Abstract

CHENNAMSETTY, NARESH. ***Molecular simulation of surfactant self-assembly: from mesoscale to multi-scale modeling.*** (Under the direction of Keith E. Gubbins)

Fully atomistic computer simulations of surfactant self-assembly are extremely challenging because of the different length scales and the associated different times scales, implying large system sizes and tediously long simulations. To overcome this, the uninteresting degrees of freedom at the atomistic level can be integrated out leading to a meso-scale model, which can span the required length and time scales with less computational burden. We use such a meso-scale model to study surfactant self-assembly and how alcohols affect this self-assembly behavior in supercritical carbon dioxide. Here the surfactants and alcohols are represented as a chain of beads where each bead represents a set of atoms. This model is implemented into lattice Monte Carlo simulations. We show that short chain alcohols act as cosurfactants by concentrating in the surfactant layer of the aggregates, strongly decreasing micellar size and increasing the number of aggregates. In contrast long chain alcohols act as cosolvents by concentrating more in the solvent and increasing the micellar size.

We then focus on systematically constructing a meso-scale model that preserves the important aspects of the atomistic model, while spanning these different length and time scales. The process of constructing this meso-scale model from the corresponding atomistic model is called coarse-graining. We first explore the rigorous coarse-graining

technique in which we match the partition function of the atomistic model with that of the meso-scale model. Such a rigorous procedure has the advantage that it leads to the reproduction of all the structural and thermodynamic properties of the atomistic model in the meso-scale model. We develop a procedure to calculate the rigorous 1, 2... N-body effective interactions using Widom's particle insertion method. We implement this rigorous procedure for a binary Ar/Kr system, where the degrees of freedom of Ar are integrated out. We observed that the structure at the pair level is well reproduced by the effective system using only effective pair potentials and ignoring all higher multi-body contributions. However, we observe deviations in the pressure for higher densities. These latter deviations are attributed to the neglect of three- and higher multi-body interactions.

For complex systems, we explore coarse-graining techniques that match the correlation functions between the atomistic and the meso-scale models. We apply this coarse-graining procedure for a system of ethanol molecules in water. In the coarse-grained model each ethanol molecule is represented by one spherical bead and the water is coarse grained out completely. We show that the potential of mean force works well as an effective potential only for low concentrations (8wt%), an integral equation approach with hypernetted chain closure approximation works well up to quite high surfactant concentrations (50 wt%), while an iterative Boltzmann scheme works very well for even the highest concentrations studied (70wt%).

Molecular simulation of surfactant self-assembly: from mesoscale to multi-scale modeling

by

NARESH CHENNAMSETTY

A dissertation submitted to the Graduate Faculty of
North Carolina State University
in partial fulfillment of the requirements for the degree of
Doctor of Philosophy

CHEMICAL ENGINEERING

Raleigh
January 5, 2006

APPROVED BY:

Keith E. Gubbins, Chair

Carol K. Hall

Jan Genzer

Richard J. Spontak

Dedication

To my parents

Biography

Naresh Chennamsetty was born on January 9, 1979 in Visakhapatnam, India, to his parents Venkateswara Rao and Satyavathi. He was raised along with his older sister Subba Lakshmi and younger brother Rama Krishna. After early education in Visakhapatnam, he obtained scholarship to attend his 11^{th} and 12^{th} standard in the APRJC, Nagarjuna Sagar, located in a beautiful place right next to the world's largest masonry dam, built across the river Krishna. Later, he went on to pursue his undergraduate studies in Chemical Engineering at the Indian Institute of Technology (IIT), Madras, India. During his 2^{nd} year at IIT, he got interested in drawing which was to become his life long passion. In his final year at IIT, he worked on the "Study of pulsatile flow within a Haemo-dialyser" under the guidance of Prof. M. S. Ananth. After graduating with a Bachelors of Technology in 2000, he went on to pursue his doctoral studies in the Chemical and Biomolecular Engineering Department at the North Carolina State University. He joined the research group of Prof. Keith E. Gubbins, where he carried out the work presented in this dissertation.

Acknowledgements

I am most thankful to my advisor, Keith Gubbins, for his invaluable support, guidance and more importantly for giving the freedom to pursue my own ideas and think independently. He would always push me towards challenging tasks that could make a difference at the most fundamental level. He would continuously ask me questions which made me reflect on my course of thought and organize myself. Working with him has been a great learning experience and I thank him for sharing his knowledge of science and other aspects of life, and for being a mentor as well as a good friend.

I like to express my immense gratitude to Henry Bock, a former post-doc in our group who went on to become an Assistant Professor at the Heriot-Watt University in Edinburgh, Scotland. He has been my coworker throughout the work on this thesis and I could not have asked for a better person to work with. I thoroughly enjoyed discussions with him which gave me a whole new perspective of my research and were most enlightening. He was very encouraging and inspiring and I have been most fortunate to work with him.

I would like to thank our collaborators Jörg Silbermann, Martin Schoen and Sabine Klapp at the Technical University-Berlin, Germany for many stimulating discussions, for sharing their ideas and for their unending enthusiasm in our collaboration. I would always cherish the days I spent in Berlin when I got the opportunity to visit them and thank them for making my stay both productive and exciting.

I am grateful to Flor Siperstein and Lauriane Scanu, former post-docs in our group, who were very helpful in guiding me during the early part of my Ph.D and getting me settled down. I thank them for always willing to help and offer their advice.

I like to thank all the Gubbins' group members that I had a chance to interact with over the years. This includes Francisco, Supriyo, Surendra, Erik, Coray, Benoit, Milen, Alberto, Jorge, Heath, Joshua, Tim, and our beloved secretary June. They made it enjoyable and fun to be part of the group. I thank the Hall's group members for being our fun neighbors and all the students, faculty and staff of the Chemical Engineering department, who made my graduate life an enjoyable experience.

I thank the National Science Foundation and the Department of Energy for providing the financial support required to carry out this research. I thank the National Partnership for Advanced Computational Infrastructure for providing the necessary supercomputing time. International cooperation with Prof. Schoen's group in Berlin was made possible through a joint grant from the National Science Foundation and the Deutsche Forschungsgemeinschaft.

Finally, I like to thank all my innumerable friends in Raleigh, who made my stay here the most memorable experience. I thank my parents for their belief in me and for provided all the help and support throughout my life. I thank them for all the hardships they went through to make me reach this point of my career. I am forever indebted to them.

Table of Contents

List of Tables

List of Figures

Chapter 1

Introduction

Surfactant self-assembly is an important phenomenon that occurs in a number of processes in our everyday life. Whether you use soap for your morning shower, drink a glass of milk for breakfast, or paint the walls of your house, surfactant self-assembly is occurring. These surfactants self-assemble both in bulk solution and from a solution onto solid surfaces to form a wide range of structures such as spheres, ellipses, cylinders, hemi-cylinders, helices, double helices, bilayers, etc. These self-assembled structures are useful in numerous applications such as enhanced separations [1], agents for drug delivery [2], biosensors [3,4,5], sol-gel nanocoatings [6], biomimetic materials [7], nano-structured functional surfaces [8] and synthesis of nano-particles [9]. One such application is in using supercritical carbon dioxide ($scCO_2$) as a solvent, where the reverse micelles formed by surfactants help solubilize polar substances (such as water and ionic compounds) and high molecular weight polymers, which are otherwise insoluble in $scCO_2$ [10,11,12]. Addition of cosurfactants such as alcohols further increases the solubilization of these substances within reverse micelles in $scCO_2$ [13,14]. Thus environmentally benign and inexpensive $scCO_2$ can replace toxic solvents in industrial applications with the help of surfactants.

Computer simulations play an important role in understanding the forces and parameters that influence the surfactant self-assembly behavior. This understanding is

required to design nano-structured materials with desired properties. The study of these self-assembling systems however, is quite challenging because of the different length scales and the associated different times scales involved, implying large system sizes and long simulations. For example, the length scale in surfactant solutions ranges from the order of 0.1 nm for atoms to tens or hundreds of nanometers for the self-assembled structures such as micelles. Similarly, the time scale ranges from the order of 1fs for atomic motion to that of ms for micellar dynamics [15]. Using a fully atomistic model to simulate such large length and time scales involves enormous computational costs. For example, a 1ns simulation of a single micelle with about 50 C_8E_5 surfactants (where C = methylene or methyl and E = ethylene oxide) in water in a cubic box of length 4nm on a single processor takes about 10 days. Thus, simulating a few micelles for ms is, at present, beyond the capability of current computers. Therefore, we need a multi-scale scheme that spans the required length and time scales, at the same time preserving the important aspects of the atomistic model (such as hydrogen bonding). Such a scheme can be achieved by integrating out the uninteresting degrees of freedom at the atomistic level, leading to a meso-scale model. For example, if we are not interested in every atomistic detail of the surfactant, we can combine sets of atoms into beads and follow the motion of the center of mass of these beads instead of all individual atoms. The process of constructing this meso-scale model from the corresponding atomistic model is called coarse-graining. The meso-scale model thus constructed still preserves some of the important aspects of the atomistic model, but can span the required length and time scales. This process of coarse-graining to obtain a meso-scale model from the atomistic model will be the main focus of our work.

1.1 OVERVIEW OF OUR WORK

We first study surfactant self-assembly in supercritical CO_2 and the effect of alcohols on their self-assembly behavior. Here we use a meso-scale model with simple interaction potentials to represent the amphiphilic nature of the surfactant and the alcohol (chapter 2). We then investigate ways to extract exact interaction potentials required for the meso-scale model from the underlying atomistic model through the process of coarse-graining (chapters 3 to 5). We first give a review of the various coarse-graining techniques available in the literature (chapter 3). We then explore both rigorous (chapter 4) and alternate coarse-graining techniques (chapter 5). We end with possible directions for future work (chapter 6). A brief overview of each chapter, with its main conclusions is given below.

In chapter 2, we study how alcohols affect surfactant self-assembly in supercritical CO_2 using lattice Monte Carlo simulations [16]. Here we use a meso-scale model where a group of atoms are combined into a bead so that the surfactant and alcohol are represented as chains of beads. Each CO_2 molecule is represented by a single bead. The alcohols function as either cosurfactants or cosolvents depending on their hydrocarbon chain length. In this meso-scale model, the interaction potentials are represented with simple, yet physically meaningful parameters (such that a part of the surfactant is solvo-phobic and an other part is solvo-philic). We observe that all studied alcohols reduce the critical micelle concentration (CMC). The reduction is stronger the

longer the hydrocarbon chain of the alcohol, and the higher the alcohol concentration. We show that short chain alcohols act as cosurfactants by concentrating in the surfactant layer of the aggregates, strongly decreasing micellar size and increasing the number of aggregates. In contrast long chain alcohols act as cosolvents by concentrating more in the solvent and increasing the micellar size.

In chapters 3-5, we explore various routes to extract effective interaction potentials in the meso-scale model which preserve the most important aspects from the atomistic model, through the process of coarse-graining. In chapter 3, we review the various coarse-graining techniques available in the literature, discussing their strengths and weaknesses. First we discuss the *rigorous* method where the partition function of the atomistic model is matched with that of the meso-scale model. Such a procedure has the advantage that it leads to the reproduction of all the structural and thermodynamic properties of the atomistic model in the meso-scale model. We also discuss alternate coarse-graining techniques where an effective potential is found that reproduces a specific property of interest, such as the pair level structure.

In chapter 4, we develop a rigorous coarse-graining technique to calculate the 1, 2 ... N-body effective interactions using Widom's particle insertion method [17]. We first apply this procedure to find the effective 2-body potentials for a binary Ar/Kr system, where the degrees of freedom of Ar are integrated out [18]. Comparison of this approach with an alternative route via the potential of mean force shows good agreement; however, Widom's particle insertion method experiences sampling difficulties at high densities.

We observed that the structure at the pair level is well reproduced by the effective system using only effective pair potentials and ignoring all higher multi-body contributions. However, we observe deviations in the pressure for higher densities. These latter deviations are attributed to the neglect of three- and higher multi-body interactions.

In chapter 5, we explore techniques used to coarse-grain complex systems by matching a specific property of interest between the atomistic and the meso-scale model. Since we are interested in exploring the nano-scale structures formed by surfactants, we find an effective potential which reproduces the structural properties, i.e. correlation functions. We apply this coarse-graining procedure for a system of ethanol molecules in water [19]. In the coarse-grained model each ethanol molecule is represented by one spherical bead and the water is coarse grained out completely. We show that the potential of mean force works well as an effective potential only for low concentrations (8wt%), an integral equation approach with hypernetted chain closure approximation works well up to quite high surfactant concentrations (50 wt%), while an iterative Boltzmann scheme works very well for even the highest concentrations studied (70wt%).

Chapters 2-5 have been adopted from the following publications

Chapter 2 N. Chennamsetty, H. Bock, L. F. Scanu, F. R. Siperstein, and K. E. Gubbins, "Cosurfactant and cosolvent effects on surfactant self-assembly in supercritical carbon dioxide"*J. Chem. Phys.*, 122, 94710 (2005)

Chapter 3 N. Chennamsetty, H. Bock, and K. E. Gubbins, "From atomistic to meso-scale: Coarse-graining techniques", manuscript in preparation.

Chapter 4 N. Chennamsetty, H. Bock, and K. E. Gubbins, "Coarse-grained potentials from Widom's particle insertion method", *Mol. Phys.*, 103, 3185 (2005)

Chapter 5 J.R. Silbermann, S.H.L. Klapp, M. Schoen, N. Chennamsetty, H. Bock, and K.E. Gubbins, "Mesoscale modeling of complex binary fluid mixtures. Towards an atomistic foundation of effective potentials" *J. Chem. Phys.,* in press

1.2 REFERENCES

1. J. B. Mcclain, D. E. Betts, D. A. Canelas, E. T. Samulski, J. M. DeSimone, J. D. Londono, H. D. Cochran, G. D. Wignall, D. ChilluraMartino, and R. Triolo, *Science* **274**, 2049 (1996).

2. C. J. Drummond, C. Fong, *Current Opinion in Colloid & Interface Science*, **4**, 449 (2000)

3. A. Kamyshny, S. Lagerge, S. Partyka, P. Relkin, S. Magdassi, *Langmuir* **17**(26), 8242 (2001).

4. J. Penalva, R. Puchades, A. Maquieira, S. Gee, B.D. Hammock, *Biosensors & Bioelectronics*, **15**, 99 (2000).

5. C. Richard, R. Balavoine, P. Schultz, T.W. Ebbesen and C. Mioskowski, *Science*, **300**, 775 (2003).

6. R.A. Caruso and M. Antonietti, *Chem. Mater.* **13**, 3272 (2001).

7. A. Sellinger, P.M. Weiss, A. Nguyen, Y.F. Lu, R.A. Assink, W.L. Gong, C.J. Brinker, *Nature* **394**, 256 (1998).

8. F. Tiberg, J. Brinck, L. Grant, *Current Opinion in Colloid & Interface Science* **4**, 411 (2000).

9. A. Manna, T. Imae, M. Iida, N. Hisamatsu, *Langmuir*, **17**, 6000 (2001)

10. M. M. Jimenez-Carmona and M. D. L. de Castro, *Anal. Chim. Acta* **358**, 1 (1998)

11. E. L. V. Goetheer, M. A. G. Vorstman, and J. T. F. Keurentjes, *Chem. Eng. Sci.* **54**, 1589 (1999).

12. J. B. Mcclain, D. E. Betts, D. A. Canelas, E. T. Samulski, J. M. DeSimone, J. D. Londono, H. D. Cochran, G. D. Wignall, D. ChilluraMartino, and R. Triolo, *Science* **274**, 2049 (1996)

13. G. J. McFann, K. P. Johnston, and S. M. Howdle, *AIChE J*. **40**, 543 (1994)

14. K. Sawada, T. Takagi, and M. Ueda*, Dyes Pigments* **60**, 129 (2004)

15. J. C. Shelley and M. Y. Shelley, *Curr. Opin. Colloid Interface Sci.*, **5**, 101 (2000).

16. N. Chennamsetty, H. Bock, L. F. Scanu, F. R. Siperstein, and K. E. Gubbins, *J. Chem. Phys.*, **122**, 94710 (2005)

17. B. Widom, *J. Chem. Phys.* **39**, 2808 (1963)

18. N. Chennamsetty, H. Bock, and K. E. Gubbins, *Mol. Phys.* **103**, 3185 (2005)

19. J.R. Silbermann, S.H.L. Klapp, M. Schoen, N. Chennamsetty, H. Bock, and K.E. Gubbins, *J. Chem. Phys.* in press

Chapter 2

Cosurfactant and cosolvent effects on surfactant self-assembly in supercritical carbon dioxide

2.1 INTRODUCTION

Supercritical carbon dioxide ($scCO_2$) is an attractive alternative to conventional solvents since it is environmentally benign, inexpensive, essentially non-toxic and has moderate critical conditions (T_C = 304.13K, P_C =73.773bar). Furthermore, its density, viscosity and dielectric properties are unusually tunable by small changes in the thermodynamic conditions (temperature and pressure), which are easy to control in practice, making supercritical carbon dioxide an unusually versatile solvent [1]. Unfortunately, the poor solvent quality of CO_2 for polar substances (such as water and ionic compounds) and high molecular weight polymers limits its wide application. One potential way to overcome this limitation is to solubilize these otherwise insoluble substances within reverse micelles formed by surfactants [2-4]. However, the low solvent strength of CO_2 also limits the solubility of many surfactants, which in turn prevents sufficient solubilization of hydrophilic substances [5]. This situation can be substantially improved by adding cosurfactants or cosolvents such as alcohols [6-10].

Surprisingly little work has been done on the effect of alcohol additives in supercritical CO_2. Liu *et al.* [9] showed that adding n-pentanol leads to an increase of the

solubility of the primary surfactant (tetraethylene glycol n-lauryl ether, $H[CH_2]_{12}[OCH_2CH_2]_4OH$, i.e. $C_{12}E_4$, where C = methylene or methyl and E = ethylene oxide) with increasing alcohol concentration at all temperatures and CO_2 pressures studied. Under constant CO_2 pressure conditions, an alcohol concentration of 1.12M caused a four-fold increase of the $C_{12}E_4$ solubility. In a similar system, McFann *et al.* [6,7] studied the solubility of water and found that 0.5-0.8 wt. % water can be solubilized in a solution of pentaethylene glycol n-octyl ether (C_8E_5) in $scCO_2$, depending on the surfactant concentration. The water load of the solution was found to increase by a factor of 4 to 5 if n-pentanol was added.

Later Sawada *et al*. [8] studied the same system and systematically investigated the dependence of the solubility of C_8E_5 on the chain length of the added alcohol. The solubility experiments revealed an optimum performance of the alcohol with a chain length of 5 carbon atoms, i.e. n-pentanol. The authors [8] further report that this behavior was independent of temperature. In agreement with McFann's results, Sawada *et al*. also found that the water solubility increased significantly with increasing n-pentanol concentration.

The solubility of the non-ionic surfactant Ls-54 in supercritical CO_2 was investigated by Liu *et al*. [10] The addition of n-propanol, n-pentanol or n-heptanol decreased the cloud point pressure (CPP) of the Ls-54/$scCO_2$ system, i.e. at constant CO_2 pressure, the solubility of Ls-54 was increased. The largest reduction of the CPP was

measured for n-propanol. On the contrary, benzyl alcohol *increased* the cloud point pressure, *reducing* the solubility of Ls-54.

Far more studies on the effect of alcohols have been carried out in water/surfactant/oil systems. In these systems it is usually desired to find a surfactant, which at given thermodynamic conditions and for a given oil, stabilizes a microemulsion middle-phase rather than water-in-oil or oil-in-water microemulsions. Winsor [11] found that the performance of the surfactant depends on the balance between surfactant-oil and surfactant-water interactions [12]. To achieve optimal performance, it may require surfactant molecules with long hydrophobic tails. However, if the surfactant tail becomes too long, the solubility of the surfactant in water may decrease to a value below the critical micelle concentration (CMC), such that neither micelles nor microemulsions can form [13]. As in the CO_2 systems, alcohol additives successfully stabilize microemulsions in water/surfactant/oil systems [14-17]. Alcohols can also decrease the CMC, depending on alcohol concentration and tail length [18-20]. Some authors suggest that the alcohol molecules operate by inserting themselves between the surfactant tails, reducing tail-tail and micelle-micelle interactions [21-23], while others argue that they act at the interface itself reducing the surface tension [24,25]. Another view is that the additives distribute mainly between the aqueous and the oil phases, altering the solvent properties [26].

These assumptions about the function of the additives led to a classification into two groups: *cosolvents* and *cosurfactants*. Cosurfactants are weakly amphiphilic

molecules, which are assumed to concentrate in the surfactant layer of the aggregates formed by the primary surfactant. Due to their weak amphiphilic character, cosurfactants alone do not form aggregates, but they strongly support aggregation of the primary surfactant. Common examples of cosurfactants are medium chain alcohols (5-8 carbon units). Cosolvents on the other hand are not necessarily amphiphilic. In CO_2 systems, their main function is to improve the solvent quality of CO_2. This is necessary since hydrocarbons are not very soluble in CO_2, preventing the solubilization of surfactants with hydrocarbon tails. Fluorocarbon surfactants are much more soluble in CO_2 than hydrocarbon surfactants, but their use is questionable, since the entire solution should be environmentally friendly.

Frequently the same molecules (alcohols) are considered as cosurfactants and cosolvents. One reason is that it is very difficult to directly measure the composition of the surfactant layer. Usually theories are fitted to the experimental results, which in turn indicate the distribution of the additive in the system [20]. In NMR measurements of a water-in-oil (n-hexane) microemulsion, a more direct observation of the distribution of additive molecules was made [27]. A large amount of cosurfactant (n-pentanol) was found at the microemulsion interface, thus qualifying n-pentanol as cosurfactant for this system. However, it must be assumed that for many additives there is no clear-cut distinction between cosurfactants and cosolvents. Additive molecules will be present in the surfactant layer as well as in the surrounding solution, thus altering the properties of the solvent as well as those of the surfactant layer.

While molecular properties such as the distribution of additive molecules are usually difficult to measure experimentally, they are natural observables in molecular simulations. Thus lattice and off-lattice simulation methods have been used to study the self-assembly and phase behavior of surfactants in supercritical carbon dioxide [28-33].

Off-lattice simulations are very attractive since they provide an association of the thermodynamic properties of the system with very detailed molecular information, at least in principle. Salaniwal *et al.* [28,29] used a hybrid full-atom/united-atom model in molecular dynamics (MD) simulations to study reverse micelles formed in a CO_2/dichain surfactant/water system. One of their systems, containing 33 surfactants, was observed over a period of 1ns. During this time one aggregate formed from a preassembled starting configuration. The size and shape of the aggregate was in reasonable agreement with experimental findings. The enclosed water in the center of the reverse micelle showed dramatic structural differences from the water located close to the surfactant head groups. A similar system was investigated by Senapati *et al.* [30] using united-atom molecular dynamics simulations. In their system, 160 dichain fluorosurfactant molecules stabilized one microemulsion droplet, which was observed over a period of 4ns. The radius of gyration of the droplet was in reasonable agreement with small-angle neutron scattering (SANS) experiments at the same thermodynamic conditions. A small section of a surfactant stabilized CO_2/water interface was studied by da Rocha and co-workers emploing full-atomistic MD simulations [31]. As these examples show, off-lattice simulations are invaluable tools to investigate CO_2/surfactant/water systems, but they are

challenging because of the various length and time scales involved. Consequently they are usually limited to relatively small systems and short times.

In this paper we are interested in thermodynamic equilibrium properties of surfactant solutions. This requires much larger systems than in the examples above where single-aggregate properties were investigated. To achieve the required system sizes, it is necessary to "trade" a detailed description of the molecules for a coarse grained model of the system. Coarse models are commonly used in stochastic dynamics methods such as Brownian dynamics (BD) or dissipative particle dynamics (DPD). Using DPD, Rekvig *et al*. [34] studied the impact of mixing different surfactants on the bending modulus of a surfactant stabilized water/oil interface. They observed that mixing long and short chain surfactants leads to more flexible interfaces compared to usage of surfactants with a chain length intermediate between the long and the short one.

Alternative coarse grained models are applied in lattice Monte Carlo simulations of surfactant systems. Recently, Zaldivar and Larson [35] studied the aggregation behaviour of binary mixed micelles in an incompressible solvent using lattice Monte Carlo simulations. In their model, the two surfactant species are distinguished by the difference in the unlike surfactant head/head interaction compared to the like surfactant head/head interaction. They observed a synergistic lowering of the CMC for surfactant mixtures with an effective unlike surfactant head/head net attraction and an increase in the opposite case. An optimum was found when both surfactant species have the same concentration in the solution. The lattice model originally developed by Larson [36-38]

has been modified for compressible fluids by Lisal *et al.* [32,39] to study surfactant solutions in supercritical carbon dioxide and used by Scanu *et al.* [33] to reproduce the correct CO_2 density dependence of the critical micelle concentration (CMC).

In this work, we use lattice Monte Carlo simulations to study the effect of alcohols on the micellization of surfactants in supercritical CO_2. Special attention is drawn to the location of additive molecules in the system. Further, we study the dependence of the CMC and the size, shape and structure of the micelles as a function of alcohol chain length and alcohol concentration. We also discuss how increasing the alcohol chain length changes the additive behavior from cosurfactant to cosolvent.

The remainder of this chapter is organized as follows: In section 2.2, we describe the model and give definitions of the properties that characterize the micellar solution. Section 2.3 is devoted to a presentation of our results. We analyze our results in two parts: The first part is concerned with the formation of the aggregates while the second part investigates structural properties, shape, size and density distributions. Finally, we summarize our findings and conclusions in section 2.4.

2.2 MODEL AND SIMULATION

Throughout we use *reduced quantities*: all lengths are reduced with the lattice constant, ℓ, the energy scale is given in units of the absolute value of the CO_2/CO_2

interaction energy, $\left|\varepsilon_{CC}^{*}\right|$ and the temperature is reduced with $k_{\mathrm{B}}/\left|\varepsilon_{CC}^{*}\right|$, where k_{B} is the Boltzmann constant.

2.2.1 Model

To study surfactant solutions in supercritical CO_2 containing additive molecules, we employ a modified version of Larson's lattice model [36-38] proposed by Lisal *et al.* [32] This model allows vacant lattice sites leading to a nonvanishing compressibility, which is essential to correctly describe supercritical fluids such as CO_2 [32,33]. In the lattice model, CO_2 molecules are represented by single beads and surfactant and additive molecules by chains of beads. The bead positions are restricted to the sites of a simple cubic lattice with lattice constant ℓ. Each bead interacts with its nearest neighbors and with neighbors that are $\sqrt{2}\ell$ and $\sqrt{3}\ell$ apart, giving a total coordination number of 26. The same vectors that connect interacting beads also connect consecutive beads in the chain molecules. The surfactant used here is denoted by H_5T_4, consisting of 5 head beads (*H*) and 4 tail beads (*T*), occupying a total of 9 lattice sites. This model molecule could represent a member of the widely used nonionic ethylene glycol surfactants, e.g. tetraethylene glycol n-octyl ether (C_8E_4), which has four ethylene oxide groups and one terminal OH group. Similarly, the additive molecules are denoted by ht_{α}, consisting of one head bead (*h*) and α tail beads (*t*), giving a total of $1+\alpha$ beads. We assume that these additive molecules represent a homologous series of linear alcohols with one terminal OH group. Head and tail groups of the model molecules are distinguished by their interaction energies with other beads in the system. In our definition we follow the

common convention that the head groups are hydrophilic, i.e. CO_2-phobic, and the tail groups are hydrophobic, i.e. CO_2-philic. Thus, in CO_2, the surfactants form *reverse micelles* (head inside, tail outside). However, for the sake of simplicity and convenience we will refer to them as "micelles".

The set of interaction energies used in this study is given in table 2.1. The surfactant/CO_2 interaction parameters are taken from Ref.33. The peculiarity of this set of interaction energies is that it correctly reproduces the experimental trends of the CMC with CO_2 density [33] while others do not [32]. We choose the interaction energies of the alcohols to be equal to those of the surfactant. The exchange energy between the alcohol head group and the surfactant head group is set to $w_{Hh} = -1$.

Exchange energies are convenient tools to characterize mixing tendencies in the solution. The exchange energy, w_{ab}, is defined as

$$w_{ab} = \varepsilon_{ab} - \frac{\varepsilon_{aa} + \varepsilon_{bb}}{2}, \qquad a \neq b. \tag{2.1}$$

Although the interaction energy between CO_2 and surfactant heads is attractive, $\varepsilon_{CH} = -1$, the corresponding exchange energy is repulsive, $w_{CH} = 1$. Thus, they repel each other because of the strong *H*/*H* attraction ($\varepsilon_{HH} = -3$). The mild repulsion of the phobic exchange energies ($w_{CH} = w_{TH} = 1$) ensures that the CMC does not occur at too low surfactant concentration [33].

Table 2.1. Interaction energies between CO_2 (*C*), surfactant head (*H*), surfactant tail (*T*), alcohol head (*h*), and alcohol tail (*t*). The surfactant/CO_2 interaction energies are taken from Ref.33. Here ε_{ab} denotes the interaction energy between different species *a* and *b*, where *a* and *b* represent *H*, *T*, *h*, *t* or *C* and w_{ab} denotes the exchange energy [see Eq. (2.1)].

Like interactions		Unlike interactions		
Type of interaction	ε_{ab}	Type of interaction	ε_{ab}	w_{ab}
C-C	-1	*C-H, C-h*	-1	1
H-H, h-h	-3	*C-T, C-t*	-3	-2
T-T, t-t	-1	*H-h*	-4	-1
		T-t	-1	0
		H-T, H-t, h-T, h-t	-1	1

2.2.2 Monte Carlo Simulations

We study the thermodynamic behavior of the lattice model described above using lattice Monte Carlo simulations in the canonical ensemble (NVT). In order to avoid finite size effects on the aggregation behavior, we simulate systems accommodating 5 to 10 micelles. This requires lattice sizes ranging from $N = 40^3$ (for higher surfactant concentrations) up to $N = 130^3$ lattice sites (for lower surfactant concentrations near the CMC). These N lattice sites are occupied by N_C CO_2 beads, $9N_{H5T4}$ surfactant beads, and $(1+\alpha)N_{ht\alpha}$ alcohol beads. Consequently, $N_v = N - \left[N_C + 9N_{H5T4} + (1+\alpha)N_{ht\alpha}\right]$ lattice sites are vacant. Periodic boundary conditions are applied in all three dimensions.

To efficiently sample configuration space, we use *complete chain regrowth* with configurational bias, *reptation,* and *twist* moves for surfactant and alcohol molecules and *particle exchange* (switch) moves for CO_2 where we attempt to move a CO_2 bead to a randomly chosen vacant site [40]. We typically run $1x10^5$ to $2x10^5$ cycles for equilibration and $4x10^5$ to $8x10^5$ cycles for evaluation of quantities of interest. Each cycle consists of $N_C + N_v$ switch moves, $9N_{H5T4}$ chain moves for the surfactants and $(1+\alpha)N_{ht\alpha}$ chain moves for the alcohol molecules. In each chain move, a molecule is randomly selected and a randomly chosen move (re-growth, reptation and twist) is performed. The different chain moves are chosen with equal probability.

In solution, surfactant molecules aggregate spontaneously. A surfactant (or additive) molecule is defined to belong to a specific aggregate if one of its head beads is a neighbor of a head bead of a surfactant (or additive) molecule that belongs to the same aggregate. A surfactant molecule is called "free" if it does not belong to any aggregate. In the simulations we determine aggregates using the *cluster multiple labeling technique* of Hoshen and Kopelman [41].

2.2.3 Thermodynamic Properties

During the simulation, we monitor several quantities such as the fraction of free surfactants, the aggregation number distribution, the radii of gyration of micelles and the density profile within a micelle. In this section we present the definitions of these properties that we will use throughout the paper.

a. Concentration

To quantify the content of the solution we use volume fractions, ϕ, in [%], henceforth called "concentration". In our lattice model, volume fractions are identical to site fractions, since *a priori* all beads have the same volume.

b. Critical micelle concentration

At low surfactant concentrations, individual surfactant molecules are dissolved in the solvent, while micelles form at higher concentrations. The threshold concentration where the first micelles appear in the system is called *critical micelle concentration* (CMC). Unfortunately, the CMC is not an *a priori* well defined point. While several definitions of the CMC exist and give similar results [42-48], we employ the definition given by Israelachvili *et al* [42]. In figure 2.1, we present a typical plot of the concentration of free surfactant molecules, ϕ^{free}, as a function of the total surfactant concentration, ϕ, at 5% alcohol *ht*. Although the alcohol might influence the value of the CMC, it is not involved in CMC determination. According to Israelachvili's definition, the CMC is given by the surfactant concentration where the line $\phi^{\text{free}} = \phi/2$ (dashed line) intersects the line representing a fit to the linear part of the curve at high surfactant concentration (solid line). The CMC thus calculated is, $\phi^{\text{CMC}} = 0.54\%$. We note that according to this definition $\phi^{\text{free}} = \phi^{\text{CMC}}/2$ at the CMC.

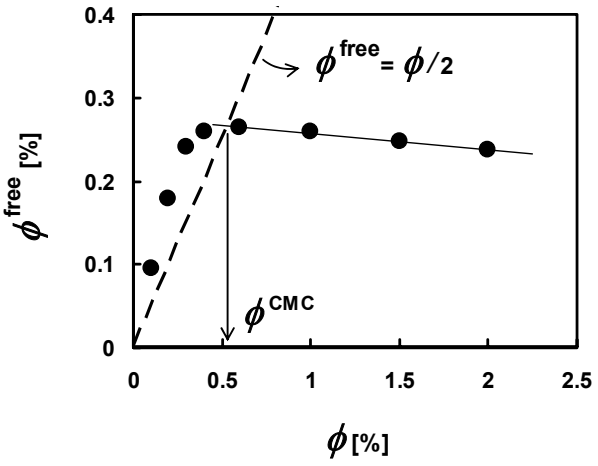

Figure 2.1. Determination of the CMC for a solution of surfactant H_5T_4 in $scCO_2$ containing 5% alcohol *ht*. The solid line is a linear fit to the simulation results at $\phi \geq 0.6\%$.

c. Aggregation number distribution

Micelles are dynamic entities with surfactant molecules entering and leaving over the course of their "life time". Therefore, surfactant solutions comprise aggregates of different aggregation numbers, M, quantified by aggregation number distributions. The commonly used aggregation number distribution, $P(M)$, which represents the fraction of surfactant molecules bound in aggregates of size M is defined as

$$P(M) = \frac{MN_M}{\sum_M MN_M} = \frac{MN_M}{N_{H5T4}}, \tag{2.2}$$

where N_M is the ensemble average of the number of aggregates of aggregation number M and N_{H5T4} is the total number of H_5T_4 surfactant molecules. In figure 2.2, a typical surfactant aggregation number distribution is shown, which is obtained at 2.5% H_5T_4 and 5% *ht*. It comprises a steeply rising part when M approaches 1, and the usual bell

shaped maximum, separated by a minimum. The symmetry of the aggregate size distribution suggests that a mean aggregation number $\bar{M}$ can be defined by

$$\bar{M} = \frac{\sum_{M>5} MN_M}{\sum_{M>5} N_M}. \tag{2.3}$$

Note that free surfactants ($M = 1$) and small aggregates ($2 \le M \le 5$) are excluded from the calculation of $\bar{M}$.

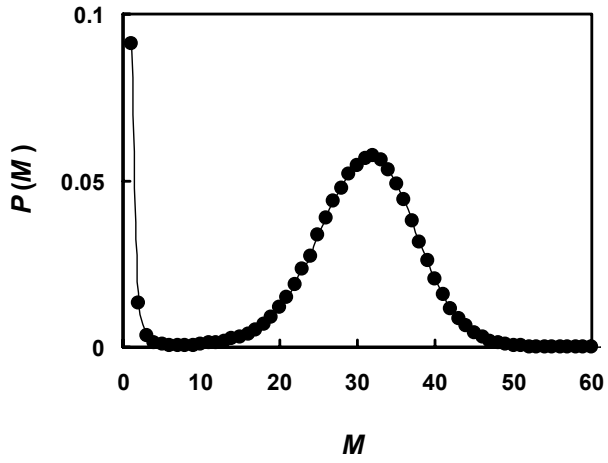

Figure 2.2. Surfactant aggregation number distribution at 2.5% surfactant H_5T_4 and 5% alcohol *ht.*

d. Radius of gyration

Convenient measures of the shape of micelles are the three "principal radii of gyration", which are obtained in the following way: At first one calculates the instantaneous gyration tensor, $\underline{\underline{R}}$, defined by [49]

$$R_{kl}^2 = \frac{1}{n}\sum_{i=1}^{n}\left[r_k(i) - r_k^*\right]\left[r_l(i) - r_l^*\right], \tag{2.4}$$

for each micelle. The sum in (2.4) runs over the n beads of all surfactant molecules which belong to the micelle, $r_k(i)$ and $r_l(i)$ are the (x, y, z) components of the position vector, $\underline{r}(i)$, of bead i and $\underline{r}^*$ is the position of the center of mass. We note that this definition implies the head and tail beads have the same mass. Next, the three eigenvalues of $\underline{\underline{R}}$ are determined and ordered, $\hat{R}_1 \le \hat{R}_2 \le \hat{R}_3$. These eigenvalues represent the principal radii of gyration of the micelle under consideration. A micelle is considered spherical if $\hat{R}_1 = \hat{R}_2 = \hat{R}_3$. The properties which are commonly called "principal radii of gyration of micelles with aggregation number M" are given by

$$R_\beta(M) = \left\langle \hat{R}_\beta(M) \right\rangle, \qquad \beta = 1,2,3, \tag{2.5}$$

where $\langle\ \rangle$ denotes the ensemble average. By considering only the head beads one obtains the principal radii of gyration of the core of the reverse micelles, $R_\beta^C(M)$. By averaging the principal radii of gyration one obtains the mean radius of gyration, $R(M)$:

$$R(M) = \frac{1}{3}\sum_{\beta=1}^{3} R_\beta(M). \tag{2.6}$$

Values of $R(M)$ obtained in solutions at different thermodynamic conditions can be used to compare the size of micelles of aggregation number, M. At constant M, a larger value of $R(M)$ indicates that the micelle extends further into the solvent compared to a micelle with a smaller $R(M)$.

e. Density profile

The structure within spherical micelles can be analyzed using radial density profiles for each species of beads *a=H, T, h, t, C, v*. The density profile, $n_a(r)$, of a particular species, *a*, is defined as

$$n_a(r) = \frac{\langle N_a(r) \rangle_M}{N_{\text{total}}(r)}, \tag{2.7}$$

where $\langle \ \rangle_M$ denotes the ensemble average for all micelles of aggregation number M, $N_a(r)$ is the number of lattice sites occupied by beads of species a at a distance r from the center of mass and $N_{\text{total}}(r)$ stands for the total number of lattice sites at this distance r. We note that $n_a(r)$ depends also on M, although we do not show this explicitly.

f. Connection to experiments

Our simulations are carried out at constant (reduced) temperature, $T = 6.4$ and constant CO_2 (reduced) number density $\rho = 0.86$. These conditions correspond to the experimental conditions of McFann *et al*. [7] discussed in the introduction.

Using corresponding state theory for the pure solvent we can relate the reduced temperature to an explicit temperature in Kelvin, through the ratio

$$\frac{T}{T_C} = \frac{T[\mathrm{K}]}{T_C[\mathrm{K}]}, \tag{2.8}$$

where T is the temperature in the present model, $T_C = 5.85$ is the critical temperature of the model [50,51], $T[\mathrm{K}]$ is the corresponding temperature in Kelvin and $T_C[\mathrm{K}] = 304.13\mathrm{K}$ is the measured critical temperature of CO_2. From Eq. (2.8), we estimate that the reduced temperature, $T = 6.4$, corresponds to $T[\mathrm{K}]$=333K in pure CO_2.

In an analogous way, one estimates the density of the *pure* solvent [32]. For the densities, corresponding states theory requires:

$$\frac{\rho}{\rho_C} = \frac{\rho[\mathrm{g/ml}]}{\rho_C[\mathrm{g/ml}]}, \tag{2.9}$$

where ρ is the volume fraction of CO_2 in the model, $\rho[\mathrm{g/ml}]$ is the corresponding density in explicit units, $\rho_C = 0.5$ is the critical density of the model and $\rho_C[\mathrm{g/ml}] = 0.4676$ g/ml is the experimentally measured critical density of CO_2. Thus the reduced number density (or volume fraction) of the pure solvent, $\rho = 0.86$, corresponds to $\rho[\mathrm{g/ml}] = 0.8$ g/ml. We note that within the present model the *reduced* number density of CO_2 and the CO_2 volume fraction are equivalent.

2.3 RESULTS

We investigate the impact of concentration and architecture of alcohols, ht_α, on the aggregation behavior of the surfactant H_5T_4 in supercritical CO_2. All simulations are carried out at constant temperature, $T = 6.4$ and constant CO_2 density $\rho = 0.86$. Here ρ is calculated by counting only lattice sites that are *not* occupied by surfactant or additive molecules, i.e. vacancy and CO_2. We assume that the solvent quality of CO_2 is constant as long as ρ is kept constant. We maintain constant solvent quality so as not to bias the interpretation of the effect of adding alcohols by a simultaneous change of the solvent quality.

2.3.1 Formation of aggregates

A characteristic property of surfactant aggregation in bulk solutions is the *critical micelle concentration* (CMC). The dependence of the CMC of H_5T_4 surfactants on the concentration of two different alcohols, *ht* and ht_4, in supercritical CO_2, is shown in figure 2.3(a). The addition of alcohol leads to a reduction of the CMC in both cases. Thus, both alcohols support aggregation of the surfactant. The CMC decreases monotonously with increasing concentration of alcohol. The decrease becomes weaker as the alcohol concentration increases. In the case of *ht*, addition of alcohol beyond 2.5% has essentially no effect on the CMC. In general, the effect of the alcohol having the longer tail group is much stronger than that of the shorter one. An alcohol concentration of 10% ht_4 lowers the CMC by a factor of 3 while 10% *ht* lowers it by less than 10%.

The dependence of the CMC of H_5T_4 surfactants on the alcohol chain length is shown in figure 2.3(b). We observe that increasing the length of the alcohol at constant alcohol concentration decreases the CMC monotonously. However, the decrease becomes weaker for $\alpha > 3$.

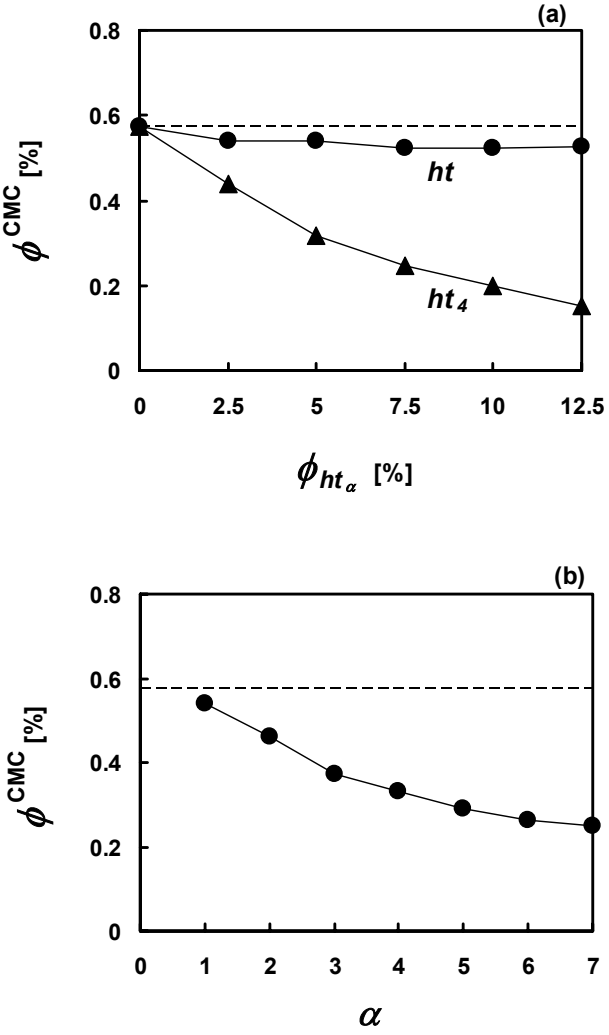

Figure 2.3. (a) CMC of surfactant H_5T_4 as a function of concentrations of alcohols *ht* and ht_4. **(b)** CMC of surfactant H_5T_4 as a function of the chain length of the alcohol (*ht* to ht_7) at constant alcohol concentration of 5%. In parts **(a)** and **(b)**, the dashed lines indicate the CMC of pure H_5T_4 surfactant without any alcohol and solid lines are drawn to guide the eye.

To our knowledge, no experimental data for the dependence of CMC on alcohol type and concentration is available in the literature for surfactant solutions in supercritical CO_2. In figure 2.4, we present experimental CMC values for an *aqueous* solution of potassium dodecanoate as a function of alcohol type and concentration [18]. Both experiments (in H_2O) and simulations (in CO_2) have been carried out at constant thermodynamic conditions of the solvent, so that a qualitative comparison is possible. Comparison of figures 2.3 and 2.4 reveals that in both simulation and experiment the impact of the longer alcohols is always stronger than that of the shorter ones and that the effect is stronger the higher the alcohol concentration. It is interesting to notice that, although the behavior of the CMC in the two solvents is very similar, the structure of the two systems is quite different. While we observe reverse micelles in the simulations of the CO_2 system, regular micelles are formed in aqueous solutions. Thus, the mechanism by which the CMC is lowered might be quite different in the two cases.

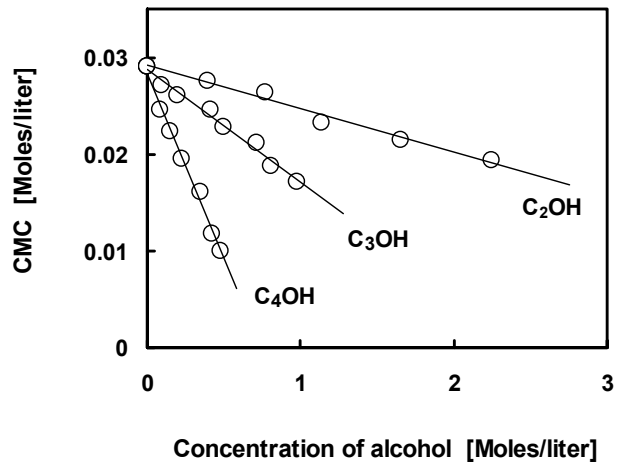

Figure 2.4. The effect of ethanol, propanol, and butanol on the CMC of potassium dodecanoate in water at $10^{\circ}C$. Data taken from Ref.18.

The results plotted in figure 2.3 clearly show that the addition of alcohols lowers the CMC and that their performance depends on concentration and chain length. Using the detailed molecular information available from our simulations, we now investigate the cause of these effects. We first study the effect of the concentration of alcohol *ht* on the mean aggregation number, $\bar{M}$, and on the composition of the micelles. In figure 2.5(a), the mean aggregation number of H_5T_4 micelles and the average number of *ht* molecules present in micelles with an aggregation number, $M = \bar{M}$ are plotted as a function of *ht* concentration at 2.5% H_5T_4. The pure H_5T_4/CO_2 system at this surfactant concentration consists of micelles with $\bar{M} = 40$. Addition of *ht* drastically decreases the mean aggregation number until at 10% *ht*, the value of $\bar{M}$ is half that of the pure system. This large reduction in the number of H_5T_4 molecules per micelle seems to be compensated by binding of *ht* molecules in micelles. Results from figure 2.5(a) indicate that each H_5T_4 molecule leaving the micelle is replaced by approximately two alcohol *ht* molecules.

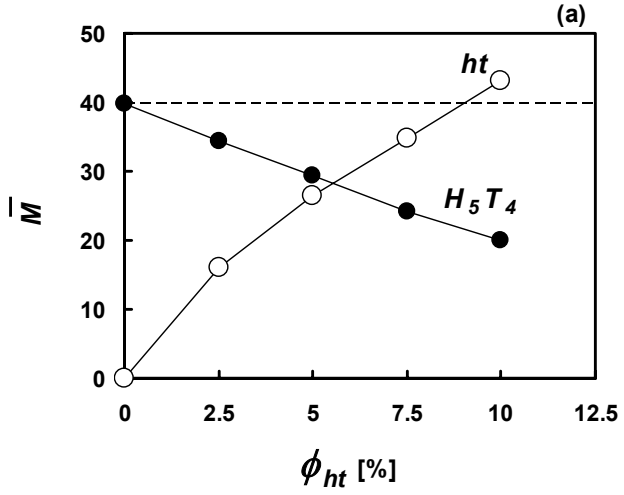

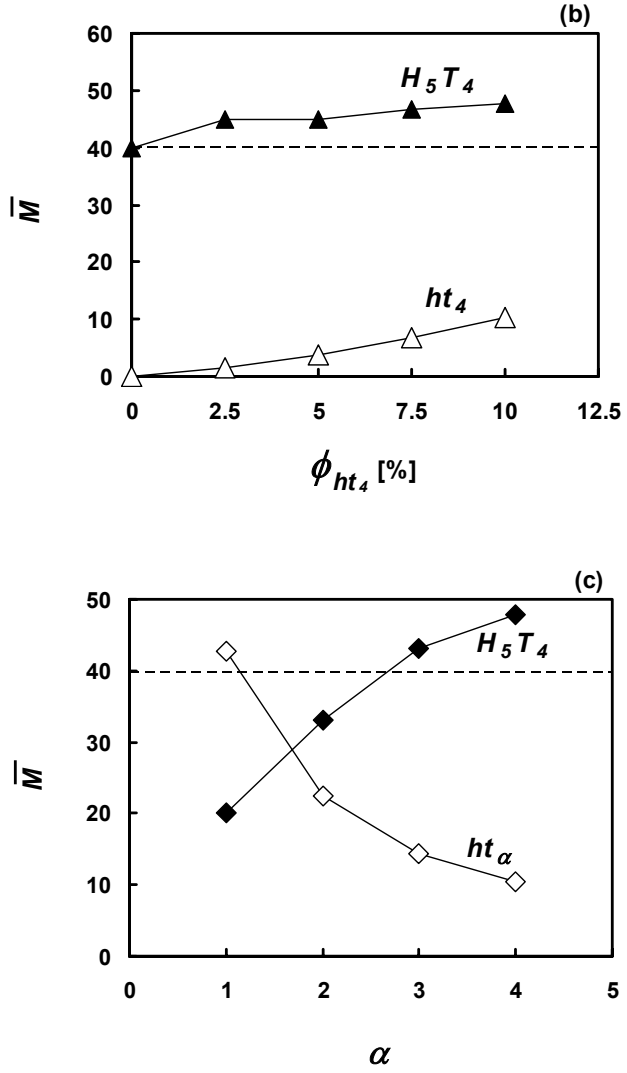

Figure 2.5. (a) Mean aggregation number of H_5T_4 micelles (filled symbols) and the average number of *ht* molecules within micelles with aggregation number $M = \bar{M}$ (open symbols) as a function of *ht* concentration at 2.5% H_5T_4. The dashed line indicates the mean aggregation number of H_5T_4 micelles formed in CO_2 without alcohol. Solid lines are drawn through the data as a guide to the eye. **(b)** Same as (a) but for ht_4. **(c)** Same as (a) but as a function of alcohol chain length at 10% alcohol concentration.

The large effect of *ht* on the aggregation number is surprising since the CMC is only lowered slightly. In contrast, the impact of ht_4 on the CMC is large but the aggregation number *increases* with increasing ht_4 concentration [figure 2.5(b)] and only a

few ht_4 molecules "enter" the micelles. From the plot in figure 2.5(c), we observe that *ht* strongly decreases the mean aggregation number of H_5T_4 micelles. However, increasing the alcohol tail length, α, continuously increases the aggregation number, such that for $\alpha > 2$ the mean aggregation number of the (10%) alcohol containing solution exceeds $\bar{M}$ of the solution without alcohol. The average number of alcohol molecules bound in micelles is large for the *ht* containing system but it decreases rapidly as α increases.

Since addition of *ht* molecules does not lower the CMC significantly and the concentration of free surfactant molecules is approximately half the CMC (figure 2.1), the number of surfactant molecules bound in micelles remains almost unchanged. On the other hand, addition of 10% *ht* halves the aggregation number. Consequently one expects the number of aggregates to increase by a factor of two. The addition of ht_4 leads to a lower CMC, i.e. more surfactant molecules are bound in micelles compared to the system without alcohol. On the other hand, addition of ht_4 increases the mean aggregation number. While a lower CMC leads to a higher number of aggregates, the increase of the mean aggregation number is reducing it. These two small opposing effects may compensate one another, i.e. one expects the number of aggregates in the solution with 10% ht_4 to be roughly equal to the one in the pure H_5T_4 solution.

In figure 2.6, we present the aggregation number distributions, $P(M)$, defined in Eq. (2.2), for H_5T_4 solution at different *ht* concentrations. As the concentration of *ht* molecules increases, the bell-shaped part of the curve shifts to lower aggregation

numbers while the shape and height do not change markedly. Since the area below the bell-shaped part of the curves is proportional to the number of surfactant molecules bound in micelles, the plots in figure 2.6 are consistent with the observation that the CMC is only weakly influenced by the addition of *ht* [figure 2.3(a)].

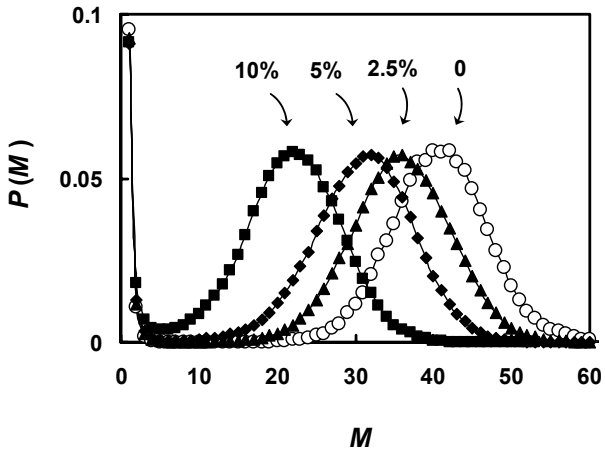

Figure 2.6. Surfactant aggregation number distributions for 2.5% H_5T_4 solution at different *ht* concentrations (0%, 2.5%, 5%, 10%).

The distribution of the number of aggregates per H_5T_4 molecule, $P^*(M)=P(M)/M$, for the pure H_5T_4 solution and for the solutions containing 10% *ht* and 10% ht_4, is shown in figure 2.7. The maximum of the curve for the solution containing 10% *ht* is about twice as high as the maximum of P^* for the pure H_5T_4 solution. Thus, addition of 10% *ht* doubles the number of micelles but halves their mean aggregation number compared to the system without alcohol. The addition of 10% ht_4, on the other hand, leads to a slight increase of the aggregation number, while the height of the maximum of P^* is slightly decreased. The lowering of the maximum is accompanied by a broadening of P^*. Both effects compensate each other, such that the

integral of the Gaussian part of P^* is almost identical for the solution containing 10% ht_4 and for the pure H_5T_4 solution. Thus, addition of 10% ht_4 does not change the number of micelles although it slightly increases the mean aggregation number. Consequently, more surfactant molecules are bound in micelles and the CMC must decrease, which is consistent with our findings presented in figure 2.3(a).

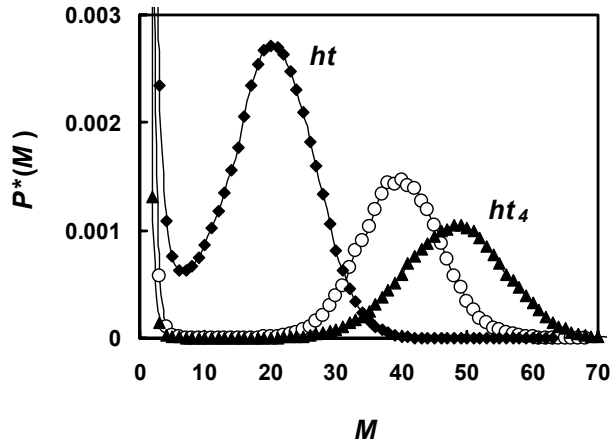

Figure 2.7. Number of aggregates per H_5T_4 molecule, $P^*(M)=P(M)/M$, as a function of aggregation number, for the pure H_5T_4 solution (open symbols) and for solutions with 10% *ht* and 10% ht_4 (closed symbols indicated in the figure) at 2.5% H_5T_4.

These observations are quite intriguing since they show that the two molecules *ht* and ht_4, which are very similar in structure, can have very different effects on the behavior of H_5T_4 surfactants in CO_2 solution. While they both lower the CMC, their impact on the mean aggregation number is *opposite*.

2.3.2 Shape, size and density distributions

The radii of gyration give information about the average shape of micelles. The three principle radii of gyration (R_1, R_2, and R_3) for the micelles formed in pure H_5T_4

solution are plotted as a function of the aggregation number in figure 2.8. As one would expect, the radii of gyration increase monotonously with aggregation number. For the present system, R_1 is about 20% smaller than R_3 indicating essentially spherical micelles. The behavior of the radii of gyration shown in figure 2.8 is representative for all studied systems, i.e. all micelles in this study are spherical.

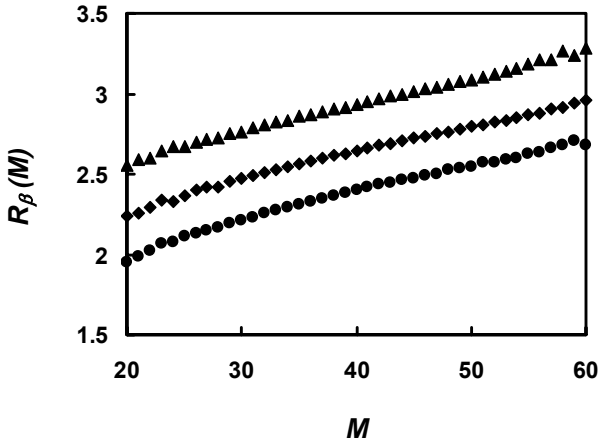

Figure 2.8. The three principal radii of gyration R_1 (●), R_2 (◆) and R_3 (▲) for micelles as a function of aggregation number for 2.5 % H_5T_4 surfactant in CO_2.

The spherical shape of micelles in all systems with and without alcohols is also apparent from snapshots presented in figure 2.9. Closer inspection of the shape of the micelles reveals that the aggregates in the *ht* containing solution [figure 2.9(b)] have less well defined, i.e. rougher interfaces than micelles in the two other systems. It appears that micelles in the pure H_5T_4 solution [figure 2.9(a)] and in the ht_4 containing solution [figure 2.9(c)] have approximately the same size, while micelles in the *ht* containing solution [figure 2.9(b)] are generally smaller. This is consistent with our expectation, since the mean aggregation number in the *ht* containing solution is much smaller than in the other two solutions (see figure 2.5).

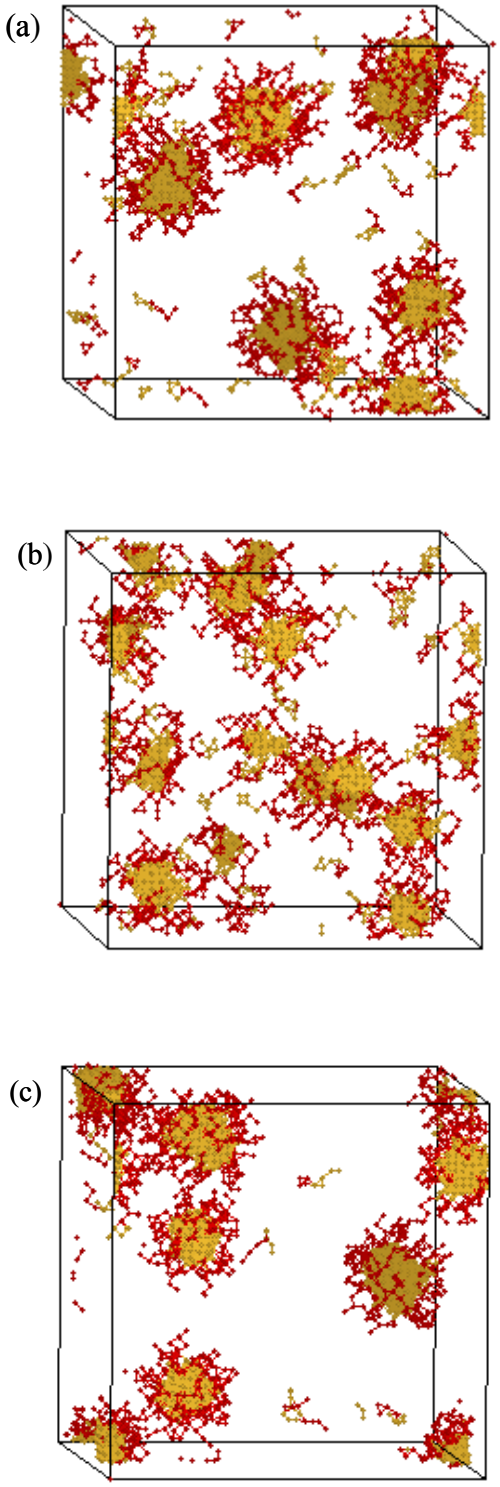

Figure 2.9. Snapshots of a 2.5% H_5T_4 solution in a simulation box of 50*50*50 lattice units containing **(a)** no alcohol, **(b)** 10% alcohol *ht* and **(c)** 10% alcohol ht_4. Only surfactant head (yellow) and surfactant tail (red) beads are shown for ease of viewing.

For a quantitative comparison of the aggregate sizes, we plot the mean radius of gyration R as a function of aggregation number for the pure, the *ht* and the ht_4 containing systems in figure 2.10(a). At the respective mean aggregation number, micelles in the *ht* containing solution ($\bar{M} = 20$) are considerably smaller than micelles in the pure H_5T_4 solution ($\bar{M} = 40$). If ht_4 instead of *ht* is added, then the mean aggregation number increases ($\bar{M} = 48$) as well as the size of the micelles.

To study the impact of the addition of alcohol on the size of micelles one needs to compare micelles of the different solutions having the *same* aggregation number. Micelles in the *ht* containing solution have slightly larger R values than micelles in the pure H_5T_4 solution, while micelles in the ht_4 containing solution have slightly lower R values [figure 2.10(a)]. If we consider only the head groups of H_5T_4 to calculate the radius of gyration for the micellar *core*, R^C, we observe the same trend [figure 2.10(b)]. The micellar size, R, at a given aggregation number increases with the addition of *ht* because of the excluded volume effect caused by binding of *ht* molecules to the micellar core/corona interface. This is consistent with the roughening of the micelle, indicated in the snapshot of the *ht* containing solution in figure 2.9(b). In contrast, only a few ht_4 molecules enter the micelles [figure 2.5(b)], causing a smaller excluded volume effect than in the case of *ht*. On the other hand, replacing CO_2 molecules by ht_4 molecules reduces the solvent quality, as can be seen from the interaction parameters in table 2.1, causing the micelles to become more compact. The net effect is a very small decrease in R [figure 2.10].

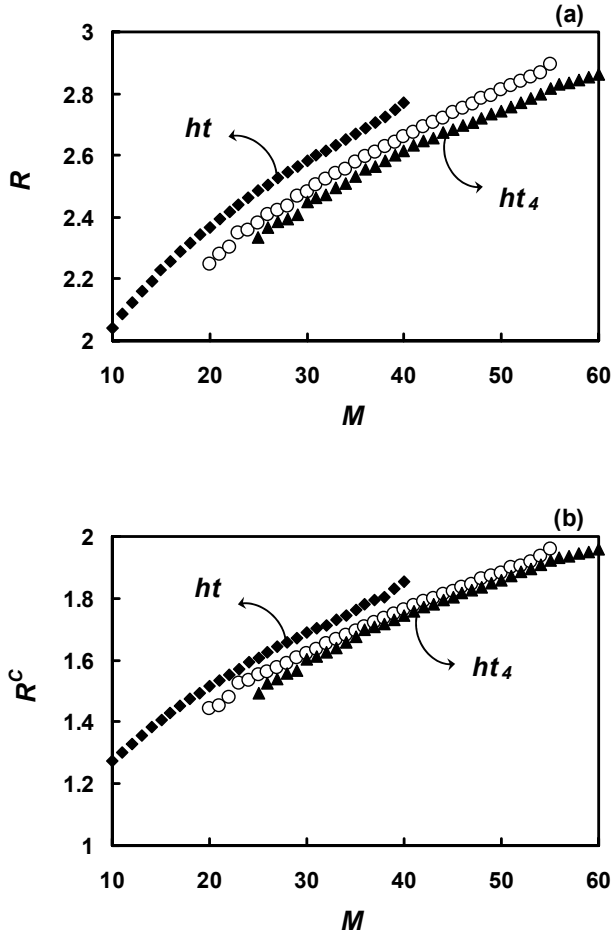

Figure 2.10. Mean radius of gyration as a function of aggregation number at 2.5% H_5T_4 for **(a)** the micelle and **(b)** the micellar core. Open symbols denote the pure H_5T_4 solution and closed symbols denote the 10% *ht* and 10% ht_4 containing solutions as indicated in the figure. For each solution, only the data range with sufficient sampling is shown.

A quantitative measure of the sharpness/roughness of the core/corona interface, i.e., the excluded volume effect, is given by the radial density profile of micelles having the same aggregation number. As "core/corona interface", we define the region of r around the inflection point of the density profiles of surfactant head groups, $n_H(r)$, shown in figure 2.11. The weaker decay of $n_H(r)$ for the *ht* containing solution

compared to the ht_4 containing solution or the pure H_5T_4 solution indicates a less well defined core/corona interface, i.e. a rougher interface. This roughness is produced by the transfer of surfactant molecules due to the excluded volume effect causing the observed increase of R [see figure 2.10 and Eq. (2.4)]. The density profiles of surfactant head groups for the ht_4 containing and the pure H_5T_4 solution are nearly identical, suggesting a negligible impact of ht_4 on the core/corona interface. This is consistent with our earlier observation that only a few ht_4 molecules "enter" the micelles [see figure 2.5(b)].

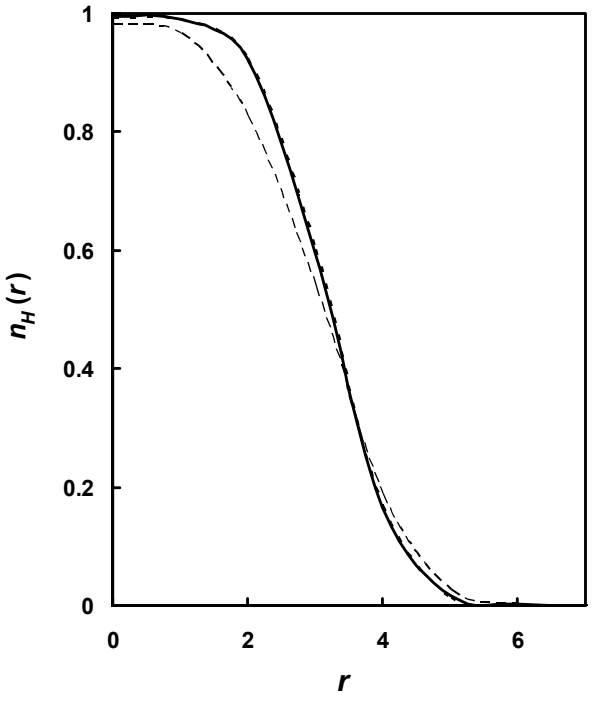

Figure 2.11. Radial density profiles of surfactant head groups (H) within micelles of aggregation number $M = 35 \pm 1$ formed in pure 2.5% H_5T_4 (solid line), with 10% ht added (dashed line) and with 10% ht_4 (dotted line). Note that the curves for the pure system (solid line) and for 10% ht_4 (dotted line) are coinciding.

The complete density profile within micelles formed in the 10% *ht* containing solution is shown in figure 2.12(a) and reveals that many *ht* molecules are located at the core/corona interface. The *ht* alcohol head groups concentrate at the core-side of the interface, while there is a depletion of alcohol head groups in the micellar corona [figure 2.12(b)]. On the other hand, *ht* tail groups are preferentially located at the corona-side of the interface. This indicates a preferential orientation of *ht* molecules perpendicular to the core/corona interface. The same behavior is observed for the longer alcohols. The concentration of *ht* head groups close to the interface is much higher than in the surrounding solution. This high value of *ht* density is consistent with the earlier observed high number of *ht* molecules bound in micelles [see figure 2.5(a)].

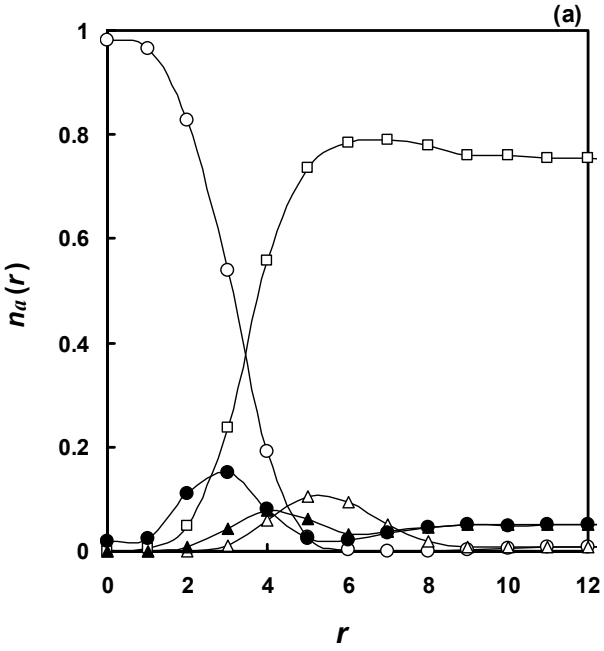

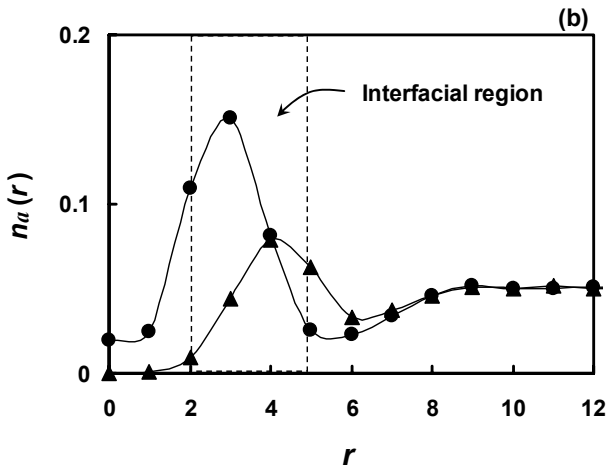

Figure 2.12. **(a)** Radial density profiles for *H* (○), *T* (△), *C* (□), *h* (●) and *t* (▲) within micelles of aggregation number $M = 35 \pm 1$ formed in a solution with 2.5% H_5T_4 and 10% *ht*. **(b)** same as (a) but only *h* (●) and *t* (▲) are shown.

The density profiles in figure 2.12 suggest that the roughening of the micelle is caused by binding of *ht* molecules to the interface of the micelles. Such a roughening does not exist in the case of ht_4. Thus, we expect the density of ht_4 molecules at the interface to be much lower than that of *ht* molecules. In figure 2.13(a), we compare the density profiles of alcohol head groups for systems containing different alcohols, ht_α. As α increases, one observes a *decrease* of the head group density at the interface. The value of the density maximum for *ht* is several times larger than that of ht_4. This is consistent with our earlier findings presented in figure 2.5 that the mean number of alcohol molecules bound in micelles is several times larger for *ht* than for ht_4. We note that (because of the orientation of the cosurfactant molecules perpendicular to the core/corona interface) the *total* density of cosurfactant head and tail groups at the micellar core/corona interface also decreases with increasing cosurfactant tail length [figure 2.13(b)].

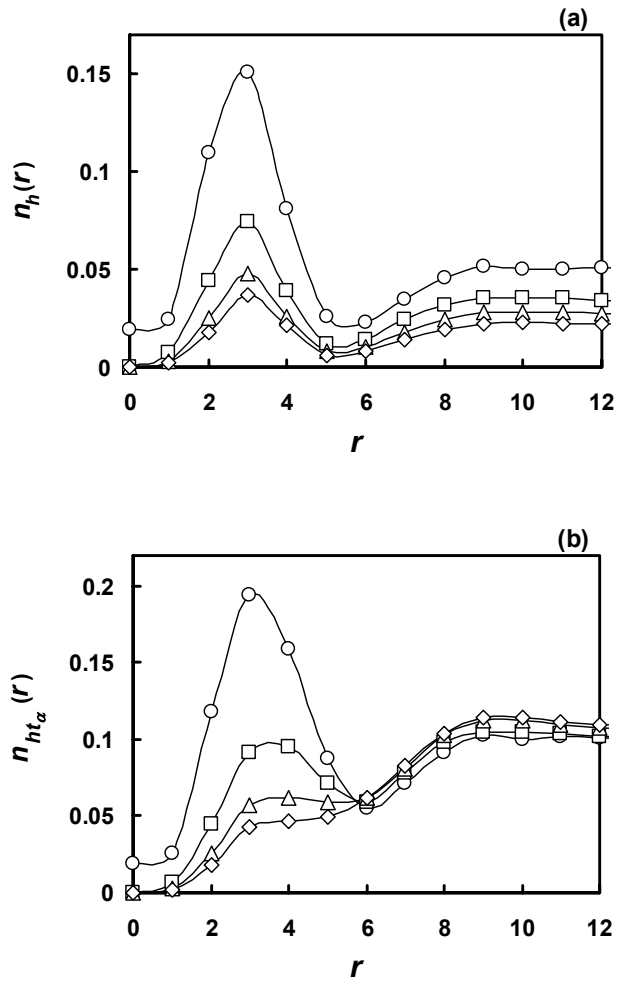

Figure 2.13. **(a)** Radial density profiles of alcohol head groups within micelles of size $M = 35 \pm 1$ formed in a solution with 2.5% H_5T_4 and 10% ht (○), ht_2 (□), ht_3 (△) or ht_4 (◇) respectively. **(b)** Same as in (a) but for the total of alcohol head and tail groups.

2.4 SUMMARY AND CONCLUSIONS

CO_2 is an attractive, environmentally friendly solvent but not a good solvent for polar substances. However, reverse micelles formed by surfactants in CO_2 can incorporate polar molecules. The solubilization capacity of these reverse micelles

depends on many factors such as the solubility of the surfactant, the CMC, and the structural properties of the aggregates. The primary goal of adding additives to a surfactant solution is to increase the solubility of a solute without increasing the concentration of the original surfactant. To choose an appropriate additive it is necessary to know how additives affect the aggregation behavior of the surfactant solution. As a first step, we have studied the impact of alcohol additives on the self-assembly of the surfactant H_5T_4 in supercritical CO_2. In particular, we have investigated the dependence of the aggregation behavior on the length, α, of linear alcohols ht_α and their concentration.

All alcohols investigated here *decrease* the CMC. The effect is stronger the longer the alcohol is. Also for each alcohol, the CMC decreases with increasing alcohol concentration. For *ht*, we observe that the effect levels off at a concentration of approximately 2.5%. Thus, further increase of the alcohol concentration has little effect on the CMC. If, however, a lower CMC is desired, an alcohol with a longer tail can be used. Clearly, a reduction of the CMC, i.e. micelle formation at lower concentrations, allows solubilization of a solute at lower surfactant concentrations. This is important if the surfactant concentration is limited, e.g. by its own solubility.

While all ht_α alcohols lower the CMC, their impact on the mean aggregation number and the number of aggregates depends strongly on the alcohol chain length α. At 2.5% H_5T_4, addition of 10% ht_4 causes the aggregation number to *increase* slightly, whereas the number of aggregates remains constant. In contrast, the number of

aggregates doubles and the aggregation number *halves* if *ht* is added. In the latter case, *ht* molecules replace a large number of surfactant molecules in the aggregates. Both effects, an increase in the number of aggregates as well as an increase in aggregation number and size of the micelles, should increase the total amount of solute that can be incorporated in the aggregates. However, there is a striking difference; in the system with more but smaller aggregates, the total surface area per unit volume of solute would be much higher than in the case of a few big micelles. Thus, by changing the length of the alcohol it might be possible to adjust the surface to volume ratio of microemulsion droplets.

The main difference in the behavior of *ht* and ht_4 molecules in the solution is that *ht* molecules concentrate at the interface of the micelles while ht_4 molecules do not. We believe that the higher loss in configurational entropy of ht_4 compared to *ht* molecules prevents ht_4 molecules from binding to the micellar core/corona interface. Consequently, *ht* molecules alter the properties of micelles directly, whereas the effect of ht_4 on the properties of the aggregates is minor. However, the effect of ht_4 on the CMC is large. This CMC reduction arises from the decrease in solvent quality due to the presence of ht_4 molecules. Consequently, *ht* is a clear *cosurfactant* while ht_4 would be considered a *cosolvent*. The transition from one to the other is, however, *gradual*, as our results for alcohols with intermediate chain length show.

2.5 REFERENCES

1. J. M. DeSimone, *Science* **297**, 799 (2002).

2. M. M. Jimenez-Carmona and M. D. L. de Castro, *Anal. Chim. Acta* **358**, 1 (1998).

3. E. L. V. Goetheer, M. A. G. Vorstman, and J. T. F. Keurentjes, *Chem. Eng. Sci.* **54**, 1589 (1999).

4. J. B. Mcclain, D. E. Betts, D. A. Canelas, E. T. Samulski, J. M. DeSimone, J. D. Londono, H. D. Cochran, G. D. Wignall, D. ChilluraMartino, and R. Triolo, *Science* **274**, 2049 (1996).

5. K. A. Consani and R. D. Smith, *J. Supercrit. Fluids* **3**, 51 (1990).

6. G. J. McFann, Ph.D. Thesis, The University of Texas at Austin (1993).

7. G. J. McFann, K. P. Johnston, and S. M. Howdle, *AIChE J.* **40**, 543 (1994).

8. K. Sawada, T. Takagi, and M. Ueda, *Dyes Pigments* **60**, 129 (2004).

9. J. C. Liu, B. X. Han, G. Z. Li, Z. M. Liu, J. He, and G. Y. Yang, *Fluid Phase Equilib.* **187**, 247 (2001).

10. J. C. Liu, B. X. Han, J. L. Zhang, T. C. Mu, G. Z. Li, W. Z. Wu, and G. Y. Yang, *Fluid Phase Equilib.* **211**, 265 (2003).

11. P. Winsor, *Solvent Properties of Amphiphilic Compounds* (Butterworths, London, 1954).

12. J. L. Salager, "Microemulsions", in *Handbook of Detergents*, edited by G. Broze (Marcel Dekker, New York, 1998).

13. M. J. Rosen, *Surfactants and Interfacial Phenomena* (Wiley, New York, 1978).

14. A. Graciaa, J. Lachaise, C. Cucuphat, M. Bourrel, and J. L. Salager, *Langmuir* **9**, 669 (1993).

15. A. Graciaa, J. Lachaise, C. Cucuphat, M. Bourrel, and J. L. Salager, *Langmuir* **9**, 3371 (1993).

16. M. Miñana-Perez, A. Graciaa, J. Lachaise, and J. L. Salager, *Colloids Surf. A* **100**, 217 (1995).

17. J. L. Salager, A. Graciaa, and J. Lachaise, *J. Surfactants Detergents* **1**, 403 (1998).

18. K. Shinoda, "The Formation of Micelles", in *Colloidal Surfactants*, edited by K. Shinoda, T. Nakagawa, B. Tamamushi, and T. Isemura (Academic Press, New York, 1963).

19. A. Castedo, J. L. Del Castillo, M. J. Suarez-Filloy, and J. R. Rodriguez, *J. Colloid Interface Sci.* **196**, 148 (1997).

20. D. J. Jobe, R. E. Verrall, B. Skalski, and E. Aicart, *J. Phys. Chem.* **96**, 6811 (1992).

21. D. J. Mitchell and B. W. Ninham, *J. Chem. Soc. Faraday Trans. II* **77**, 601 (1981).

22. M. J. Hou and D. O. *Shah, Langmuir* **3**, 1086 (1987).

23. V. K. Bansal, D. O. Shah, and J. P. Oconnell, *J. Colloid Interface Sci.* **75**, 462 (1980).

24. P. G. Degennes and C. Taupin, *J. Phys. Chem.* **86**, 2294 (1982).

25. N. Asgharian, P. Otken, C. Sunwoo, and W. H. Wade, *Langmuir* **7**, 2904 (1991).

26. M. Kahlweit, R. Strey, and G. Busse, *J. Phys. Chem.* **95**, 5344 (1991).

27. G. Palazzo, F. Lopez, M. Giustini, G. Colafemmina, and A. Ceglie, *J. Phys. Chem. B* **107**, 1924 (2003).

28. S. Salaniwal, S. T. Cui, H. D. Cochran, and P. T. Cummings, *Langmuir* **17**, 1773 (2001).

29. S. Salaniwal, S. T. Cui, H. D. Cochran, and P. T. Cummings, *Langmuir* **17**, 1784 (2001).

30. S. Senapati, J. S. Keiper, J. M. DeSimone, G. D. Wignall, Y. B. Melnichenko, H. Frielinghaus, and M. L. Berkowitz, *Langmuir* **18**, 7371 (2002).

31. S. R. P. da Rocha, K. P. Johnston, and P. J. Rossky, *J. Phys. Chem. B* **106**, 13250 (2002).

32. M. Lisal, C. K. Hall, K. E. Gubbins, and A. Z. Panagiotopoulos, *J. Chem. Phys.* **116**, 1171 (2002).

33. L. F. Scanu, K. E. Gubbins, and C. K. Hall, *Langmuir* **20**, 514 (2004).

34. L. Rekvig, B. Hafskjold, and B. Smit, *J. Chem. Phys*. **120**, 4897 (2004).

35. M. Zaldivar and R. G. Larson, *Langmuir* **19**, 10434 (2003).

36. R. G. Larson, L. E. Scriven, and H. T. Davis, *J. Chem. Phys*. **83**, 2411 (1985).

37. R. G. Larson*, J. Chem. Phys*. **89**, 1642 (1988).

38. R. G. Larson, *J. Phys. II* **6**, 1441 (1996).

39. M. Lisal, C. K. Hall, K. E. Gubbins, and A. Z. Panagiotopoulos, *Mol. Simul.* **29**, 139 (2003).

40. D. Frenkel and B. Smit, *Understanding Molecular Simulation: From Algorithms to Applications* (Academic Press, London, 1996).

41. J. Hoshen and R. Kopelman, *Phys. Rev. B* **14**, 3438 (1976).

42. J. N. Israelachvili, D. J. Mitchell, and B. W. Ninham*, J. Chem. Soc. Faraday Trans. II* **72**, 1525 (1976).

43. C. Tanford, *The hydrophobic effect: Formation of micelles and biological membranes* (Wiley, New York, 1980), pp. 90-95.

44. E. Ruckenstein and R. Nagarajan, *J. Phys. Chem*. **79**, 2622 (1975).

45. S. K. Talsania, Y. M. Wang, R. Rajagopalan, and K. K. Mohanty, *J. Colloid Interface Sci.* **190**, 92 (1997).

46. S. K. Talsania, L. A. Rodriguez-Guadarrama, K. K. Mohanty, and R. Rajagopalan, *Langmuir* **14**, 2684 (1998).

47. M. A. Floriano, E. Caponetti, and A. Z. Panagiotopoulos, *Langmuir* **15**, 3143 (1999).

48. A. Z. Panagiotopoulos, M. A. Floriano, and S. K. Kumar, *Langmuir* **18**, 2940 (2002).

49. J. Rudnick and G. Gaspari, *Science* **237**, 384 (1987).

50. A. D. Mackie, A. Z. Panagiotopoulos, and S. K. Kumar, *J. Chem. Phys*. **102**, 1014 (1995).

51. Note that in Ref. 50 the temperature scale is given in units of $\left|w_{Cv}^{*}\right| = \frac{1}{2}\left|\varepsilon_{CC}^{*}\right|$.

Chapter 3

From atomistic to meso-scale: Coarse-graining techniques

3.1 INTRODUCTION

So far we have used a meso-scale model to study alcohol effects on surfactant self-assembly (chapter 2). In this chapter we discuss how we can construct a meso-scale model that preserves the important aspects arising from the atomistic model, through the process of coarse-graining. We then review the various coarse-graining techniques available in the literature. In our meso-scale model thus far, the alcohol and the surfactant were represented as a chain of beads, where each bead represents a set of atoms. The interactions between these beads were represented with simple, yet physically meaningful parameters (such that a part of the surfactant is solvo-phobic and other part is solvo-philic). Such a meso-scale model with simple interaction parameters is useful to study qualitative trends and understand the general physics of the system. In many applications however, we would also like this meso-scale model to quantitatively predict the properties of a real system. This requires that our meso-scale model preserve the important aspects arising from a more fundamental level of description (such as the hydrogen bonding at the atomistic level). In this situation, one could ask: why not use the atomistic model itself to study surfactant self-assembly? In principle, we could study these phenomena using an atomistic model, where each atom is modeled explicitly. Although these atomistic models are quite reliable, we are limited by the enormous

computational burden involved in simulating complex systems such as surfactant self-assembly. This is because of the wide range of length and time scales involved in studying such systems. For example, the length scale in surfactant solutions ranges from the order of 0.1 nm for atoms to hundreds of nanometers for the self-assembled structures such as micelles. Similarly, the time scale ranges from the order of 1fs for atomic motion to that of ms for micellar dynamics [1]. Therefore, using a fully atomistic model to simulate such large length and time scales involves enormous computational costs (as discussed earlier in chapter 1). In the meso-scale models however, these atoms are combined into beads leading to a decrease in the number of degrees of freedom. Thus the meso-scale models allow us to span the large length and time scales, with much less computational cost. The challenge then is to construct a meso-scale model that preserves the important aspects of the atomistic model, while spanning these length and time scales. The process of constructing this meso-scale model from the corresponding atomistic model is called coarse-graining. In coarse-graining, we first start from a fully atomistic model of the system and then decide on the degrees of freedom to be preserved and coarse-grain out all the other degrees of freedom. This results in a coarse-grained meso-scale model where the interactions are now 'effective', because they include the effects arising from the degrees of freedom that have been coarse grained out.

In this work we restrict our attention to equilibrium properties. Ideally, one would like to coarse-grain such that the resulting meso-scale model reproduces *all* the equilibrium properties of the atomistic model (i.e. the structural properties such as the correlation functions, thermodynamic properties such as the pressure, internal energy,

etc., dielectric properties, and so on). This can be achieved by using a coarse-graining procedure that preserves the partition function of the system while going from the atomistic to the meso-scale model, because the partition function uniquely determines all the equilibrium properties of the system. This procedure to reproduce the partition function is called *rigorous* coarse-graining. Alternatively, we can adopt a less rigorous approach, and coarse-grain such that the meso-scale model reproduces a certain property of interest from the atomistic model; in general, in such approaches, properties other than the chosen one may not be accurately reproduced.

The main focus of this chapter is to review the various coarse-graining techniques available in the literature. We first review the rigorous coarse-graining technique (section 3.2) and then move on to the alternate coarse-graining techniques (section 3.3 to 3.7). In the following chapters (4 and 5), we explore these coarse-graining techniques in more depth.

3.2 RIGOROUS COARSE-GRAINING

3.2.1 Background

Rigorous coarse-graining requires that the partition function of the degrees of freedom in the coarse-grained system is identical to the partition function of the same degrees of freedom in the original atomistic system. This condition yields an equation for the effective potential in the coarse-grained system. This effective potential preserves

the overall thermodynamics and it guarantees that the correlation functions of any order between the preserved degrees of freedom are the same, whether calculated within the original atomistic system or the effective system. Following the earlier works of McMillan and Mayer [2] and others [3,4], Dijkstra *et al.* [5,6,7] obtained the expression for the effective potential through rigorously coarse-graining uncharged systems of spherical particles in the semi-grand ensemble. In a semi-grand ensemble the number of particles of one of the components and the chemical potential of the other component are fixed along with the volume and temperature. In particular Dijkstra *et al.* [7] determined the effective interactions between 'solute' A molecules by integrating over the degrees of freedom of 'solvent' B molecules in a binary A/B mixture. They showed that by treating the system in the semi-grand canonical ensemble (N_A, μ_B, V, T) where the number of A molecules (N_A) and the chemical potential of B (μ_B) are fixed, the effective potential naturally splits into a sum of a volume term, and one-body, two-body ... and N_A-body interactions. The effective Hamiltonian thus obtained for the coarse-grained system is given by:

$$H^{eff} = H_{AA} + \Omega(\mu_B), \tag{3.1}$$

where $H_{AA} = \sum_{IJ} \phi_{AA}(R_{IJ})$ is the original bare interaction between A particles and Ω is the B-mediated effective interaction. Dijkstra *et al.* [7] showed that Ω is given by

$$\Omega = \sum_{n=0}^{N_A} \Omega_n = -\beta^{-1} \ln \Xi_0 + N_A \omega_1 + \sum_{IJ} \omega_2(R_{IJ}) + \sum_{IJK} \omega_3(\boldsymbol{R}_I, \boldsymbol{R}_J, \boldsymbol{R}_K) + \cdots. \tag{3.2}$$

The first term on the far right side of (3.2), the volume term, can be identified as the grand canonical potential of a pure fluid of species B (where Ξ_0 is its grand canonical

partition function). The rest are the one-body (ω_1), two-body (ω_2), three-body (ω_3)... etc. terms. A very important property of the expressions for the ω_i in (3.2) is that they do not depend on the total number of particles of species A, N_A. Thus the individual potentials ω_i are (*species A) density transferable* (but still depend on T and μ_B). On the other hand, Ω in (3.2) contains terms for all numbers of particles of species A up to N_A. Thus the density transferability is an advantage only if the series of effective interactions (3.2) converges after the first few terms. In chapter 4 we give explicit expressions for ω_1, ω_2,.. and describe how we devised a technique to compute these rigorous one, two... N_A-body potentials using Widom's particle insertion method. We also present calculations for the first few terms in Eq. (3.2) for a binary mixture of Argon and Krypton, where the degrees of freedom of Argon are integrated out [8].

3.2.2 Choice of ensemble

As discussed in the previous section, rigorous coarse-graining in the semi-grand canonical ensemble leads to an effective potential which naturally splits into a sum of independent volume term, one-body, two-body ... and N_A-body interactions. As we go higher in this expansion, these terms are usually decreasing in magnitude. Therefore, the series can be truncated at some point, and the limited calculations to date suggest that truncation can be either at the two-body or the three-body level, without a significant error in the reproduction of the properties. The terms beyond three-body are computationally very demanding. Therefore the split into these independent terms is

very useful. This split however may not be possible with rigorous coarse-graining in other ensembles. For example, Louis [9] uses the Asakura Oosawa (AO) model system to demonstrate the outcome of coarse-graining in different ensembles. This AO model consists of N_c big particles treated as simple hard spheres, and N_p small spheres whose interaction with the big particles is hard sphere like, but whose interaction with other small particles is ideal gas like [10]. By tracing-out the degrees of freedom of small particles in this AO model in two different ensembles, Louis [9] obtained the following expressions for the effective Hamiltonian,

Semi-grand ensemble:

$$H^{eff}(N_C, z_p, V; \{r_i\}) = H_{CC} - z_p V + z_p N_C V_1 - z_p \sum_{i<j} V_2(r) \tag{3.3a}$$

Canonical ensemble:

$$H^{eff}(N_C, N_p, V; \{r_i\}) = H_{CC} + N_p \, log\left[\frac{N_p}{V - N_C V_1}\right] - N_p - N_p \, log\left[1 + \frac{1}{V - N_C V_1} \sum_{i<j} z_p V_2(r)\right] \tag{3.3b}$$

Here H_{cc} is the bare Hamiltonian of just the big particles, V is the total volume, V_1 is the volume excluded by each big particle, and V_2(r) has the standard AO form [10]. We observe that in the semi-grand ensemble (3.3a) the effective Hamiltonian already splits into sum of a volume term and an effective pair potential. In the canonical ensemble (3.3b) however, the effective Hamiltonian contains a logarithmic term which can no longer be written as a sum over independent interactions. In general, coarse-graining in

the canonical ensemble leads to an N-body interaction term, which cannot be further simplified. Calculating this N-body term and implementing it into meso-scale simulations is extremely challenging. Therefore, the rigorous coarse-graining procedure needs to be carried out in the semi-grand canonical ensemble, where the degrees of freedom to be conserved are treated canonically, and the degrees of freedom to be coarse-grained out are treated grand-canonically. With this we obtain an effective Hamiltonian which is a sum of independent N_i-body terms. If this series converges quickly, it can be truncated and used to reproduce the properties of the original atomistic system.

3.2.3 Rigorous coarse-graining of complex systems

The split into the independent N_i-body terms through rigorous coarse-graining has been derived for a simple binary mixture with short range interactions and without any intra-molecular degrees of freedom [7]. For systems with long-ranged Coulomb interactions however, the Mayer expansion used in deriving these independent many-body terms diverges [7]. Moreover, the semi-grand ensemble poses problems for coarse-graining these charged systems. This is because of the addition and deletion moves required to maintain the chemical potential of these charged particles, which in turn affect the overall charge neutrality required for this system. In such a situation, the canonical ensemble becomes a natural choice. However, as discussed in the previous section (3.2.1), coarse-graining in the canonical ensemble leads to an effective Hamiltonian which can no longer be written as a sum over *independent* many-body interactions.

Although there have been attempts at coarse-graining charged systems by using approximate expressions in the canonical ensemble [11,12,13], the problem of rigorous coarse-graining these systems is yet to be resolved.

There are also challenges in rigorous coarse-graining systems with intra-molecular degrees of freedom, such as surfactants, where we wish to integrate out some of the intra-molecular degrees of freedom. As we have discussed earlier, rigorous coarse-graining requires using a semi-grand ensemble, which means the intra-molecular degrees of freedom have to be treated in the grand-canonical ensemble. In order to maintain the chemical potential in this ensemble, we need to use the addition and deletion moves for the atoms within a molecule, which changes the molecular structure itself.

In view of these difficulties involved in rigorously coarse-graining systems with charges or with intra-molecular degrees of freedom, alternate methods have been developed in the literature to determine the effective potentials. We discuss these alternate methods in the following sections starting with the 'Potential of Mean Force' which is actually *rigorously correct* in the limit of infinite dilution of A.

3.3 POTENTIAL OF MEAN FORCE

The effective potential, u^{eff}, is sometimes approximated by the potential of mean force (PMF), defined as $u^{eff} = -\beta^{-1} \ln g(R)$, where $g(R)$ is the pair correlation function

from the atomistic model. We can show that this is *rigorously correct* in the limit of infinite dilution, i.e. the potential of mean force is equal to the effective potential obtained through equating the partition functions. To illustrate this point, consider the same binary A/B mixture discussed in section 3.2.1, where the component B is coarse grained out. Now consider a case of just *two* A particles in the solution of B particles. This corresponds to the most dilute system of A with at least pair level interactions between A particles. Since no B particles are present in the *effective* system, the effective pair interaction and the potential of mean force are identical in this two-A-particle system (Ref.[14] Chap. 2.5). Thus, we can write:

$$\omega_2(R_{12}) + \phi_{AA}(R_{12}) = -\beta^{-1} \ln g^{eff}(R_{12}) \tag{3.4}$$

where $\omega_2(R_{12}) + \phi_{AA}(R_{12})$ is the rigorous effective pair potential {from Eq.'s (3.1),(3.2)} and $g^{eff}(R_{12})$ is the pair correlation in the effective two A-particle system. Moreover, since we coarse-grain rigorously, the $g^{eff}(R_{12})$ in the effective system is the same as that of the pair correlation function $g^{at}_{AA}(R_{12})$ in the original atomistic binary A/B mixture (discussed more in detail in next chapter, section 4.2.1). Therefore we can write:

$$\omega_2(R_{12}) + \phi_{AA}(R_{12}) = -\beta^{-1} \ln g^{at}_{AA}(R_{12}) \tag{3.5}$$

Thus the rigorous two body part of the effective potential, $\omega_2 + \phi_{AA}$, can be calculated via the potential of mean force. In order to calculate this however, we need to simulate a system with just two A particles in a sea of B particles. The simulation of such a system with just two A-particles to find $g^{at}_{AA}(R_{12})$ needs enormous computational power to get

any good statistics. Therefore, in practice the $g^{at}_{AA}(R_{12})$ is calculated with not just two A particles, but with a sufficiently dilute system of A.

The potential of mean force has been widely used in the literature as an approximation for the effective potential. For example, in the study of surfactant n-decyltrimethylammonium chloride ($CH_3(CH_2)_9–N(CH_3)_3^+Cl^–$) in water, the effective potential was approximated as the potential of mean force between different groups [$(CH_3)_4N^+$], CH_4 and $Cl^–$ ion in water [15]. The resulting effective potential was implemented in Langevin dynamics simulations, where no water molecules were explicitly treated. Simulating this system for a period of 12ns, the early stages of surfactant self-assembly were observed. In the study of polymeric systems [16], the potential of mean force was shown to be inadequate in reproducing the correct structure at high densities because of the significant contribution from the three-body and higher terms. The contribution from these three and higher-body terms can be included *within* the effective pair potential using integral equations, which are discussed below.

3.4 INTEGRAL EQUATION TECHNIQUES

Integral equations along with a suitable closure relation can be used to extract effective potentials from a known pair correlation function, $g(R)$. For example, if we are interested in coarse-graining out the degrees of freedom of B from a binary A/B mixture, then the pair correlation function between A molecules in the mixture can be used to find

the effective pair potential through integral equations. Note that the effective pair potential thus obtained already includes the contributions from three and higher body interactions.

The integral equation approach to find the effective potentials is as follows: First we start with the Ornstein-Zernike integral equation [17], which relates the total pair correlation function with the direct correlation function,

$$h(R_{12}) = c(R_{12}) + \rho_1 \int h(R_{23})\, c(R_{13})\, dR_3 \tag{3.6}$$

where $h(R_{12}) = g(R_{12}) - 1$ is the total correlation function from the fully atomistic system, $c(R_{12})$ is the direct correlation function and the spatial integration is to be carried out with respect to a third reference bead. This direct correlation function can be related to the effective potential through one of the closure relations. Closures are approximate relations which arise from exact diagrammatic expansions of g(R) in terms of c(R) but with certain classes of diagrams ignored. The common closures used are the Hypernetted chain (HNC) and the Percus-Yevick (PY) given by [14],

HNC: $\beta u(R) = h(R) - c(R) - \ln g(R)$ (3.7)

PY: $\beta u(R) = \ln\left\{1 - \left[c(R)/g(R)\right]\right\}$ (3.8)

The PY closure is known to yield very accurate results for short-range hard interactions, whereas the HNC is more accurate for long-range soft potentials [18]. Thus using equations (3.7) or (3.8) along with (3.6), we can extract an effective pair potential from the pair correlation function obtained through fully atomistic simulation.

This integral equation procedure has been used widely in the literature to extract effective potentials for complex systems such as polymers. The $g(R)$ between the center of mass of polymers derived from a self-avoiding walk (SAW) lattice model was inverted using HNC closure to obtain the effective potential [19,20,21]. These effective potentials were found to be finite at all distances even at full overlap indicating their 'soft' character. These potentials also showed a clear (though small) density dependence. In chapter 5 (section 5.3.2), we employ these integral equations to find the effective potential between ethanol molecules by coarse-graining out the water and the internal degrees of freedom of ethanol [22]. There we observe that the integral equations perform well until intermediate concentrations (50wt% ethanol in water) in reproducing the atomistic pair correlation function, but give deviations at higher concentrations.

We now move on to a coarse-graining approach where one finds these effective potentials by directly matching the correlation functions between the atomistic and the meso-scale model.

3.5 MATCHING CORRELATION FUNCTIONS

In this coarse-graining approach the mapping rule is that the effective system has to reproduce a certain set of correlation functions of the original system, e.g. a pair

correlation function. Reproducing a pair correlation function leads to the matching the pair level structure between the atomistic and the meso-scale models. Strictly speaking, it would be desirable to find all the effective potentials from N-body and lower terms which reproduce all of the correlation functions from N^{th} order and lower from the original atomistic model. Here 'N' refers to the total number of particles (or 'beads') in the effective system. In practice however, the determination of correlations beyond 3^{rd} order is a huge task and so is the process of inverting them to find the effective potentials. Therefore, usually correlations up to the pair level from the atomistic model are inverted to find an effective pair potential. The uniqueness of such an effective pair potential is guaranteed by the *uniqueness theorem* which says that if the effective system contains only pair interactions, there is a *unique* pair potential that corresponds to a given pair correlation function [23,24]. It is, however, rare to find an effective system with just 2-body interactions and no higher terms, since coarse-graining usually leads to a system with many-body interactions, even though the original atomistic system contains only pair interactions (as discussed in section 3.2.1). Therefore, the effective pair potential found by inverting the pair correlation functions already includes contributions from the three and higher body interactions. Because of this added contributions, the effective pair potential becomes density *dependent* (unlike the rigorous 2-body potential derived in the semi-grand ensemble which is density *independent*). This is called the "transferability problem" since the effective pair potential found at a certain density cannot be used at another density [9]. Also this effective potential designed to reproduce the structure may not reproduce other properties of the system (such as the internal energy). This is called the "representability problem" [9].

Therefore, the effective potentials derived to reproduce a certain property (pair level structure in this case) may not accurately reproduce other properties, nor reproduce the same property at a different state point. In spite of these limitations, these potentials can still be used to reproduce the property of interest, and might be transferable within a certain range of state variables, especially at low concentrations when the contribution from the 3-body and higher interactions are negligible. Moreover, since it is very challenging to perform rigorous coarse-graining for complex systems with Coulomb charges or with intra-molecular degrees of freedom, we have to resort to alternate procedures which reproduce the property of our interest.

Now the question is how to find an effective potential that reproduces a given atomistic pair correlation function, $g(R)$. Although the uniqueness theorem says that there is a unique pair potential, there is no standard procedure to find this potential. At low densities, it is known that the $g(R)$ is well reproduced by the potential of mean force (PMF) (as discussed in section 3.3). At higher densities however, the PMF fails to reproduce $g(R)$ and various techniques have been developed to find an effective potential that reproduces a given $g(R)$. One such technique is through the "simplex algorithm" which has been used to find the effective potentials in polymeric systems [25,26,27]. The simplex algorithm is a multi-dimensional optimization procedure and was used to optimize the parameters of a pre-selected effective potential. The convergence criterion was that the effective potential reproduces the pair correlation functions from the atomistic model. The resulting effective potentials using this algorithm were found to be

successful in reproducing the atomistic pair correlation functions. This procedure however has drawbacks such as the slow convergence of the analytical potentials and the manual process of having to pre-select a good functional form for the potential. Soper [28] introduced another technique called 'iterative Boltzmann inversion' used to find an effective potential by inverting a given pair correlation function. Here the effective potential is iteratively improved based on the difference between the correlation functions from the atomistic and the meso-scale models. This procedure has been successfully used for coarse-graining polymeric systems [29,30]. We have used this iterative Boltzmann procedure to find the effective potential between the center of mass of ethanol molecules in water [22] (discussed in section 5.3.3).

3.6 EMPIRICAL COARSE-GRAINING

In empirical coarse-graining, the parameters for a pre-selected form of the effective potential (such as Lennard-Jones) are fitted to data such as densities, solubilities, phase transition data, etc. which are extracted from experiments or simulations using higher level models [31,32,33]. For example, in coarse-graining phospholipids, Shelley *et al*. [31] represented each $(-CH_2-)_3$ unit as a single bead and the interaction between these beads was assumed to be Lennard-Jones 9-6 potential. The parameters for this potential were chosen such that the bulk density and vapor pressure obtained from simulations of both dodecane and nonane agree reasonably well with experimental values. In this system, the solvent water was also coarse-grained in a

similar manner where three water molecules are represented as a single bead and the interaction between these beads assumed to be a Lennard-Jones 6-4 potential. The parameters for this potential were chosen such that they reproduce the experimental bulk density and vapor pressure of water. The effective potentials between the remaining beads in the phospholipids were found by matching the pair correlation functions between the atomistic and the meso-scale models. Although these empirical methods are successful in reproducing the properties they are parameterized to (such as the density, solubility etc), they may not reproduce any other property. Another shortcoming of this empirical approach is the lack of a basis in statistical mechanics.

3.7 OTHER COARSE-GRAINING METHODS

Apart from the above coarse-graining techniques (sections 3.2 to 3.6), a variety of other techniques have also been employed to derive the effective potentials. Here we briefly discuss some of these coarse-graining techniques. Izvekov and Voth [34] developed a force-matching procedure to directly obtain the forces acting on coarse-grained sites through the force data from an explicit atomistic MD simulation. The resulting coarse-grained model was able to successfully match the structural properties, i.e the pair correlation functions of a fully atomistic model of a lipid bilayer. Akkermans and Briels [35] derived an effective potential that minimizes the variational free energy of a coarse-grained polymer melt, starting from the Gibbs-Bogoliubov inequality. The resultant effective potential however, gives a pair correlation function which is less

structured than the original atomistic system. McCoy and Curro [36] obtained effective potentials between CH_4, CH_3, CH_2 and CH sites by taking direct angular averages in a Monte Carlo simulation. They observed that the resulting effective potentials are temperature dependent. Adhikari *et al.* [37] derived the effective potentials between different moieties of a surfactant directly from *ab initio* calculations and used them in a meso-scale model to perform lattice Monte Carlo simulations. Using this meso-scale model to simulate a surfactant templated assembly of cobalt dots, they could quantitatively reproduce the experimental cobalt nano-particle size. Klapp *et al.* [38] derived effective pair potentials for simple 'toy' models (between an atom and a diatomic, and between disk shaped supramolecular units) by truncating the three-body and higher terms in the Mayer cluster expansion of the effective potential. The resulting effective potentials were observed to be much softer in relation to the corresponding atomic potentials.

Thus, there are a wide variety of coarse-graining techniques in the literature which were successful in reproducing one or more of the structural or thermodynamic properties of the original atomistic model in the meso-scale model.

3.8 SUMMARY AND CONCLUSIONS

Fully atomistic simulations of systems which self-assemble are very challenging because of the different length scales and the associated different time-scales involved.

Through coarse-graining, a meso-scale model can be constructed which preserves the important aspects arising from that atomistic model, while spanning these length and time scales. In this chapter, we reviewed various such coarse-graining techniques developed in the literature to build a meso-scale model from the original atomistic model.

In the rigorous coarse-graining technique, the partition function of the meso-scale model is matched with that of the atomistic model. It was shown that rigorous coarse-graining for a binary A/B mixture, where the degrees of freedom of B are integrated out, leads to an effective potential that naturally splits into a sum of a volume term, one-body, two-body ... and N_A-body interactions in the semi-grand ensemble [7]. These individual terms are also species A density *transferable* (but still depend on T and μ_B). The advantage of the rigorous coarse-graining technique is that it reproduces all the structural, thermodynamic and other equilibrium properties of the atomistic model in the meso-scale model.

While the rigorous coarse-graining procedure for simple uncharged systems has been worked out, there are still challenges in rigorous coarse-graining more complex systems with charges and intra-molecular degrees of freedom. These complex systems have been coarse-grained using alternate techniques which match a specific property of interest between the atomistic and the meso-scale models. However, apart from the property of interest, these alternate techniques may not reproduce any other property, or the same property at a different state point (such as at a different density, temperature,

etc.). Therefore, extreme care should be used in using these alternate techniques in predicting properties other than those that they are designed to reproduce.

One such alternate technique is the use of the Potential of Mean Force (PMF). The PMF is actually *rigorously correct* in the limit of infinite dilution. In practice however, a sufficiently dilute system is used to determine the effective potential through the PMF. Care must be taken if this potential is used at higher concentrations, since it can give significant errors due to the contribution from the three-body and higher interaction terms which are not accounted in PMF. These three and higher-body terms can be accounted to some extent by using integral equations along with one of the closures, such as the hypernetted chain (HNC) or the Percus-Yevick (PY) approximation.

Another common coarse-graining technique is through matching pair correlation functions between the atomistic and the meso-scale models. The effective pair potential thus obtained already includes the contributions from the 3-body and higher interactions. This makes the effective potential density dependent, unlike the rigorous effective potentials which are density independent. In empirical coarse-graining the parameters of a pre-selected potential are fitted to data extracted from experiments or simulations using higher level models. The major shortcoming of this method is the lack of a basis in statistical mechanics. Other coarse-graining techniques such as a force matching procedure or minimizing the variational free energy were developed which were successful in reproducing some of the properties of the atomistic system in the meso-scale model.

The specific coarse-graining technique to use depends on the particular system and property of interest. Certainly, it is desirable to use the rigorous coarse-graining method since it preserves both the structure and thermodynamics of the original system. However, the rigorous approach is quite challenging except for some simple systems. The problems in rigorously coarse-graining complex systems (such as charged particles or molecules with intra-molecular degrees of freedom to be integrated out) are yet to be resolved. Therefore, in coarse-graining complex systems such as polymers or surfactants, alternative approaches are widely used.

In conclusion, there are a variety of techniques available to coarse-grain the system from an atomistic to a meso-scale model. Whenever possible, a rigorous coarse-graining approach needs to be adopted since it reproduces all the equilibrium properties of the original atomistic system. If the system is too complex, so that the rigorous approach is not viable, an alternate approach can be adopted which reproduces the property of interest.

3.9 REFERENCES

1. J. C. Shelley and M. Y. Shelley, *Curr. Opin. Colloid Interface Sci.*, **5**, 101 (2000).

2. W. G. McMillan and J. E. Mayer, *J. Chem. Phys.*, **13**, 276 (1945).

3. J. S. Rowlinson, *Mol. Phys.*, **52**, 567 (1984)

4. H. N.W. Lekkerkerker, W. C. K. Poon, P. N. Pusey, A. Stroobants and P. B. Warren, *Europhys. Lett.*, **20**, 559 (1992)

5. M. Dijkstra, R. van Roij, R. Evans, *Phys. Rev. Lett*. **81**, 2268 (1998).

6. M. Dijkstra, R. van Roij, R. Evans, *Phys. Rev. Lett*. **82**, 117 (1999).

7. M. Dijkstra, R. van Roij, R. Evans, *Phys. Rev. E* **59**, 5744 (1999).

8. N. Chennamsetty, H. Bock, and K. E. Gubbins, *Mol. Phys.* **103**, 3185 (2005)

9. A. A. Louis, *J. Phys.: Condens. Matter,* **14**, 9187 (2002)

10. S. Asakura and F. Oosawa, *J. Polym. Sci. Polym. Symp*, **33**, 183 (1958)

11. R. van Roij and J. P. Hansen, *Phys. Rev. Lett.* **79**, 3082 (1997)

12. R. van Roij, M. Dijkstra and J. P. Hansen, *Phys. Rev. E*, **59**, 2010 (1999)

13. L. Belloni, *J. Phys.: Condens. Matter*, **12**, R549 (2000)

14. J. P. Hansen, I. R. McDonald, *Theory of simple liquids*, (2nd Ed.), Academic, London (1986).

15. H. Shinto, S. Morisada, M. Miyahara, and K Higashitani, *Langmuir*, **20**, 2017 (2004)

16. P. G. Bolhuis, A. A. Louis, and J. P. Hansen, *Phys. Rev. E*, **64**, 21801 (2001)

17. L. S. Ornstein and F. Zernike, *Proc. Acad. Sci. Amst.*, **17**, 793 (1914)

18. F. J. Rogers and D. A. Young, *Phys. Rev. A* **30**, 999 (1984)

19. A. A. Louis, P. G. Bolhuis, J. P. Hansen, and E. J. Meijer, *Phys. Rev. Lett.*, **85**, 2522 (2000)

20. P. G. Bolhuis, A. A. Louis, J. P. Hansen, and E. J. Meijer, *J. Chem. Phys.*, **114**, 4296 (2001)

21. P. G. Bolhuis, A. A. Louis, *Macromolecules*, **35**, 1860 (2002)

22. J.R. Silbermann, S.H.L. Klapp, M. Schoen, N Chennamsetty, H. Bock, and K.E. Gubbins, *J. Chem. Phys.* in press.

23. R. L. Henderson, *Phys. Lett.* **49A**, 197 (1974)

24. C. G. Gray and K. E. Gubbins, *Theory of Molecular fluids*, Vol 1, p. 178, Oxford University Press, Oxford (1984)

25. R. Faller, H. Schmitz, O. Biermann, F. Müller-Plathe, *J Comput. Chem.* **20**, 1009 (1999)

26. H. Meyer, O. Biermann, R. Faller, D. Reith, F. Müller-Plathe, *J Chem. Phys.* **113**, 6264 (2000)

27. D. Reith, H. Meyer, F. Müller-Plathe, *Macromolecules* **34**, 2335 (2001)

28. A. K. Soper, *Chem. Phys.*, **202**, 295 (1996).

29. D. Reith, M. Pütz, F. Müller-Plathe, *J. Comput. Chem.*, **24**, 1624 (2003).

30. H. S. Ashbaugh, H. A. Patel, S. K. Kumar, S. Garde, *J. Chem. Phys.*, **122**, 104908 (2005)

31. J.C. Shelley, M.Y. Shelley, R.C. Reeder, S. Bandyopadhyay, M.L. Klein, *J. Phys, Chem. B*, **105**, 4464 (2001).

32. J.C. Shelley, M.Y. Shelley, R.C. Reeder, S. Bandyopadhyay, P.B. Moore, M.L. Klein, *J. Phys, Chem. B*, **105**, 9785 (2001).

33. G. Srinivas, J. C. Shelley, S. O. Nielsen, D. E. Discher, and M. L. Klein, *J Phys. Chem. B*, **108**, 8153 (2004)

34. S. Izvekov, G. A. Voth, *J. Phys. Chem. B*, **109**, 2469 (2005)

35. R. L. C. Akkermans, and W. J. Briels, *J Chem. Phys.*, **115**, 6210 (2001)

36. J. D. McCoy and J. G. Curro, *Macromolecules*, **31**, 9362 (1998)

37. N. P. Adhikari, X. Peng, A. Alizadeh, S. Ganti, S. K. Kayak, and S. K. Kumar, *Phys. Rev. Lett.*, **93**, 188301 (2004)

38. S. H. L. Klapp, D. J. Diestler, and M. Schoen, *J Phys. Condens. Matter*, **16**, 7331 (2004)

Chapter 4

Rigorous coarse-grained potentials from Widom's particle insertion method

4.1 INTRODUCTION

In this chapter we explore the rigorous coarse-graining approach to construct a meso-scale model from the corresponding atomistic model [1]. Rigorous coarse graining is based on the requirement that the partition function of the degrees of freedom of the effective system is identical to the partition function of the same degrees of freedom in the original system. This yields an equation for the effective interactions. Dijkstra, van Roij and Evans [2] have shown that in a binary mixture, where the preserved component ('solute', A) is treated canonically while the degrees of freedom which are coarse grained out ('solvent', B) form a grand canonical ensemble, the total effective interaction can be written as a series of a volume term and one-, two-, and higher-body terms. The individual contributions have the beneficial property that they are *A-density transferable*, i.e. they are correct for any density of species A (with all other state variables fixed). On the other hand, this series of contributions contains terms for all numbers of particles. Thus, the density transferability is an advantage only if the series can be truncated after the first few terms. The results of Ref. [2] show that by taking into account only the effective pair interaction the phase diagrams of a number of binary hard sphere mixtures can be reproduced very well.

The expressions for the effective interactions given in Ref. [2] represent test-particle equations and can be evaluated using Widom's particle insertion method [3]. Here we use Widom's method to coarse grain a binary mixture of Argon ('solvent', B) and Krypton ('solute', A). Coarse graining this mixture results in a pure fluid (Krypton) with effective interactions, while Argon is coarse grained out. We compare the performance of Widom's method and an alternative method employing the potential of mean force at different Argon densities. The pair approximation of the effective system is then tested against simulations of the full system.

The chapter is organized as follows: In section 4.2 we briefly describe the derivation of the effective potentials (following Ref.[2]), derive an alternative expression and present details of the model and the simulation technique. In section 4.3 we collect the results of our simulations and conclude in section 4.4.

4.2 MODEL AND SIMULATIONS

4.2.1 The effective Potentials

The objective of this work is to study coarse graining of a two component mixture using Widom's test particle insertion method [3] and to compare it to an alternative method employing the potential of mean force. The statistical mechanics of coarse

graining of binary mixtures without internal degrees of freedom of the two components has been presented in detail by Dijkstra, van Roij and Evans in Ref. [2]. Here we summarize only the general idea of the derivation.

We consider a mixture of structureless, spherical molecules of components A (the 'large' particles or 'solute') and B (the 'small' particles or 'solvent'). Assuming pair-wise additivity for the mixture, the potential energy part of its Hamiltonian is given by

$$H = H_{\mathrm{AA}} + H_{\mathrm{AB}}^{(N_1)} + H_{\mathrm{BB}} \tag{4.1}$$

and

$$H_{\mathrm{AA}} = \sum_{IJ} \phi_{\mathrm{AA}}(R_{IJ}), \quad H_{\mathrm{BB}} = \sum_{ij} \phi_{\mathrm{BB}}(r_{ij}), \quad H_{\mathrm{AB}}^{(N_{\mathrm{A}})} = \sum_{I}^{N_{\mathrm{A}}} \sum_{i}^{N_{\mathrm{B}}} \phi_{\mathrm{AB}}(r_{Ij}), \tag{4.2}$$

where N_{A} and N_{B} are the number of particles of component A and B, respectively, $\boldsymbol{R}_I$ is the position of particle I of component A, $\boldsymbol{r}_i$ is the position of particle i of species B, $R_{IJ} = \|\boldsymbol{R}_I - \boldsymbol{R}_J\|$, $r_{Ij} = \|\boldsymbol{R}_I - \boldsymbol{r}_j\|$, $r_{ij} = \|\boldsymbol{r}_i - \boldsymbol{r}_j\|$, and the sums in H_{AA} and H_{BB} run over all pairs of particles. The semi-grand canonical partition function of the two-component system is given as:

$$\Psi(N_{\mathrm{A}}, \mu_{\mathrm{B}}, V, T) = \left(N_{\mathrm{A}}! \Lambda_{\mathrm{A}}^{3N_{\mathrm{A}}}\right)^{-1} \int_{V^{N_{\mathrm{A}}}} d\boldsymbol{R}^{N_{\mathrm{A}}} \exp(-\beta H_{\mathrm{AA}}) \sum_{N_{\mathrm{B}}=0}^{\infty} \frac{z_{\mathrm{B}}^{N_{\mathrm{B}}}}{N_{\mathrm{B}}!} \int_{V^{N_{\mathrm{B}}}} d\boldsymbol{r}^{N_{\mathrm{B}}} \exp\left[-\beta\left(H_{\mathrm{AB}}^{(N_{\mathrm{A}})} + H_{\mathrm{BB}}\right)\right], \tag{4.3}$$

where μ_{B}, $\Lambda_{\mathrm{B}} = h(2\pi m_{\mathrm{B}} k_{\mathrm{B}} T)^{-1/2}$, and $z_{\mathrm{B}} = \exp(\beta\mu_{\mathrm{B}})\Lambda_{\mathrm{B}}^{-3}$ are the chemical potential, the thermal de Broglie wave length and the fugacity of species B, respectively, V is the volume, T the temperature, k_B Boltzmann's constant and $\beta = (k_B T)^{-1}$.

We seek to map the original system to an effective one-component system (of species A) by 'coarse graining out' species B. Thus, the effective system is a canonical ensemble governed by the effective Hamiltonian:

$$H^{\text{eff}} = H_{\text{AA}} + \Omega(\mu_{\text{B}}), \tag{4.4}$$

which leads to the canonical partition function:

$$Q^{\text{eff}}(N_{\text{A}}, V, T; \mu_{\text{B}}) = \left(N_{\text{A}}! \Lambda_{\text{A}}^{3N_{\text{A}}}\right)^{-1} \int_{V^{N_{\text{A}}}} d\boldsymbol{R}^{N_{\text{A}}} \exp\{-\beta[H_{\text{AA}} + \Omega(\mu_{\text{B}})]\}. \tag{4.5}$$

Requiring that the integrands of the $\boldsymbol{R}^{N_{\text{A}}}$ integrations in (4.3) and (4.5) are equal, the effective potential $\Omega(\mu_{\text{B}})$ is defined as:

$$\exp[-\beta\Omega(\mu_{\text{B}})] = \sum_{N_{\text{B}}=0}^{\infty} \frac{z_{\text{B}}^{N_{\text{B}}}}{N_{\text{B}}!} \int_{V^{N_{\text{B}}}} d\boldsymbol{r}^{N_{\text{B}}} \exp\left[-\beta\left(H_{\text{AB}}^{(N_{\text{A}})} + H_{\text{BB}}\right)\right], \tag{4.6}$$

which ensures that $Q^{\text{eff}} = \Psi$.

As shown in Ref. [2], the advantage of the semi-grand canonical ensemble is that the effective potential splits naturally in a sum of a volume term, a one-body term, and two-, three-,…, N_{A}-body interactions:

$$\Omega = \sum_{n=0}^{N_{\text{A}}} \Omega_n = -\beta^{-1} \ln \Xi_0 + N_{\text{A}}\omega_1 + \sum_{IJ} \omega_2(R_{IJ}) + \sum_{IJK} \omega_3(\boldsymbol{R}_I, \boldsymbol{R}_J, \boldsymbol{R}_K) + \cdots. \tag{4.7}$$

The first term on the far right side of (4.7), the volume term, can be identified as the grand canonical potential of a pure fluid of species B (where Ξ_0 is its grand canonical partition function). The one-body term ω_1 is given by

$$\omega_1 = -\beta^{-1} \ln\left\langle \exp(-\beta H_{\mathrm{AB}}^{(1)}) \right\rangle_0 , \tag{4.8}$$

where $\langle \cdots \rangle_0$ denotes the (grand canonical) ensemble average in the pure fluid of species B at chemical potential μ_{B}. We note that because of the continuous symmetry of fluids [4] ω_1 is a constant, i.e. it is not position dependent. As pointed out in Ref. [2], ω_1 is an effective contribution to the chemical potential of species A due to the presence of component B, which is consistent with the linear N_{A} dependence of the one-body contribution to Ω in (4.7). The effective pair-interaction ω_2 is given as

$$\omega_2(\boldsymbol{R}_1, \boldsymbol{R}_2) = -\beta^{-1} \ln\left\langle \exp(-\beta H_{\mathrm{AB}}^{(2)}) \right\rangle_0 - 2\omega_1 \tag{4.9a}$$

$$= -\beta^{-1} \ln\left\langle \exp(-\beta H_{\mathrm{AB}}^{(2)}) \right\rangle_1 - 1\omega_1 , \tag{4.9b}$$

where $\langle \cdots \rangle_1$ in the alternative expression (4.9b) denotes the (grand canonical) ensemble average in the pure fluid of species B at chemical potential μ_B containing one particle (particle 1) of species A at a *fixed* position, $\boldsymbol{R}_1$. From (4.9a) we realize that due to the spherical symmetry of species A and the continuous symmetry of fluids the effective pair potential depends only on the relative distance between particles 1 and 2. Thus the effective pair potential is spherically symmetric, $\omega_2(R_{12}) = \overline{\omega_2(\boldsymbol{R}_1, \boldsymbol{R}_2)}$, where the overbar denotes averaging over all coordinates of the two particles except the interparticle distance, R_{12}.

The effective interactions in (4.8) and (4.9) represent test-particle equations which can be evaluated using Widom's particle insertion method (see Sec. 4.2.2).

An alternative route to obtain ω_2 becomes apparent by considering an *effective* system containing only *two* particles of species A. Since no B particles are present in the effective system, the effective pair interaction and the potential of mean force are identical in this two-A-particle system (Ref.[5] Chap. 2.5). Thus, we can write:

$$\omega_2(R_{12}) = -\beta^{-1} \ln g^*(R_{12}) \tag{4.10}$$

and the pair correlation function, $g^*(R_{12})$, is given as

$$g^*(R_{12}) = \frac{\exp\left[-\beta\Omega(N_A = 2, \mu_B\right]}{\int_{V^{N_A}} d\boldsymbol{R}^{N_A} \exp\left[-\beta\Omega(N_A = 2, \mu_B)\right]} = \frac{\sum_{N_B=0}^{\infty} \frac{z_B^{N_B}}{N_B!} \int_{V^{N_B}} d\boldsymbol{r}^{N_B} \exp\left[-\beta\left(H_{AB}^{(2)} + H_{BB}\right)\right]}{\int_{V^{N_A}} d\boldsymbol{R}^{N_A} \sum_{N_B=0}^{\infty} \frac{z_B^{N_B}}{N_B!} \int_{V^{N_B}} d\boldsymbol{r}^{N_B} \exp\left[-\beta\left(H_{AB}^{(2)} + H_{BB}\right)\right]}, \tag{4.11}$$

where the denominators are the configuration integrals of the effective and the full system, respectively, and we have used, (4.3), (4.5), and (4.6). The far right side of (4.11) is the pair correlation function of particles 1 and 2 of species A in a fluid of species B at chemical potential μ_B containing only these two *not directly interacting* particles of species A (compare Hill Ref. [6] Chap. 37). Thus, the combination of (4.10) and (4.11) represents an alternative way to calculate ω_2. To improve sampling of the pair correlation function it proves more convenient to consider the potential of mean force in a system where particles 1 and 2 *interact* [7]. If they interact via ϕ_{AA} we recover the original semi-grand canonical ensemble containing *two* particles of species A. In *this* system the potential of mean force, $\omega_2(R_{12}) + \phi_{AA}(R_{12})$ is given as

$$\omega_2(R_{12}) + \phi_{\mathrm{AA}}(R_{12}) = -\beta^{-1} \ln g(R_{12}) \,. \tag{4.12}$$

We note that ω_2 is not affected by ϕ_{AA}. Thus any pair potential could be used instead of ϕ_{AA} which might offer a convenient way to improve sampling in more complex systems.

A very important property of the expressions for the ω_i in (4.8), (4.9), and (4.12) is that they do not depend on the total number of particles of species A, N_{A}. Thus the individual potentials ω_i are (*species A) density transferable* (but still depend on T and μ_{B}). On the other hand, Ω in (4.7) contains terms for all numbers of particles of species A up to N_{A}. Thus the density transferability is an advantage only if the series of effective interactions (4.7) converges after the first few terms.

Truncating the series in (4.7) after the effective pair interaction is an approximation and will affect the structure and the equation of state of the system. Therefore, we compare the pressures of the original and the effective system. Since the coarse system is a canonical ensemble its pressure, P, is given as [6]

$$P = \beta^{-1} \left(\frac{\partial \ln Q^{\mathrm{eff}}}{\partial V} \right)_{N_{\mathrm{A}},T} . \tag{4.13}$$

Following the procedure detailed in Ref. [6] (Chap. 30) we obtain:

$$P = \frac{N_{\mathrm{A}}}{\beta V} - \left\langle \frac{\partial}{\partial V} \left(H_{\mathrm{AA}} + \Omega \right) \right\rangle , \tag{4.14}$$

where $\langle\cdots\rangle$ denotes the canonical average in the effective system. The partial derivative of H_{AA} in (4.14) is given by

$$\frac{\partial}{\partial V}H_{\mathrm{AA}} = \frac{1}{3V}\sum_{IJ}\phi'_{\mathrm{AA}}(R_{IJ})R_{IJ}\,, \tag{4.15}$$

where $\phi'_{\mathrm{AA}}(R_{IJ}) = \partial\phi_{\mathrm{AA}}(R_{IJ})/\partial R_{IJ}$. The partial derivative of the effective interaction Ω as given by (4.7) with respect to V yields:

$$\frac{\partial}{\partial V}\Omega = -P_0 + \frac{1}{3V}\sum_{IJ}\omega'_2(R_{IJ})R_{IJ} + \cdots, \tag{4.16}$$

where $P_0 = V^{-1}\beta^{-1}\ln\Xi_0$ is the pressure of the pure fluid of species B at chemical potential μ_{B}, $\omega'_2(R_{IJ}) = \partial\omega_2(R_{IJ})/\partial R_{IJ}$, and '…' denotes higher-body terms. We note that the one-body term does not contribute to the pressure because it is constant. Combining (4.14), (4.15), and (4.16) and ignoring contributions from effective three-body interactions and higher-body terms we find for the pressure in the effective system:

$$P \approx \frac{N_{\mathrm{A}}}{\beta V} + P_0 - \frac{1}{3V}\left\langle\sum_{IJ}\left[\omega'_2(R_{IJ}) + \phi'_{\mathrm{AA}}(R_{IJ})\right]R_{IJ}\right\rangle. \tag{4.17}$$

Using (4.6) for Ω we can derive an alternative expression for (4.16) that does not involve the approximation of truncating the series (4.7):

$$\left(\frac{\partial}{\partial V}\Omega\right)_{\mu_{\mathrm{B}},T} = -\frac{\langle N_{\mathrm{B}}\rangle_{N_{\mathrm{A}}}}{\beta V} + \left\langle\frac{\partial}{\partial V}\left(H_{\mathrm{AB}}^{N_{\mathrm{A}}} + H_{\mathrm{BB}}\right)\right\rangle_{N_{\mathrm{A}}}. \tag{4.18}$$

Combining (4.14), (4.15), and (4.18) we obtain

$$P = \frac{N_{\mathrm{A}} + \langle N_{\mathrm{B}}\rangle_{\mathrm{orig}}}{\beta V} - \frac{1}{3V}\left\langle\sum_{IJ}\phi'_{\mathrm{BB}}(R_{IJ})R_{IJ} + \sum_{I=1}^{N_{\mathrm{A}}}\sum_{i=1}^{N_{\mathrm{B}}}\phi'_{\mathrm{AB}}(r_{Ij})r_{Ij} + \sum_{ij}\phi'_{\mathrm{BB}}(r_{ij})r_{ij}\right\rangle_{\mathrm{orig}}, \tag{4.19}$$

where $\langle \cdots \rangle_{\text{orig}}$ denotes the average in the original system. Eq. (4.19) is identical to the expression one obtains from $P = -(\partial \Psi / \partial V)_{N_A, \mu_B, T}$ for the original system. As expected, since the present coarse graining method is exact, it preserves the equation of state. All deviations of (4.17) from the exact value (4.19) are solely due to truncation of the series of effective interactions in (4.7).

4.2.2 The Model

In this paper we use as an example the binary (bulk) mixture Argon/Krypton. (Throughout we assume the convention component B/component A.) The liquid/gas phase behaviour of this mixture is well known [8] and can be reproduced by a binary Lennard-Jones (LJ)(12,6) mixture [9,10], assuming pair-wise additivity and employing the Lennard-Jones potential:

$$\phi(r) = 4\varepsilon \left[\left(\frac{\sigma}{r} \right)^{-12} - \left(\frac{\sigma}{r} \right)^{-6} \right], \tag{4.20}$$

where ε and σ are the energy and the size parameter of the LJ potential, respectively. The LJ parameters for the Ar/Kr mixture are given in table 4.1 and were taken from Ref. [9]. The parameters for the pure fluids have been fitted to liquid/gas equilibrium data, while the parameters for the cross interaction (Ar/Kr) are obtained by employing standard Lorentz-Berthelot mixing rules:

$$\varepsilon_{ij} = \left(\varepsilon_{ii}\varepsilon_{jj}\right)^{\frac{1}{2}}, \quad \sigma_{ij} = \frac{1}{2}\left(\sigma_{ii} + \sigma_{jj}\right). \tag{4.21}$$

All interactions were cut off at $5\sigma_{\mathrm{Ar}}$.

Table 4.1. Potential Parameters (Parameters are taken from Ref. [9])

Component	Ar/Ar	Kr/Kr	Ar/Kr
ε/K	117.5	161.0	137.5
σ/Å	3.390	3.607	3.499

We coarse grain the Ar/Kr mixture by mapping it onto an effective Kr fluid where we ignore all contributions to Ω in Eq.(4.7) beyond the pair level. Two methods to compute the effective pair potentials are tested:

I. ω_2 from Widom's particle insertion method, Eq.(4.9b)

II. ω_2 from the potential of mean force, Eq.(4.12).

I. Coarse graining by Widom's particle insertion is based on the calculation of ω_2 following Eq. (4.9b): We run a Monte Carlo (MC) simulation in the semi-grand canonical ensemble containing one Krypton atom and a fluid of Argon atoms at fixed chemical potential μ_{Ar}. The size of the cubic simulation box is $(10\sigma_{\mathrm{Ar}})^3$ and has periodic boundary conditions. A 'test particle' is placed on the nodes of a simple cubic lattice with lattice constant, $\ell = 10\sigma_{\mathrm{Ar}}/15$, and $\exp(-\beta H_{\mathrm{AB}}^{(2)}) = \exp\left[-\beta\phi_{\mathrm{AB}}(R_{12})\right]$ is

evaluated at each position. The ensemble average is computed by averaging over 10^6 configurations which are 2000 MC steps apart. As a check for consistency we calculate ω_1 from (4.8) and compare it to the value of $-\beta^{-1}\ln\left\langle\exp(-\beta H_{\mathrm{AB}}^{(2)})\right\rangle_1$ at large R_{12}. Since $\lim_{R_{12}\to\infty}\omega_2(R_{12})=0$ we expect $\lim_{R_{12}\to\infty}\left[-\beta^{-1}\ln\left\langle\exp(-\beta H_{\mathrm{AB}}^{(2)})\right\rangle_1\right]=\omega_1$.

II. Coarse graining using the potential of mean force. As shown in Sec. 4.2.1 the effective pair interaction ω_2 is alternatively given as the potential of mean force between Krypton atoms 1 and 2 in the semi-grand canonical ensemble containing these two Krypton atoms and a fluid of Argon atoms at μ_{Ar}. Strictly, to obtain ω_2 using (4.12) we would have to calculate the Kr/Kr pair correlation function, $g(R_{12})$, in exactly this system. For better sampling we compute $g(R_{12})\cong g(R)$ in a system containing typically 20 Krypton atoms in an Argon fluid in a cubic simulation box of dimensions $(10\sigma_{\mathrm{Ar}})^3$. This is an approximation since the system should strictly contain only two Kr atoms in a macroscopic volume. However, at this low Krypton number density of $0.02\sigma_{\mathrm{Ar}}^{-3}$ we can expect three-body effects on $g(R)$ to be negligible.

To test the potentials we compute pair correlation functions and the pressure along an isotherm by varying N_{Kr} at constant temperature, $T=177.38\mathrm{K}$, and chemical potential of Argon, $\mu_{\mathrm{Ar}}=-15.498\varepsilon_{\mathrm{Ar}}$, in the original system, $\Psi(N_{\mathrm{Kr}},\mu_{\mathrm{Ar}},V,T)$, and the effective system, $Q^{\mathrm{eff}}(N_{\mathrm{Kr}},V,T)$.

4.3 RESULTS

4.3.1 Effective potentials

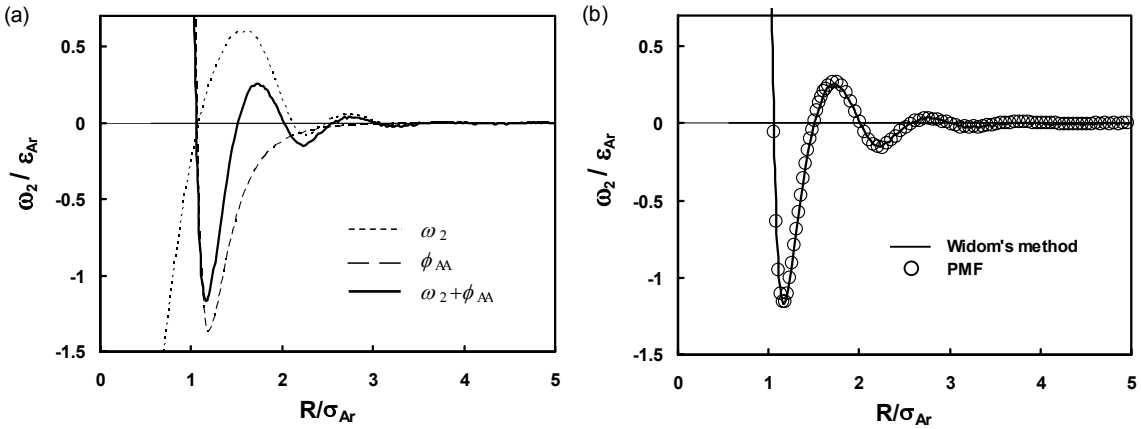

Figure 4.1. Effective potentials for the Argon/Krypton mixture. (a) Effective pair potential ω_2 calculated by Widom's particle insertion method (4.9b), the direct interaction, ϕ_{AA}, and the sum $\omega_2 + \phi_{AA}$. (b) Full pair potential, $\omega_2 + \phi_{AA}$, calculated by Widom's particle insertion method (4.9b) and via the potential of mean force (PMF) (4.12). The potentials shown here are averaged over $3*10^6$ configurations.

We compute effective density-transferable pair potentials, ω_2, via Widom's particle insertion method (4.9b) and via the potential of mean force (4.12) at different chemical potentials of Argon, μ_{Ar}, to compare the performance of the two methods. The effective potential obtained from Widom's method at $\mu_{Ar} = -15.498\varepsilon_{Ar}$, which corresponds to an Argon number density of $\rho_{Ar}^{pure} = 0.52\sigma_{Ar}^{-3}$ in pure Argon, is shown in Fig. 4.1(a). The potential is attractive at small distances, R, oscillates several times, and decays to zero within $5\sigma_{Ar}$. The general shape of the potential is consistent with that of depletion potentials of colloidal solutions which are similar in nature [11]. As shown in

Fig. 4.1(a) the full Kr/Kr potential of the effective (one-component) system, $\omega_2 + \phi_{AA}$, is dominated by the direct interaction, ϕ_{AA}, at small R and becomes increasingly influenced by ω_2 as R increases. This is consistent with the general observation that effective potentials are typically longer ranged than direct interactions.

The full effective potential, $\omega_2 + \phi_{AA}$, can also be calculated via the potential of mean force (Fig. 4.1(b)). As shown in Fig. 4.1(b), both potentials agree within the weak noise after averaging over $3*10^6$ configurations. This agreement is expected since both methods are exact. However, the potential of mean force was calculated at finite Kr number density, $\rho_{Kr} = 0.02\sigma_{Ar}^{-3}$, while (4.12) requires two Kr atoms in V. The larger number of Kr atoms is necessary for efficient sampling of $g(R)$ but it has the potential danger of affecting $\omega_2 + \phi_{AA}$ by 3- and higher-body effects. In the present case no such effect was observed. Within this approximation both methods performed about equally well. We note that in fluids Widom's method yields ω_2 and additionally ω_1 in one simulation, since for fluids we can expect $\lim_{R\to\infty} \omega_2(R) = 0$ (see (9)). In other words, the insertion of the second Kr atom far away from the first one is not affected by the first Kr atom and is thus identical to insertion in pure Argon. The value of ω_1 we found in this way agrees very well with the one obtained directly from (4.8). However, knowledge of ω_1 is usually not an important advantage since ω_1 does not influence the structure or the phase behavior; it is, however, relevant for properties such as the chemical potential of Krypton and the entropy [2].

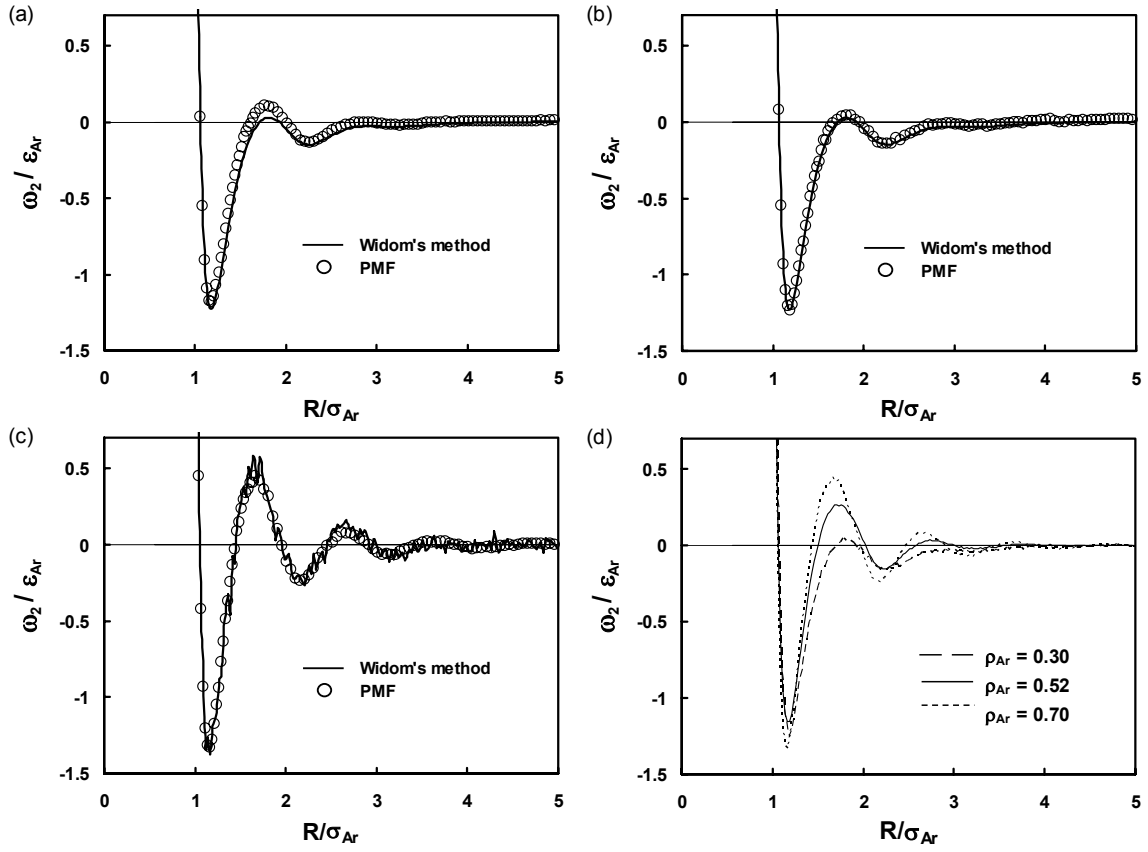

Figure 4.2 Effective potentials for the Argon/Krypton mixture, $\omega_2 + \phi_{AA}$, calculated by Widom's particle insertion method (4.9b) and via the potential of mean force (PMF) (4.12): (a) $\mu_{Ar} = -16.111\varepsilon_{Ar}$ (corresponding to $\rho_{Ar}^{pure} = 0.30\sigma_{Ar}^{-3}$) and $\rho_{Kr} = 0.02\sigma_{Ar}^{-3}$, (b) $\mu_{Ar} = -16.111\varepsilon_{Ar}$ and $\rho_{Kr} = 0.005\sigma_{Ar}^{-3}$, (c) $\mu_{Ar} = -13.670\varepsilon_{Ar}$ ($\rho_{Ar}^{pure} = 0.70\sigma_{Ar}^{-3}$), and (d) comparison of the effective potentials at different μ_{Ar} leading to different ρ_{Ar} as indicated in the figure.

At a lower chemical potential of Argon, $\mu_{Ar} = -16.111\varepsilon_{Ar}$, ($\rho_{Ar}^{pure} = 0.30\sigma_{Ar}^{-3}$) both methods converge relatively fast and give smooth potential curves after averaging over 10^6 configurations (Fig. 4.2(a)). However, they differ significantly around the first peak. This difference disappears when we reduce the Kr density to $\rho_{Kr} = 0.005\sigma_{Ar}^{-3}$ (Fig. 4.2(b)). This leads to the interesting conclusion that higher-body effects become

important at lower Kr densities if the Argon density is lowered by lowering its chemical potential. This is a clear disadvantage of the potential of mean force route and Widom's method should be preferred.

At high chemical potentials of Argon, $\mu_{Ar} = -13.670\varepsilon_{Ar}$, ($\rho_{Ar}^{pure} = 0.70\sigma_{Ar}^{-3}$) the convergence of the potential of mean force is as good as for low μ_{Ar} (Figs. 4.2(b) and (c)). On the contrary, Widom's method does not converge well (Fig. 4.2(c)). This problem is equivalent to the well known sampling problem of Widom's method to calculate chemical potentials at high densities [e.g. 12]. More sophisticated insertion methods to compute chemical potentials at high density exist [e.g. 13] but the potential of mean force route should perhaps be preferred due to its effectiveness and simplicity.

4.3.2 Test of the Potentials

a) Structure

The potentials calculated in Sec. 4.3.1 are now tested regarding their ability to reproduce the Krypton structure of the full system. Therefore we calculate Kr/Kr pair correlation functions, $g(R)$, for a number of systems with different Kr densities at constant temperature $T = 177.38K$ and chemical potential of Argon, $\mu_{Ar} = -15.498\varepsilon_{Ar}$ using the effective potential obtained from Widom's method.

At the smallest Kr density $\rho_{Kr} = 0.02\sigma_{Ar}^{-3}$ we observe excellent agreement between $g_{eff}(R)$ obtained in the effective system and the Kr/Kr pair correlation function

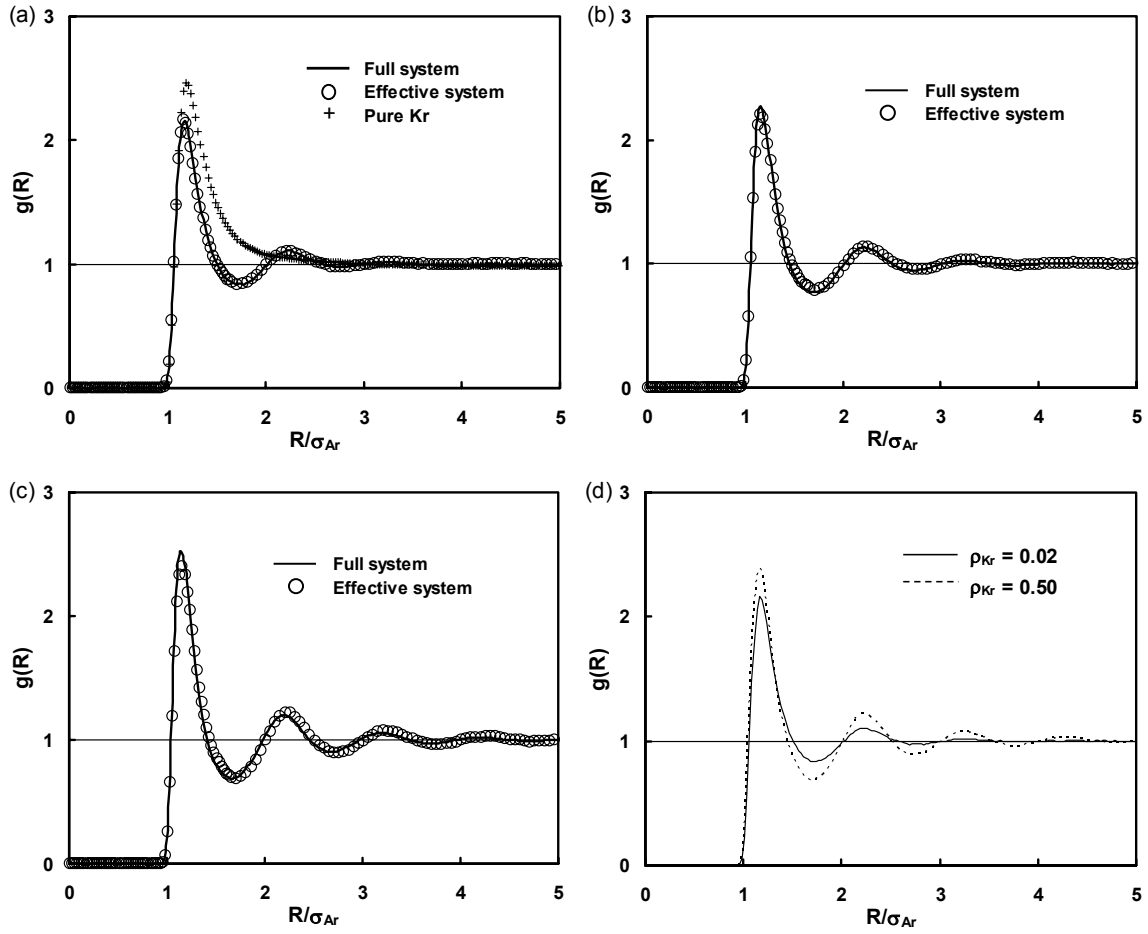

Figure 4.3 Krypton/Krypton pair correlation functions, $g(R)$, calculated directly in the full system Eq.(4.1) and the effective system Eq.(4.4) at: (a) $\rho_{\mathrm{Kr}} = 0.02\sigma_{\mathrm{Ar}}^{-3}$, (b) $\rho_{\mathrm{Kr}} = 0.2\sigma_{\mathrm{Ar}}^{-3}$, (c) $\rho_{\mathrm{Kr}} = 0.5\sigma_{\mathrm{Ar}}^{-3}$. As a reference, part (a) includes $g(R)$ calculated in pure Kr, i.e. using only ϕ_{AA}. (d) Comparison of the pair correlation functions of the effective system shown in parts (a) and (c).

of the atomistic system, $g_{\mathrm{at}}(R)$, (Fig. 4.3(a)). Comparison of $g_{\mathrm{eff}}(R)$ to the pair correlation function calculated for pure Krypton, i.e. using only ϕ_{AA}, shows that the presence of the second component (Argon) induces significant structure formation, which is well reproduced by the effective pair interaction.

As the Kr density increases the system becomes more and more structured which is well reproduced by the effective interactions (Fig. 4.3). However, a closer look at Figs. 4.3(b) and (c) reveals that the height of the first peak of $g_{\text{at}}(R)$ is not completely reached by the effective system. It also appears that the first peak of $g_{\text{eff}}(R)$ is slightly widened compared to $g_{\text{at}}(R)$ which shifts all higher peaks of $g_{\text{eff}}(R)$ to larger R.

In general, using only effective interactions up to the pair level and ignoring all others reproduces the pair structure quite well and causes only slight deviations in the pair correlation at Kr densities up to $\rho_{\text{Kr}} = 0.5\sigma_{\text{Ar}}^{-3}$.

b) Equation of state

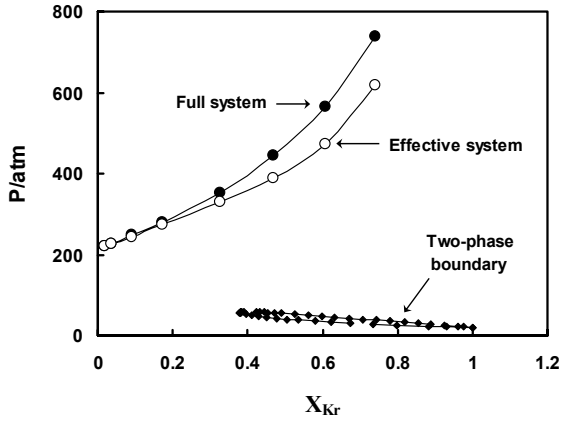

Figure 4.4 Pressure/Composition isotherms at $T = 177.38K$ and $\mu_{\text{Ar}} = -15.498\varepsilon_{\text{Ar}}$ for the atomistic and the effective system are shown. The experimental data for the liquid/gas two-phase boundary was taken from Ref. [8]. Lines are included for ease of viewing. Since the composition of the effective system is not directly accessible it was assumed to be the same as that of the full system at equal Kr densities.

The well reproduced structure implies that the effective potentials work quite well in representing the full system. The goal of thermodynamic studies is usually to investigate phase transitions and the equation of state. Therefore we test the ability of the effective system to reproduce the pressure. In Fig. 4.4 the pressure, P, of the effective system (4.17) and the atomistic system (4.19) as a function of composition, X_{Kr}, at $T = 177.38K$ and $\mu_{\mathrm{Ar}} = -15.498\varepsilon_{\mathrm{Ar}}$ is presented. The isotherm is located above the critical pressure of the mixture, thus, no influences from phase transitions are to be expected. As long as Kr is dilute, $X_{\mathrm{Kr}} < 0.2$ (which corresponds to a Kr density of $\rho_{\mathrm{Kr}} < 0.1\sigma_{\mathrm{Ar}}^{-3}$) the pressure is well reproduced by the effective system. At larger values of the composition, however, the pressure deviates significantly. At $X_{\mathrm{Kr}} = 0.74$ calculations using the effective potentials predict a pressure which is 16% too small. The absolute value of the pressure difference of 121bar is even more alarming since it is larger than the entire liquid/gas two-phase region of the mixture at this temperature (Fig. 4.4). The difference must be attributed to the neglect of three- and higher multi-body interactions.

4.4 CONCLUSIONS

Binary mixtures (species A and B) in the semi-grand canonical ensemble can be mapped onto one-component systems (species A) in the canonical ensemble by

integrating over the degrees of freedom of component B. Conveniently, the resulting effective potentials are species-A-density transferable. We compare two methods to calculate effective pair potentials:

I. Widom's particle insertion (4.9b)

II. potential of mean force (4.12).

Both methods are exact but have performance limits. Although the potential of mean force route is exact in principle, we have to resort to an approximation for efficient sampling of the required pair correlation function of component A. Therefore $g_{\text{eff}}(R)$ is calculated in the semi-grand canonical ensemble at small but finite densities of *component A*, ρ_{A}. However, if ρ_{A} is small enough the effect of the approximation of non-vanishing density, ρ_{A}, is negligible. Unfortunately, it is not known *a priori* if a certain density is indeed small enough. Our results indicate that this boundary depends on the state point. The major advantage of the potential of mean force method is its simplicity and good performance at high densities of component B associated with high chemical potentials, μ_{B}.

Widom's particle insertion method is exact and performs well up to moderately high densities of component B. However, high densities of component B lead to sampling difficulties with the particle insertion method, as is well known from studies of chemical potentials in pure fluids using this method. As a slight advantage Widom's method yields the effective one-body interaction, which the potential of mean force route

does not. This quantity, however, is not relevant if phase behaviour, structure, pressure, etc. are the properties of interest; it influences properties such as the chemical potential of component A and the entropy.

In summary, Widom's method is preferred at low densities of component B, ρ_B while the potential of mean force method is more efficient at larger ρ_B.

The pair approximation works well for the pair structure; deviations of the pair correlation function of the effective system from those of the full system are usually small. While these deviations of the pair correlation function are small, their impact on other properties can be large. The equation of state, for instance, is not very well reproduced as higher densities of component A are approached; large absolute deviations of the pressure are observed. These errors in the pressure suggest that effective three- and possibly higher multi-body interactions need to be included.

4.5 REFERENCES

1. N. Chennamsetty, H. Bock, and K. E. Gubbins, *Mol. Phys.* **103**, 3185 (2005)

2. M. Dijkstra, R. van Roij, R. Evans, *Phys. Rev. E*, **59**, 5744 (1999).

3. B. Widom, *J. Chem. Phys.*, **39**, 2808 (1963).

4. P.M. Chaikin, T.C. Lubensky, *Principles of condensed matter physics*, Cambridge University Press, Cambridge (1995).

5. J.P. Hansen, I.M McDonald, *Theory of simple liquids*, (2nd Ed.), Academic, London (1986).

6. T.L. Hill, *Statistical Mechanics*, Dover, New York (1956).

7. This ensemble proves more computationally convenient than the one without interactions between 1 and 2 since it allows better sampling of R_{12}. If 1 and 2 do not interact proper sampling will be difficult because 1 and 2 will overlap most of the time.

8. J.A. Schouten, A. Deerenberg, N.J. Trappeniers, *Physica A*, **81**, 151 (1975).

9. A.Z. Panagiotopoulos, *Int. J. Thermophys.*, **10**, 447 (1989).

10. V.K. Shen, J.R. Errington, *J. Chem. Phys.*, **122**, 064508 (2005).

11. A.A.Louis, A.Allahyaov, H.Löwen, R. Roth, *Phys. Rev. E*, **65**, 061407 (2002).

12. K.S. Shing, K.E. Gubbins, *Mol. Phys.*, **43**, 717 (1981).

13. K.S. Shing and K.E. Gubbins, *Mol. Phys.*, **46**, 1109 (1982).

Chapter 5

Coarse-graining by matching correlation functions

5.1 INTRODUCTION

In this chapter we explore coarse-graining techniques for complex systems by matching a specific property of interest between the atomistic and the meso-scale model [1]. In particular, we match the correlation functions. In the previous chapter, we have seen how the *rigorous* potentials can be determined using Widom's particle insertion method. We have calculated these potentials for a binary mixture of Ar and Kr, where the degrees of freedom of Ar are integrated out. This is a simple mixture with short range interactions and no intra-molecular degrees of freedom. When we deal with complex systems such as surfactant solutions, there are long range Coulomb charges and intra-molecular degrees of freedom that need to be coarse-grained out. As discussed in the chapter 3 (Section 3.2.4), the *rigorous* coarse-graining approach for such complex systems turns out to be very challenging. With charged systems, the problem is that the Mayer expansion used to derive the independent N-body terms diverges. Moreover it is not known how to treat the internal degrees of freedom grand-canonically, as required for rigorous coarse-graining. Therefore, for such complex systems, a variety of *alternative* coarse-graining approaches were used. These alternative approaches usually involve finding an effective potential that reproduces a specific property of interest from the

atomistic system into the coarse-grained system. Since we are interested in exploring the nano-scale structures formed by surfactants, we are interested in reproducing the structure in the coarse-grained system. Therefore, we find an effective potential which reproduces the structural properties, i.e. correlation functions. In particular we reproduce the pair correlation function from the atomistic system in the coarse-grained system. If there are no three body and higher interactions, the uniqueness theorem [2,3] guarantees there is a unique pair potential that corresponds to a given pair correlation function. Therefore, if these 3-body and higher terms are negligible, we can find a unique effective potential that reproduces a given pair correlation function.

Our long term goal is to develop a reliable coarse-graining procedure for the simulation of surfactant self-assembly both in bulk solution and onto surfaces. In coarse-graining these systems, we combine a group of atoms into a bead and the pair correlation function, $g_{ref}(R)$, between these beads is determined in the atomistic simulation. Here 'R' represents the distance between the center of mass of these beads. Then we find an effective potential that reproduces this $g_{ref}(R)$. We first explored the coarse-graining procedure for a system of ethanol molecules in water because ethanol resembles the structural units of the head groups of the polyethylene oxide surfactants. In the coarse-grained model, each ethanol molecule is represented by one spherical bead and the water is coarse grained out completely. Thus we integrate out all the degrees of freedom of water and also the internal degrees of freedom of ethanol. We first determine the $g_{ref}(R)$ between the center of mass of these ethanol molecules in the atomistic system. Then we determine an effective potential which reproduces this $g_{ref}(R)$ in the coarse-grained

system. Although the uniqueness theorem guarantees that the effective potential thus found is unique, the solution of this inverse problem is not straightforward in practice, since the exact relation between the pair correlation function and pair potential is generally unknown. In this chapter, we explore various approaches to find the effective potential that reproduces the pair correlation function from the atomistic model. The effective potential thus found is implemented into the meso-scale dissipative particle dynamics (DPD) simulations.

In Section 5.3 of this paper we discuss and compare numerical results for three different strategies by which we extract $\Phi(R)$ from $g_{ref}(R)$. These strategies vary in the degree of sophistication with which the inverse problem is tackled. At the lowest of these we employ the concept of the potential of mean force as the effective potential governing the interaction between a pair of ethanol beads [16]. At the next higher level of sophistication we incorporate the Ornstein–Zernike equation amended by the hypernetted–chain (HNC) closure. This method has been successfully employed to describe polymeric systems as soft colloids [4,5,6] and to extract effective potentials from scattering data for dendrimers [7]. At the third level of sophistication we invoke the numerical so–called Boltzmann inversion scheme originally proposed by Soper [8,9]. A similar (quasi–exact) scheme is the inverse MC method recently employed to derive effective pair potentials in NaCl mixtures [10]. Our results indicate that the integral equation methods yield very good results at small and moderate (ethanol) densities, while at large densities it is necessary to employ the (computationally quite expensive)

Boltzmann inversion scheme. We also find a significant state dependence of the derived effective potentials. Our conclusions are summarized in Sec. 5.4.

5.2 TECHNICAL ASPECTS OF COMPUTER SIMULATIONS

5.2.1 Molecular dynamics simulations at the atomistic level

In this work we are dealing with binary fluid mixtures composed of ethanol and water at various concentrations. Specifically, we employ mixtures containing 8, 26, 46, and 70 weight percent (wt%) of ethanol. The simulations at the atomistic level are based upon the DLPOLY simulation package [11]. These mixtures are realized by initially placing the center of mass of 64, 256, 512, or 1024 ethanol molecules at sites of a simple–cubic lattice in a simulation box whose side length is 40 Å. Initially, all these molecules have the same orientation. The simulation box is then filled with a configuration of pure water molecules preequilibrated at a temperature T = 300K. Positions of water molecules are adjusted such that initially the minimum spacing between each water and ethanol molecule is 1 Å to avoid exceedingly large initial intermolecular forces between any pair of molecules. In cases where the center–of–mass distance between a water and an ethanol molecule is smaller than 1 Å, the water molecule in question is removed from the simulation cell. This initial configuration is then further equilibrated at constant T = 295K and pressure P = 1atm using the Nosé–Hoover thermostat and barostat [12] as implemented in the DLPOLY simulation package. Bond

length constraints were imposed by the SHAKE algorithm [13]. The duration of this equilibration period amounts to 1ns with a time step of $\delta t = 1fs$.

The initial equilibration period of the water–ethanol mixture is followed by a production run at the same T and P for a period of 5–8ns using the same magnitude of the time step as in the equilibration period. Longer runs are employed for systems containing fewer ethanol molecules to guarantee sufficiently good sampling statistics for thermal averages.

In all simulations we use the OPLS–AA interaction parameters for ethanol molecules [14] and the SPC/E model for water [15]. The short–range (i.e., Lennard–Jones) interaction between water and ethanol is modeled via the Lorentz–Berthelot mixing rules [16]. Short–range Lennard–Jones interactions are cut off at intermolecular separations of 12 Å. Long–range electrostatic interactions are handled via the so–called smooth–particle mesh Ewald summation technique [17]. To minimize surface effects, periodic boundary conditions supplemented by the minimum image convention are used in all three spatial directions.

5.2.2 Dissipative particle dynamics simulations

At the mesoscopic level we realize that ethanol molecules are 2.55 times heavier than water molecules. Hence, one expects a water molecule to move more rapidly than an ethanol molecule. In fact, over the range of concentrations studied in this paper, the

experimental ratio of self–diffusion constants of water to ethanol varies between 1.26 (10 wt%) and 1.84 (70 wt%) [18]. Thus, as a first approximation we replace the water molecules interacting with an ethanol molecule by a stochastic force acting on the latter. In addition, we simplify the treatment of ethanol by coarse–graining its molecular structure, that is we represent each ethanol molecule by a (spherical) bead of "diameter" $R_b \approx 5$ Å. As a consequence of the coarse–grained molecular structure the beads interact via an effective rather than a "true" intermolecular interaction potential, u. The effective potential, Φ(R) where R denotes the distance between the centers of mass of a pair of beads, inevitably depends on the thermodynamic state of the fluid, that is on temperature and density of the coarse–grained molecules. As we shall see below, R_b corresponds to the first minimum of Φ(R). For distances $R \leq R_b$ the conservative force

$$F_{ij}^{C} = -\nabla_i \Phi(R_{ij}) = -F_{ij}^{C} \tag{5.1}$$

on bead i due to bead j is purely repulsive by analogy with the atomistic Lennard–Jones potential, where the force becomes repulsive for intermolecular distances $r \leq 2^{1/6}\sigma$. The far right side of Eq. (5.1) is a statement of Newton's third law. Hence, in this simplified treatment we replace the binary fluid mixture at the atomistic level by an effective pure fluid with coarse grained molecular structure. Hence, we introduce stochastic forces via

$$F_{ij}^{R} = \sigma\omega^{R}(R_{ij})\zeta_{ij}\hat{e}_{ij} = -F_{ji} \tag{5.2}$$

which is pairwise additive by analogy with F_{ij}^{C}. In Eq. (5.2), σ is the amplitude and ω^{R}(R) describes range and spatial variation of the random force. In Eq. (5.3), ζ_{ij} is a

random number sampled on the interval [0, 1] and $\hat{e}_{ij} = (R_i - R_j)/R_{ij}$ is a unit vector pointing from the center of mass of bead *j* to that of bead *i*.

However, on account of the stochastic forces, energy is not conserved in the coarse–grained, effective pure fluid. Therefore, we supplement conservative and stochastic forces by dissipative ones which serve as a thermostat to maintain a constant temperature (i.e., total energy) in the system. Assuming again pairwise additivity we express the dissipative force through

$$F_{ij}^{D} = -\gamma\omega^{D}(R_{ij})(\hat{v}_{ij}.\hat{e}_{ij}).\hat{e}_{ij} \tag{5.3}$$

where γ and $\omega^{D}(R_{ij})$ are defined analogously to σ and $\omega^{R}(R_{ij})$ in Eq. (5.2), respectively.

For a system in which molecules are subject to a total force

$$F_i = \sum_{j\neq i=1}^{N} F_{ij} = \sum_{j\neq i=1}^{N} (F_{ij}^{C} + F_{ij}^{R} + F_{ij}^{D}) \tag{5.4}$$

the equation of motion can be integrated numerically using dissipative particle dynamics (DPD) simulations [19,20]. In DPD one imposes two additional constraints on random and dissipative forces, namely

$$\omega^{R}(R_{ij}) = \sqrt{\omega^{D}(R_{ij})} \tag{5.5a}$$

$$\sigma = \sqrt{2\gamma k_B T} \tag{5.5b}$$

which serve to guarantee that the distribution of microstates (i.e., configurations) generated complies with the canonical–ensemble phase space probability density [21]. In

our simulations we use the DPD–adapted version of the velocity Verlet algorithm suggested by Vattulainen *et al.* to integrate the equation of motion [22].

However, the reader should realize that for the present paper, where we focus exclusively on static properties, a dynamical simulation technique is not really required. In fact, we might as well have employed Monte Carlo simulations or integral equation approaches to name explicitly a few alternative approaches. We focus on DPD simulations because in the longer run we will be interested in studying the mapping of atomistic dynamics onto the mesoscopic scale as well. In view of this longer term goal it thus seems sensible to use an approach which allows us to study static as well as dynamic properties at a mesoscopic level of description. This rationale prompted us to prefer DPD in this work over any other technique focusing predominantly on static properties.

5.3 RESULTS

We coarse-grain a fully atomistic model of ethanol molecules in water into a meso-scale model consisting only of ethanol beads. Our aim is to find an effective potential between these ethanol beads in the meso-scale model which gives the same pair correlation function as in the fully atomistic model. Therefore, we first perform fully atomistic simulations to determine the pair correlation function between the center of mass of ethanol beads, $g_{ref}(R)$ in the atomistic system. Then we find an effective potential

that reproduces this $g_{ref}(R)$ in the meso-scale model. We have employed three different approaches to find this effective potential 1) Potential of mean force, 2) Integral equations and 3) iterative Boltzmann inversion.

5.3.1 Potential of mean force

The potential of mean force is defined as

$$\Phi(R) = -\beta^{-1} \ln g_{ref}(R) \tag{5.6}$$

where $R \equiv |\boldsymbol{R}_1 - \boldsymbol{R}_2|$ is the distance between the centers of mass of a pair of ethanol beads. As discussed in chapter 3 (section 3.3), this relation holds for an infinitely dilute system, where the contribution from 3-body and higher interaction terms in negligible. Here we test to see until what concentration the relation given in (5.6) holds for this system of ethanol in water.

Fig. 5.1 shows plots of g (R) at various ethanol concentrations obtained from fully atomistic MD simulations and the corresponding mesoscale DPD simulations. These results are obtained as follows. In the fully atomistic simulations, where interactions between all atoms in all molecules are considered explicitly, the center–of–mass pair correlation function g_{ref} (R) is calculated. From this quantity an effective potential (of mean force) Φ(R) is then obtained from Eq. (5.6) individually for each concentration. Using this Φ(R) as input in the subsequent DPD simulations [see Eqs. (5.1) – (5.5)] to

model the interaction between pairs of ethanol beads we may calculate the ethanol bead–bead pair correlation function g (R). We may then define

$$\Delta g(R) = g(R) - g_{ref}(R) \tag{5.7}$$

as a quantitative measure reflecting the degree to which the effective bead interactions at the mesoscale can be represented by Φ(R). Ideally, if the procedure described above would be exact, Δg (R) would vanish identically so that Δg (R) is a quantitative measure of the degree to which the potential of mean force governing the temporal evolution of the system of ethanol beads in DPD is capable of reproducing the correct center–of–mass distribution obtained from the fully atomistic, first–principles MD simulations.

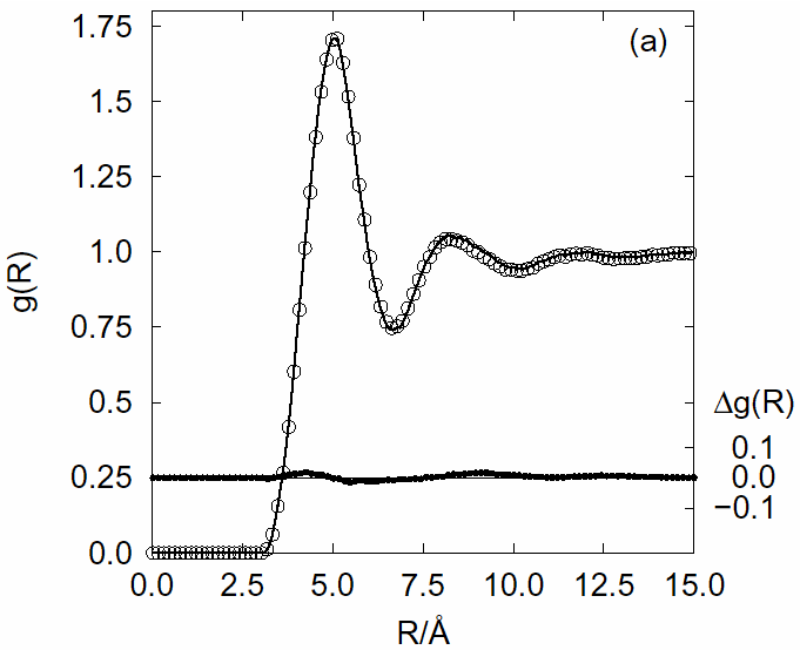

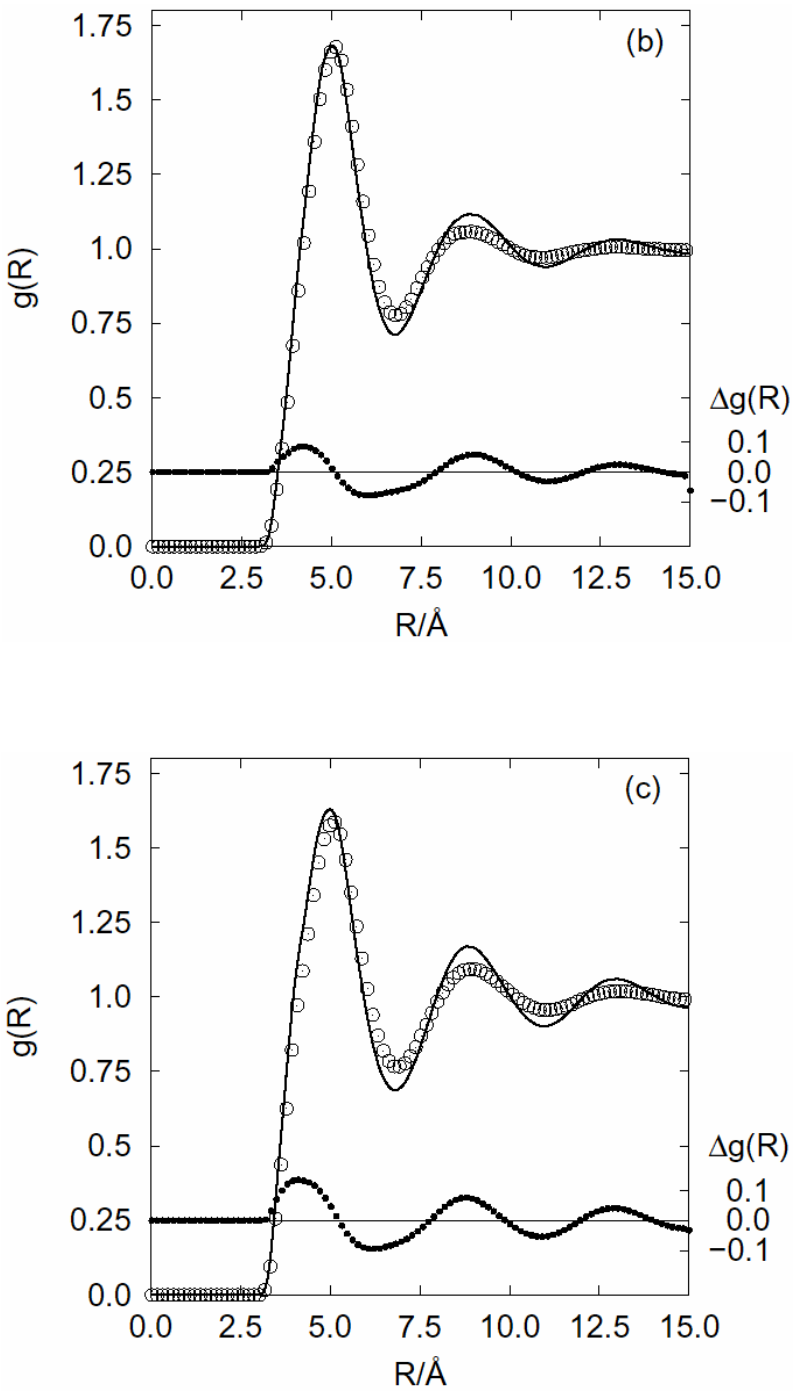

Figure. 5.1. Radial pair correlation function for the center–of–mass distribution of ethanol molecules in binary water–ethanol mixtures from fully atomistic MD simulations (o) and mesoscale DPD simulations (—) where Φ(R) is taken directly from Eq. (5.6); also shown is Δg (R) (•) [right ordinate, see Eq. (5.7)]. (a) 8wt%, (b) 46wt%, and (c) 70wt% of ethanol.

At the lowest ethanol concentration of 8wt%, Δg (R) nearly vanishes indicating that, as one would have anticipated, the assumption of additive effective interactions is reasonable in the limit of vanishing ethanol concentration. However, closer scrutiny reveals small but significant deviations between the pair correlation function calculated in DPD compared with its fully atomistic counterpart even at this low ethanol concentration. This effect becomes more pronounced at all higher ethanol concentrations as plots in Figs. 5.1(b) and (c) clearly show. In general, Δg (R) is an oscillatory function where the magnitude $|\Delta g$ (R)| can reach 10% for certain values of R at the highest ethanol concentration of 70wt%. Clearly, for this high concentration the potential of mean force extracted from a fully atomistic MD simulation is unable to reproduce the correct structure at the mesoscale on account of the neglected higher–order correlations in the assumption of Eq. (5.6), which become increasingly important at higher ethanol concentrations.

At this point one may wonder whether or not the effective potentials calculated from Eq. (5.6) are "transferable" in the sense that Φ(R) obtained at any one concentration of ethanol is capable of reproducing the correct structure at another one. To investigate this issue we take as a reference system the one containing 8wt% of ethanol. Results displayed in Fig. 5.1(a) already showed that if one uses the potential of mean force at this low concentration in a DPD simulation the correct structure is obtained as the comparison

with parallel results from the fully atomistic simulation reveals. Hence, we already concluded that for a sufficiently low concentration the potential of mean force provides a sufficiently realistic description of the effective interaction between ethanol beads in DPD.

To test the transferability of this particular effective potential to systems in which the density of ethanol beads corresponds to a much higher concentration we then use it to model the interbead interactions in a system containing 70wt% of ethanol. Quite expectedly, results plotted in Fig. 5.2 clearly show that this causes a pronounced deviation between g (R) and g_{ref} (R) both calculated for systems at this higher concentration (i.e., ethanol–bead density). Moreover, it is instructive to compare the structure at 70wt% from the previous case and the one discussed above in conjunction with Fig. 5.1(c) where Φ(R) was calculated directly from g_{ref} (R) obtained at this higher concentration. As our results plotted in Fig. 5.2 reveal the deviation between the two data sets [i.e., g_{ref} (R) and g (R)] is somewhat more pronounced in the previously discussed case in which Φ(R) was taken as the potential of mean force obtained for the lower density corresponding to only 8wt% of ethanol. In other words, the non-transferability of effective potentials adds (but is subdominant) to the failure of the potential of mean force to adequately describe the interbead interactions at higher concentrations of ethanol. We have checked that this trend increases continuously as one goes from the lowest to the highest ethanol concentration considered in this work.

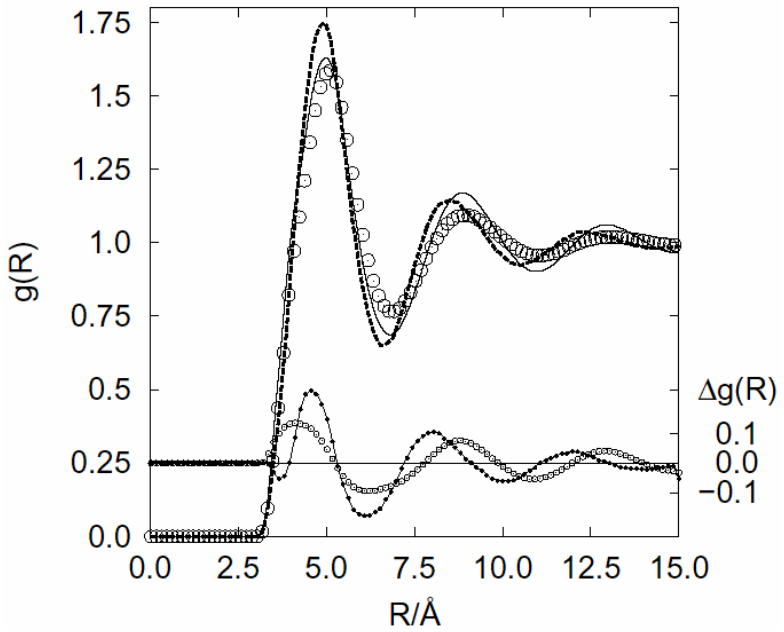

Figure 5.2. As Fig. 5.1, but only for mixtures containing 70wt% of ethanol, respectively where g_{ref} (R) (o) are obtained from fully atomistic MD simulations; DPD simulations are based upon Φ(R) given in Eq. (5.6) obtained for a system corresponding to an ethanol concentration of 8wt% (− − −) and 70wt% (—), respectively. Also shown are the respective deviations Δg (R) [see Eq. (5.7)] (right ordinate) for an ethanol concentration of 8wt% (–•–) and 70wt% (◦) (see text).

Finally, comparing plots in Figs. 5.1(a)–(c) one realizes that for the thermodynamic states considered here the variation in the corresponding atomistic g_{ref} (R) is rather minute. On the contrary, a relatively strong impact of the thermodynamic conditions is normally observed in the case of "simple" pure Lennard–Jones fluids (see, for example, Figs. 4.2 – 4.4 in Ref. [3]). The relative insensitivity of the present g_{ref} (R)

with respect to thermodynamic conditions can be rationalized as follows. First, the volume fraction

$$\phi = \frac{N_1 v_1 + N_2 v_2}{V} \tag{5.8}$$

of the binary mixtures in the atomistic simulations does not vary appreciably as one changes the concentration of ethanol over the present range. In Eq. (5.8), V is the total volume of the system, N_α is the number of molecules of species α, and $v_\alpha = \pi d_\alpha^3 / 6$ is the volume of a molecule of that species which we assume to be spherical of diameter d_α. More specifically, the volume fraction varies between ϕ= 0.28 (8wt% of ethanol) and ϕ = 0.22 (70wt% of ethanol). This is because ethanol and water do not differ that much in size. Second, we are considering correlations between the centers of mass of ethanol molecules and not those between individual interaction sites in those molecules. With respect to the arrangement of the centers–of–mass of ethanol molecules the fluid can be expected to be less structured since one averages over internal degrees of freedom.

In conclusion, we observe that the PMF approach fails at high concentrations of ethanol in water. This failure is due to the unaccounted 3-body and higher terms in the PMF approximation. The contribution from these 3-body and higher terms can be at least partly accounted using integral equations along with a suitable closure relation. We now explore this approach for our system of ethanol in water.

5.3.2 Integral equation

The Ornstein-Zernike Integral equations along with a suitable closure relation can be used to extract effective potentials from a known pair correlation function, $g_{ref}(R)$. The Ornstein–Zernike integral equation is given by [23],

$$h_{ref}(R_{12}) = c_{ref}(R_{12}) + \rho_1 \int h_{ref}(R_{23})\, c_{ref}(R_{13})\, dR_3 \tag{5.9}$$

where $h_{ref}(R_{12}) = g_{ref}(R_{12}) - 1$ and $c_{ref}(R_{12})$ are the total and direct correlation functions at the fully atomistic level and the spatial integration is to be carried out with respect to a third reference bead. This direct correlation function can be related to the effective potential through one of the closure relations. Here we use the Hypernetted chain (HNC) given by [16],

$$\beta\Phi(R) = h_{ref}(R) - c_{ref}(R) - ln\, g_{ref}(R) \tag{5.10}$$

which differs from the potential of mean force by the additional term h(R) − c(R) [cf.,Eq. (5.6)]. Using Φ(R) we perform a meso-scale DPD simulation from which we obtain g (R) and Δg (R).

Plots in Fig. 5.3 show that using the more sophisticated expression for Φ(R) from Eq. (5.10) improves the description of structure at the mesoscopic level. In particular at

intermediate [see Fig. 5.3(a)] ethanol concentrations the agreement between g_{ref} (R) and g(R) from DPD is remarkable. At higher concentrations [see Fig. 5.3(b)], however, even Eq. (5.10) begins to fail in predicting a suitable effective potential for the interaction of a pair of DPD beads. Nevertheless, it seems noteworthy that this "failure" is mostly restricted to small interbead separations. Given that Φ(R) is an oscillatory long–range potential according to the plots presented in Figs. 5.1 and 5.3 this seems consistent with the fact that the HNC closure is known to work better for long–range potentials but fails to account for short–range repulsive interactions [16].

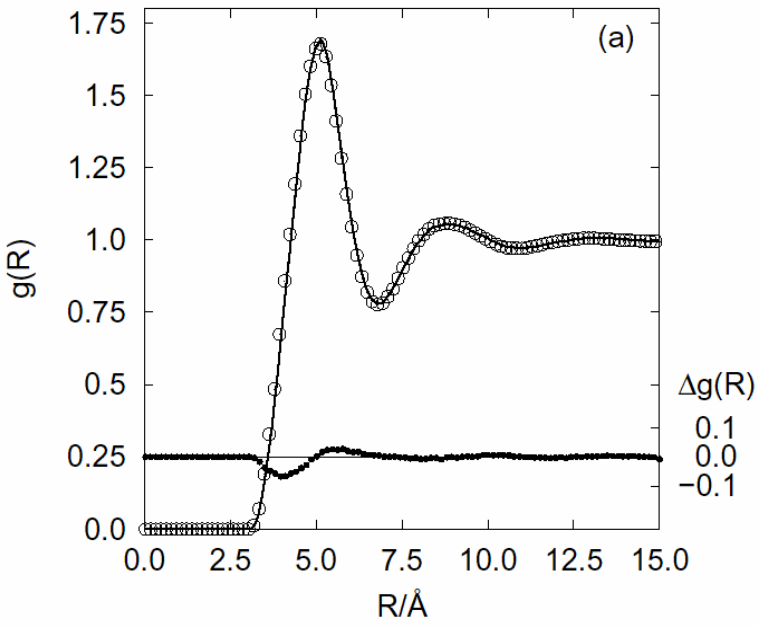

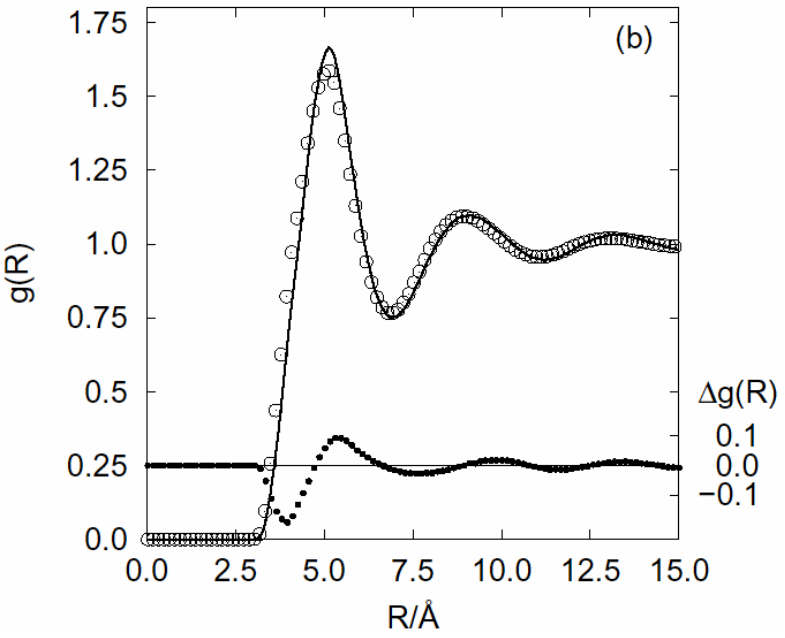

Figure 5.3. As Fig. 5.1, but only for mixtures containing 46wt% (a) and 70wt% (b) of ethanol, respectively. Here, DPD simulations are based upon Φ(R) given in Eq. (5.9).

5.3.3 Iterative Boltzmann inversion

Even though we demonstrated in the preceding section that the partial incorporation of interbead correlations beyond the pair correlation level improves the representation of the structure at the mesoscopic level, the agreement with the fully atomistic reference $g_{ref}(R)$ is not entirely satisfactory at higher ethanol concentrations, as plots of Δg (R) for ethanol concentrations of 46wt% and 70wt% in Figs. 5.3(a) and (b) clearly indicate. The reason is that Eq. (5.10) itself is not exact, but an approximation whose performance in extracting effective potentials is not yet well explored. Hence, we

are seeking a representation of Φ(R) free of these deficiencies even at the highest ethanol concentrations considered in this work.

To solve these deficiencies, we explored the iterative Boltzmann inversion procedure introduced by Soper [8] and used in polymer physics to extract effective interaction potentials from structural information [9]. This iterative procedure follows the relation,

$$\Phi_{i+1}(R) = \Phi_i(R) + \beta^{-1} \frac{g_i(R)}{g_{ref}(R)} \tag{5.11}$$

Initially, we approximate $\Phi_1(R) = -\beta\, ln\, g_{ref}(R)$ [see Eq. (5.6)]. With $\Phi_1(R)$ we perform a DPD simulation from which we calculate $g_1(R)$. This, in turn permits us to refine Φ(R) through Eq. (5.11). Iterations are halted if $\max_R |\Delta g(R)| \leq 0.02$. Even though there is no specific reason to assume that the iterative Boltzmann inversion scheme converges under all circumstances, results plotted in Fig. 5.4 reveal its remarkable success under the present conditions. As can be seen from Figs. 5.4(a)-(d) the structure of the effective one–component fluid agrees quite nicely with the one represented by $g_{ref}(R)$ obtained from the fully atomistic simulation of the binary ethanol–water mixture up to the highest ethanol concentration of 70wt%. Thus, our results indicate that for the ethanol–water mixture it is possible to map the detailed intermolecular interactions at the atomistic level onto a state–dependent, pairwise additive potential for an effective one–component fluid.

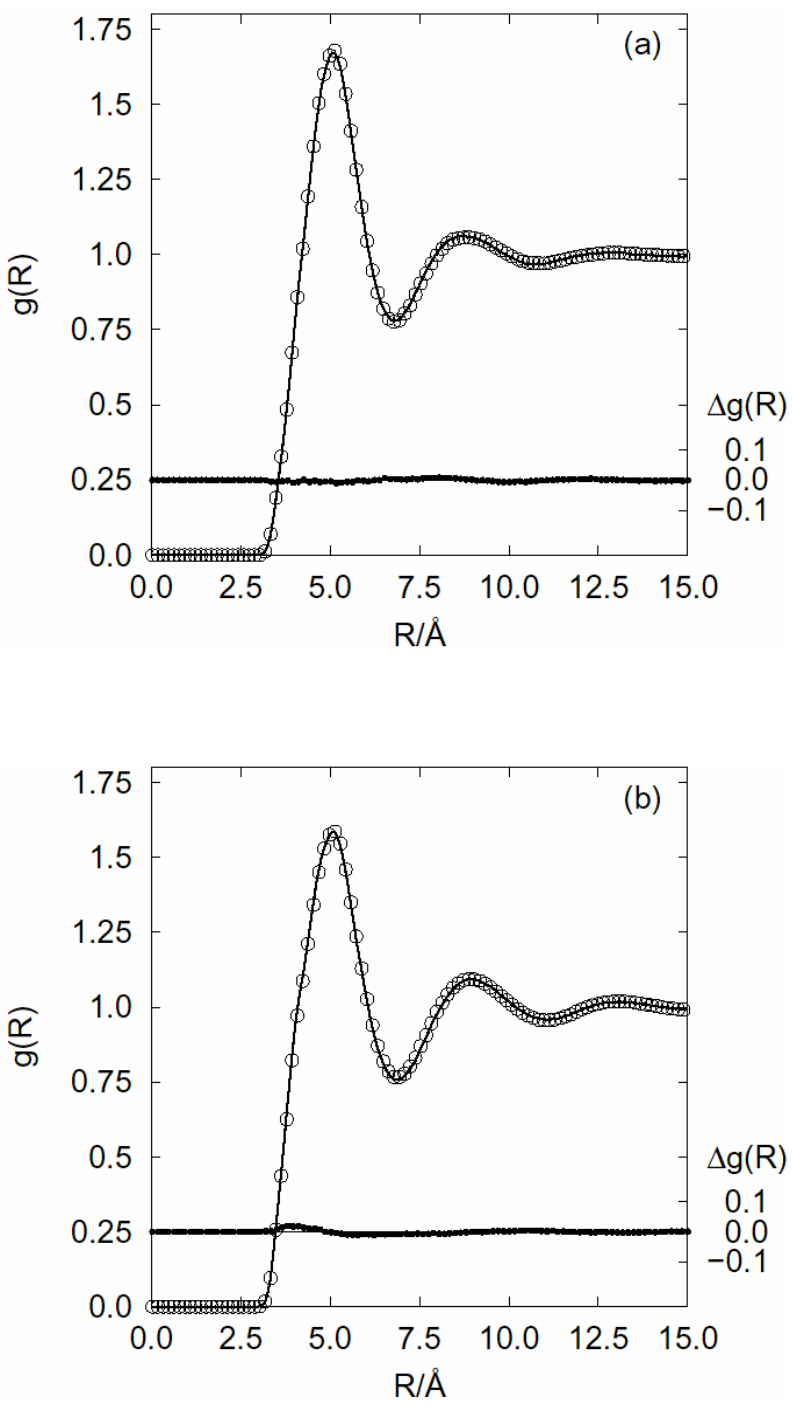

Figure 5.4. As Fig. 5.1, but only for mixtures containing 46wt% (a) and 70wt% (b) of ethanol, respectively. Here, DPD simulations are based upon Φ(R) as obtained from the Boltzmann inversion method outlined in Sec. 5.3.3.

5.3.4 Potentials

We now compare directly the effective potentials Φ(R) obtained by the various approaches described in Sections 5.3.1 – 5.3.3. As one expects, Φ(R) is a damped oscillatory function of the center–of–mass position *R* between a pair of ethanol beads (see Fig. 5.5). At the atomistic level it is standard textbook knowledge that the (damped) succession of maxima in g (R) for "simple" fluids indicates formation of spherical shells of molecules around each reference molecule [16]. In this spirit we interpret the succession of minima in g (R) as fingerprints of the formation of shells of ethanol beads surrounding the reference bead located at R = 0. In view of this notion it seems justified to take as an (admittedly somewhat arbitrary) definition of a bead "diameter" the first zero of Φ(R). Based upon this interpretation we realize that the effective potential decays to zero over a length scale which is approximately 4 times larger than the size of an ethanol bead. The depth of the deepest attractive well in Φ(R) is comparable to, but a bit shallower than, one would expect for a typical intermolecular interaction potential of, say, the Lennard–Jones type.

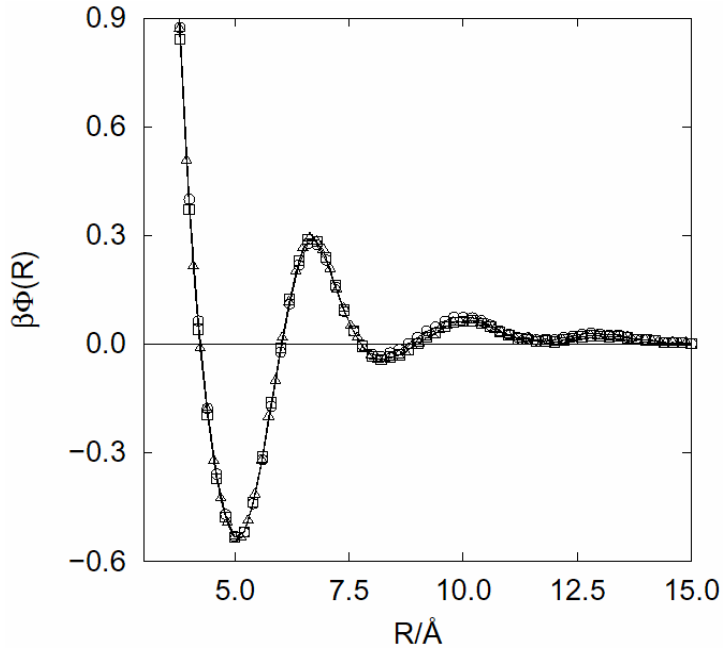

Figure 5.5. Effective pair potential Φ(R) as a function of center–of–mass position R between a pair of ethanol beads for a mixture containing 8wt% of ethanol. Results are obtained from Eqs. (5.6) (□), (5.9) (o), and the Boltzmann inversion scheme (see Sec. 5.3.3) (△).

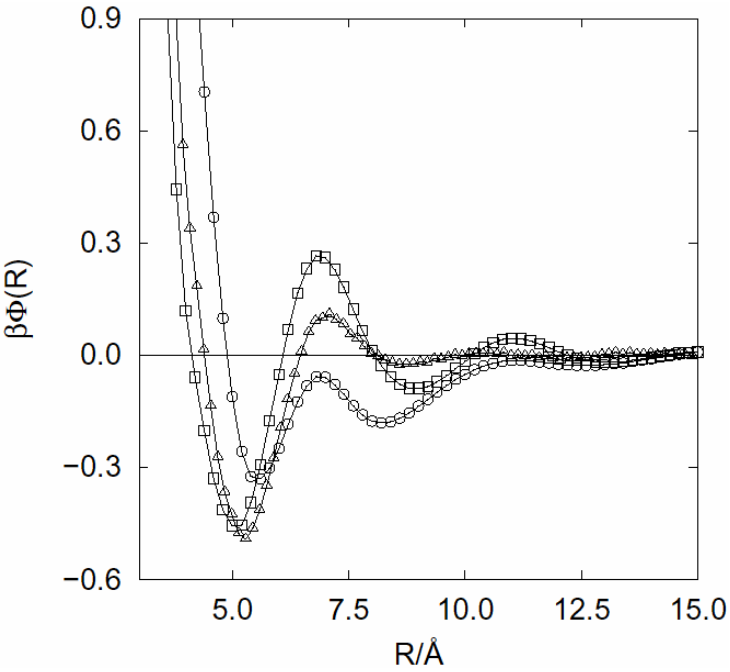

Figure 5.6. As Fig. 5.5, but for a mixture containing 70wt% ethanol.

On account of the relative "softness" of ethanol beads we also notice that the position at which neighboring shells appear varies. For example, whereas the first minimum in Φ(R) is located at $R \simeq 5\,\text{Å}$, the second one is already shifted to a smaller interbead separation of about 8.7Å. This appears to be roughly √3 times the position of the value at which the first minimum of Φ(R) is located. The location of minima in Φ(R) is thus consistent with a hexagonal packing of beads around (each) reference bead. As one would have anticipated from the discussion in Sections 5.3.1 – 5.3.3 all three approaches give the same Φ(R).

It is then interesting to analyze a case in which only the Boltzmann inversion scheme leads to reliable results for the effective potential Φ(R). Plots in Fig. 5.6 reveal that for a mixture containing 70wt% ethanol the overall structure of Φ(R) differs appreciably from that for the mixture with 8wt% ethanol (see Fig. 5.5). However, there are substantial quantitative differences between the various methods. Fig. 5.6 shows that the short range repulsive and attractive portions of Φ(R) agree reasonably between Eq. (5.6) and the Boltzmann inversion scheme. However, at larger interbead separations, Eq. (5.6) tends to overestimate both the height of repulsive barriers and the depth of minima in Φ(R) in comparison with the curve based upon Boltzmann inversion. However, the location of both repulsive barriers and attractive wells in Φ(R) is predicted correctly in DPD simulations based upon Eq. (5.6) as plots in Fig. 5.6 also show.

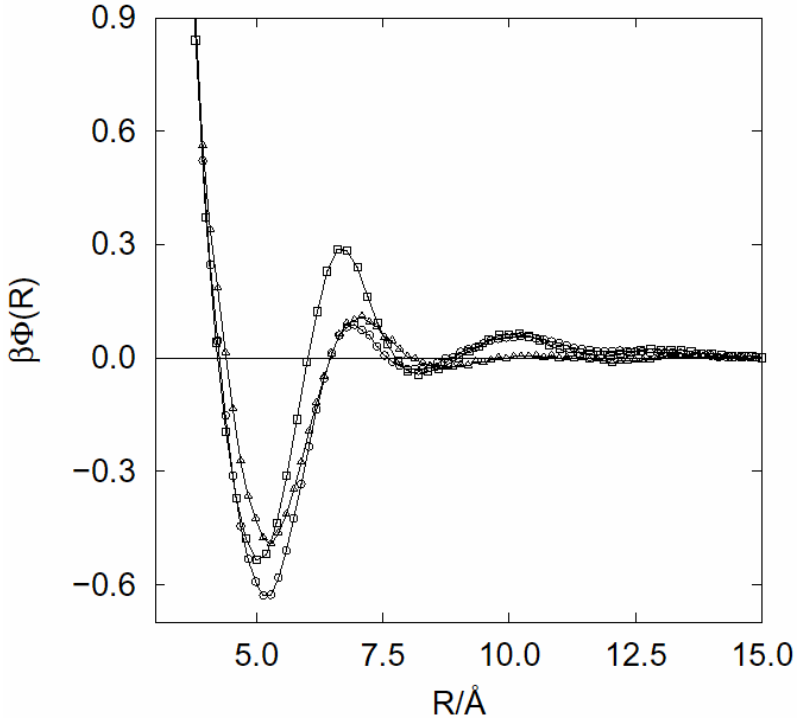

Figure 5.7. As Fig. 5.5, but for mixtures containing 8 (□) using Eq. (5.6), 46 (o), and 70wt% ethanol (△). The latter two data sets are obtained via the Boltzmann inversion technique (see Sec. 5.3.3).

At the highest ethanol concentration of 70wt%, DPD simulations based upon the HNC closure give a representation of Φ(R) which is quite distinct from the other two approaches as the plots in Fig. 5.6 indicate. However, as we demonstrated in Figs. 5.1 and 5.2 the effective potential derived on the basis of the HNC closure [see Eq. (5.10)] still exhibits a much better performance in terms of the correct reproduction of fluid structure than the one derived from Eq. (5.6) (i.e., the potential of mean force). The potential calculated via Eq. (5.10) underestimates short–range repulsive and attractive

interactions as well as the potential minima. However, the range of interbead interactions is predicted more correctly than that from Eq. (5.6), that is Φ(R) from Eq. (5.10) decays to zero at separations at which its counterpart from the Boltzmann inversion scheme also vanishes.

5.3.5 State dependence

In this paper we varied the ethanol concentration over a wide range. It thus seems instructive to investigate the impact of the change in concentration on the effective interaction potential Φ(R). We restrict the discussion to results obtained from the Boltzmann inversion scheme because this turned out to be the only one giving reliable results over the entire concentration range investigated in this work. From the plots in Fig. 5.7 one concludes that the ethanol concentration has little effect on the short(est) range repulsive branch of Φ(R). In addition, the location of the first and higher–order minima remains largely unaffected by increasing the amount of ethanol in the aqueous solutions.

However, there are substantial quantitative changes as one increases the ethanol concentration from 8 to 70wt%. For example, the first minimum in Φ(R) becomes deeper as one goes from a mixture containing 8wt% ethanol to one in which the ethanol concentration amounts to 46wt%; by increasing the ethanol concentration to 70wt% the

minimum becomes shallower again. At $R \simeq 6.8$ Å, Φ(R) appears to exhibit a repulsive barrier which turns out to be largest for the smallest ethanol concentration. The location of this repulsive barrier is relatively insensitive to variations in ethanol concentration at the highest concentrations, as a comparison between Φ(R) for 46wt% and 70wt% clearly shows. The curves pertaining to mixtures containing 8wt% and 46wt% ethanol, respectively, exhibit a secondary repulsive barrier at $R \simeq 10$ Å which is more or less absent from the curve pertaining to a mixture containing 70wt% ethanol. Thus, increasing the ethanol concentration reduces the range of the effective potential considerably, as the corresponding plots in Fig. 5.7 reveal.

5.4 SUMMARY AND CONCLUSIONS

The purpose of this study is to investigate strategies to extract effective (i.e., state–dependent) but pairwise additive, coarse–grained potentials from computer simulations carried out at the atomistic level, where the interactions between all atoms forming the molecules, their charge distribution, and flexibility of the molecular structure are taken into account. As a model system we take aqueous ethanol mixtures in which the concentration of ethanol was increased over the range 8wt% – 70wt%. This system was selected on the basis that it is known not to exhibit any phase separation for the thermodynamic states considered in this work.

The potential describing the coarse–grained interactions in the DPD simulations of this work is derived in two consecutive steps. In the first one we represent molecules of both species (i.e., water and ethanol molecules) as spherical beads by integrating out molecular (i.e., internal) degrees of freedom. This gives rise to an effective potential depending only on the center–of–mass coordinates of the beads. This (effective) potential, which should be viewed as a free energy rather than a potential energy, cannot be split into pairwise additive contributions on account of the coarse–graining process. In fact, as pointed out by Bolhuis and Louis [24] and also by Louis [25] this effective potential should not be confused with a "true" Hamiltonian from which all system properties in the coarse–grained model system can be obtained. Rather our effective potential was designed such that we can map the structure of ethanol beads obtained in a fully atomistic MD simulation with the solvent (i.e., water) present onto the one obtained for an effective pure ethanol fluid in DPD where the impact of the solvent is treated only implicitly. The latter constitutes the second step of our coarse–graining pocedure.

The key question then is: Can we represent this effective potential approximately by pairwise additive potentials $\Phi(R)$ acting between a pair of ethanol beads seperated by a distance R (in the *implicit* presence of water beads)? We tackle this question at three levels of sophistication, namely we assume

1. $\Phi(R)$ is represented by the potential of mean force,
2. $\Phi(R)$ is identified with the potential arising in the HNC closure

3. Φ(R) to be again expressed by the potential of mean force plus a small correction which we calculate by the Boltzmann inversion technique.

On the basis of these three approaches we perform DPD simulations for a one-component fluid of beads in which the interaction between a pair of beads is governed by Φ(R). In these simulations we calculate the center–of–mass pair correlation function for the beads g (R) and investigate its deviation Δg (R) from the corresponding correlation function g_{ref}(R) obtained in the fully atomistic MD simulations.

Our results show that approximating Φ(R) represented by the potential of mean force is inadequate at all but the lowest concentration of 8wt% ethanol regardless of the interbead separation. This deficiency can be cured to some extent by introducing the Ornstein-Zernike equation as a basis for calculating Φ(R) via the HNC closure approximation. The latter incorporates to some extent three–body (and higher–order) correlations neglected at the lower level of approximation (i.e., the one involving only the potential of mean force). Indeed, our results show that this approach works well up to intermediate concentrations, but fails at the highest ethanol concentration considered in this study. It is, however, noteworthy that longer–range (pair) correlations are still quite well represented in DPD simulations, even at the highest concentration where the HNC closure breaks down for short–range interactions, in accord with observations made earlier for atomistic fluids [16].

The only approach suitable over the entire range of concentrations and for all interbead separations is the Boltzmann inversion scheme. This numerical technique is successful because higher–order correlations make only a relatively small contribution under the present conditions. For example, as we illustrate by the plot in Fig. 5.1(c), $|\Delta g(R)| \simeq 0.1$ for the highest ethanol concentration even if we approximate $\Phi(R)$ at the lowest level of sophistication by the potential of mean force. The iterative incorporation of these higher-order correlations may be expected to be easily possible based upon the fact that the periodicity of the underlying effective interactions is already well represented by assuming that $\Phi(R)$ is given by the potential of mean force. We therefore conclude that for the present (admittedly ideal) binary mixture one can obtain reliable pairwise additive effective interaction potentials permitting one to map a fully atomistic model onto a coarse–grained one with the same structural characteristics. In a separate publication we shall attempt to extend this approach to dynamic properties as well.

In closing we emphasize two features of $\Phi(R)$ which are particularly important from a computational point of view: First, the calculated potentials exhibit a significant state-dependence in the sense that varying the concentration causes subtle changes in $\Phi(R)$ which are nonmonotonic and cannot easily be predicted from the knowledge of $\Phi(R)$ at any one concentration. This is in marked contrast to the observations recently made in a study of the effective center–of–mass potentials in NaCl mixtures, where the impact of varying (salt) concentrations was found to be negligible [10]. Second, within the present level of coarse–graining the resulting effective potentials are not as “soft” as

the (quadratic) potentials commonly used in DPD simulations. In particular, they still exhibit a pronounced short–range repulsive contribution. This implies that, for the present problem, the main computational advantage of coarse–graining is not a larger time–step, but mainly the fact that the number of interactions to be considered in the simulations is greatly reduced by more than two orders of magnitude on the atomistic level to 1 on the mesoscale. To illustrate the gain in computational efficiency we determined the amount of time typically required to follow the dynamics of the ethanol–water mixture for a period of 1ns. In terms of the CPU time required it turns out that the DPD simulations require between a factor of 50–100 less compared with the parallel MD simulations. However, the price to pay is a less detailed picture of the molecular dynamics on account of the coarse–graining process underlying the mesoscale simulations.

5.5 REFERENCES

1. J.R. Silbermann, S.H.L. Klapp, M. Schoen, N. Chennamsetty, H. Bock, and K.E. Gubbins, *J. Chem. Phys*, in press.

2. R. L. Henderson, *Phys. Lett.* **49A**, 197 (1974)

3. C. G. Gray and K. E. Gubbins, *Theory of Molecular fluids*, Vol 1, p. 178, Oxford University Press, Oxford (1984), p. 178.

4. A. A. Louis, P. G. Bolhuis, J. P. Hansen, and E. J. Meijer, *Phys. Rev. Lett.* **85**, 2522 (2000).

5. A. A. Louis, P. G. Bolhuis, and J. P. Hansen, *Phys. Rev. E.* **62**, 7961 (2000).

6. P. G. Bolhuis and A. A. Louis, *Macromolecules* **35**, 1860 (2002).

7. C. N. Likos, M. Schmidt, H. Löwen, M. Ballau, D. Pötschke, and P. Lindner, *Macromolecules* **34**, 2914 (2001).

8. A. K. Soper, *Chem. Phys.*, **202**, 295 (1996).

9. D. Reith, M. Pütz, F. Müller–Plathe, *J. Comput. Chem.* **24**, 1624 (2003).

10. A. P. Lyubartsev, M. Karttunen, I. Vattulainen, A. Laaksonen, *Soft Materials* **1**, 121 (2003).

11. T. R. Forester and W. Smith, DLPOLY v. 2.14, (Daresbury Laboratory, Daresbury, 2003).

12. S. Melchionna, G. Ciccotti, and B. L. Holian, *Mol. Phys.* **78**, 533 (1993).

13. J. P. Ryckaert, G. Ciccotti, and H. J. C. Berendsen, *J. Comput. Phys.* **23**, 327 (1977).

14. W. L. Jorgensen, D. S. Maxwell, and J. Tirado Rives, *J. Am. Chem. Soc.* **118**, 11225 (1996).

15. H. J. C. Berendsen, J. R. Grigera, and T. P. Straatsma, *J. Phys. Chem* **91**, 6269 (1987).

16. J. P. Hansen and I. R. McDonald, Theory of Simple Liquids, 2nd ed., (Academic, London, 1986), p. 179.

17. U. Essmann, L. Perera, M. L. Berkowitz, T. Darden, H. Lee, and L. G. Pedersen, *J. Chem. Phys.* **103**, 8577 (1995).

18. E. J. W. Wensink, A. C. Homann, P. J. van Maaren, and D. van der Spoel, *J. Chem. Phys.* **119**, 7308 (2003).

19. P. J. Hoogerbrugge and J. M. V. A. Koelman, *Europhys. Lett.* **19**, 155 (1992).

20. J. M. V. A. Koelman and P. J. Hoogerbrugge, *Europhys. Lett.* **21**, 363 (1993).

21. P. Español and P. B. Warren, *Europhys. Lett.* **30**, 191 (1995).

22. I. Vattulainen, M. Karttunen, G. Besold, and J. M. Polson, *J. Chem. Phys.* **116,** 3967 (2002).

23. L. S. Ornstein and F. Zernike, *Proc. Acad. Sci. Amst.*, **17**, 793 (1914)

24. P. G. Bolhuis and A. A. Louis, *Macromolecules* **35** 1860 (2002).

25. A. A. Louis, *J. Phys.: Condens. Matter* **14**, 9187 (2002).

Chapter 6

Future directions

6.1 COARSE-GRAINING SURFACTANT SYSTEMS

We plan to extend our coarse-graining procedure for the study of surfactant self-assembly in bulk and on surfaces. In particular, we will investigate the self-assembly of alkyl oligo (ethylene oxide) surfactants (represented as C_xE_y where C=methylene and E=ethylene oxide) in bulk water and onto silica and graphite surfaces. The coarse-graining approach will be similar to that of the ethanol/water system. We perform the atomistic simulations using the OPLS-AA force field for the surfactant and SPC/E model for water. In the meso-scale model, the surfactant will be modeled as a chain of beads where each bead represents either an ethylene oxide group or two methylene groups. The pair correlation functions between the center of mass of these beads (for all combinations) will be estimated from the atomistic simulations. Due to the complexity in the number of pair correlation functions to be inverted simultaneously, we will exclude water from the meso-scale model as a starting point. These pair correlations will be used to determine the effective potentials for use in the meso-scale simulations. The procedures used earlier to invert correlation functions for ethanol/water system (integral equations and iterative Boltzmann inversion) will be also applied here for surfactant

systems. Later the approach will be extended to include solvent in the meso-scale simulations to obtain correct dynamics.

After dealing with the bulk systems, we also plan to apply the coarse-graining procedure for the self-assembly of ethylene oxide surfactants from aqueous solution onto (i) silica planar surfaces and (ii) graphite planar surfaces. A comparison of the behavior on carbon and silica surfaces is important because of differences in the strength of the fluid-solid interaction and surface homogeneity for the two cases. It is well known that the silica surfaces containing silanol groups are hydrophilic while graphite surfaces are hydrophobic. The difference in the solid-fluid interactions between these two materials is expected to have an important impact in the types of self-organized surfactant structures that are formed at different conditions. To find the effective potentials for interactions with the surface, the correlation functions obtained between the surfactant and the surface from atomistic simulations will be subsequently inverted.

6.2 RIGOROUS COARSE-GRAINING COMPLEX SYSTEMS

The most challenging step will be the extension of rigorous coarse-graining techniques developed for simple binary mixtures to more complex systems with charges and internal degrees of freedom. Though this is quite difficult and computationally intensive, the success of this rigorous technique will lead to the reproduction of all the

structural and thermodynamic properties of the atomistic system in the meso-scale system. The first step in this direction will be going from the simple binary mixture to that of the chain molecules in a solvent, with only short-range interactions (no Coulomb charges). The solvent will be a structureless spherical atom. The chain molecule will be a freely joined chain of atoms, with no other internal degrees of freedom. Rigorously coarse-graining this system will help us understand the general physics of chain systems such as surfactants and polymers. Later the approach can be extended to systems with more internal degrees of freedom and which also include Coulomb charges.